

The Effect of Salts on the Conformational Stability of Proteins

by

David L. Beauchamp

A Thesis submitted to the Faculty of Graduate Studies of

The University of Manitoba

in partial fulfilment of the requirements of the degree of

MASTER OF SCIENCE

Department of Chemistry

University of Manitoba

Winnipeg

Copyright © 2012 by David L. Beauchamp

TABLE OF CONTENTS

Abstract.....	vi
Acknowledgements.....	vii
List of Tables.....	viii
List of Figures.....	ix
Chapter 1. Introduction.....	1
1.1 The importance of proteins.....	2
1.2 Protein structure and the folding process.....	2
1.3 Water as a universal solvent and the hydrogen bond.....	5
1.4 Linear and bent hydrogen bonds.....	6
1.5 Vibrational spectroscopy to study the hydrogen bond.....	7
1.6 The hydrophobic effect.....	10
1.7 Electrostatic interactions and salt effects.....	15
1.8 Models systems.....	18
1.9 Contact pair formation of phenol and acetate/formate as a model system.....	19
1.10 Ribonuclease t1 as a model system.....	20
1.11 The folding of ribonuclease t1.....	23
1.12 Fluorescence spectroscopy.....	24
1.13 Fluorescence in proteins.....	29
1.14 Collisional quenching.....	30
1.15 Static quenching.....	32

1.16	Deviations from linear Stern-Volmer plots.....	33
1.17	Contributions brought by thesis.....	34
	References.....	36
Chapter 2.	Materials and Methods.....	44
2.1.	Chapter 3	
2.1.1.	Materials.....	45
2.1.2.	Methods.....	45
2.2.	Chapter 4	
2.2.1.	Materials.....	46
2.2.2.	Dialysis.....	46
2.2.3.	UV-vis spectroscopy.....	47
2.2.4.	Fluorescence spectroscopy.....	48
2.3.	Chapter 5	
2.3.1.	Materials.....	48
2.3.2.	Fluorescence spectroscopy.....	48
2.3.3.	Measurements of protein unfolding energy.....	49
	References.....	53
Chapter 3.	The Effect of Lithium Ions on the Hydrophobic Effect: is the Lithium Anomaly a Real Anomaly?.....	54
3.1	The hydrophobic effect and hydrogen bonding.....	55
3.2	The effect of salts on the hydrophobic effect.....	55
3.3	The lithium anomaly.....	56
3.4	Potential explanations of the lithium anomaly.....	57
3.5	Contact pair formation of phenol and acetate or formate as a simple model.....	58

3.6 Mechanism of phenol quenching by acetate and formate.....	59
3.7 Fluorescence quenching and the Stern-Volmer equation.....	60
3.8 Collisional quenching vs static quenching in the phenol-acetate system.....	62
3.9 Defining the phenol-carboxylate system.....	66
3.10 Isolating the hydrophobic contribution to the contact pair formation.....	67
3.11 Contribution of the solvation energy to the formation of the contact pair.....	69
3.12 Introducing the H parameter.....	70
3.13 Influence of salts on the hydrophobic contribution to the formation of the encounter complex.....	75
3.14 Alternative explanation for the observed lithium anomaly.....	75
3.15 Conclusions.....	77
References.....	78

Chapter 4. Studying Salt Effects on Protein Stability Using Ribonuclease t1 as a Model

System.....	81
4.1 Overview.....	82
4.2 Characterizing the thermodynamics of RNase t1 unfolding.....	89
4.3 Effect of alkali chlorides on the unfolding of RNase t1.....	93
4.4 The effect of zinc on the unfolding of RNase t1.....	94
4.5 The effect of magnesium on the unfolding of RNase t1.....	100
4.6 Applicability of the binding model.....	102
4.7 Contribution of salting-in and salting-out effects to protein stability.....	104
4.7.1 Salting-in effects: charge solvation.....	105
4.7.2 Salting-in effects: charge screening.....	106
4.7.3 Salting-out effects.....	107
4.8 Return of the lithium anomaly.....	109

4.9 Binding contribution of divalent cations to the conformational stability of RNase t1.....	111
4.10 Conclusions.....	112
References.....	115

Chapter 5. Probing the Effect of Water-Water Interactions on Enzyme Activity with Salt

Gradients: a Case-Study Using Ribonuclease t1.....	118
5.1 Overview.....	119
5.2 Characterizing RNase t1 activity.....	119
5.3 Ligand binding and fluorescence.....	122
5.4 The effect of salt on the structure of RNase t1.....	124
5.5 Potential explanations for the observed loss of enzyme activity.....	126
5.5.1. First possibility: Salt effect on pK _a values of key active site residues... 128	
5.5.2. Second possibility: The high salt concentration weakens the Coulombic interactions between the substrate and enzyme.....	128
5.5.3. Third possibility: Metal cations bind directly to the enzyme and inhibit catalysis.....	132
5.5.4. Our proposed explanation: The observed salt effect is due to the salt interacting with the water molecules of the protein's hydration shell and modulating the hydrogen bonding, leading to the stabilization of a more rigid, more compact and less active conformation of RNase t1.....	134
5.6 Conclusions.....	143
References.....	145
Summary of Work.....	148

ABSTRACT

It has long been observed that salts affect proteins in a variety of ways, yet comprehensive explanations for different salt effects are still lacking. In the work presented here, the effect of salts on proteins has been investigated through three different effects: the hydrophobic effect; their conformational stability; the hydrogen bonding network of water in a protein's hydration shell. UV-vis absorbance and fluorescence spectroscopy were used to monitor changes in two model systems, the phenol-acetate contact pair and the model enzyme ribonuclease t1. It was shown that salts affect the hydrophobicity of the contact pair according to their charge density, induced image charges play an important role in the observed salt-induced increase of ribonuclease t1 stability, and that salts affect ribonuclease t1 activity through modulation of the hydrogen bonds of water in the enzyme's hydration shell. This work contributes a greater understanding of the effect of salts on proteins.

ACKNOWLEDGEMENTS

I would like to sincerely thank Dr. Khajehpour, whose guidance and leadership has made this work possible. I would also like to thank my parents, Paul and Mariette Beauchamp, for your support and faith. Finally, I would like to thank my girlfriend Jennifer Crook, for tolerating the long hours in the lab and for always listening with interest when I needed someone to talk to and being there when I needed someone.

LIST OF TABLES

<i>Table 3-1.</i> Stern-Volmer constants measured for the quenching of phenol fluorescence by acetate and formate ions in alkali chloride solutions at various concentrations.....	65
<i>Table 3-2.</i> Parameters associated with equation 3-2, demonstrating the salt dependence of the Stern-Volmer constants obtained from the quenching of phenol by acetate and formate.....	65
<i>Table 4-1.</i> The effect of alkali chloride salts on the unfolding profile of RNase t1.....	98
<i>Table 4-2.</i> The effect of diprotic salts on the unfolding profile of RNase t1.....	98
<i>Table 4-3.</i> Parameters obtained from fitting data in Table 4-1, 4-2 to equation 4-3.....	99
<i>Table 4-4.</i> Parameters obtained from fitting data in Table 4-1, 4-2 to equation 4-3.....	99
<i>Table 4-5.</i> Parameters obtained from the data in Table 4-1 using equation 4-1.....	99
<i>Table 5-1.</i> Values of the K parameter associated with RNase t1 for each data set by fitting the data depicted in Figure 5-2 to equation 5-7b.....	133

LIST OF FIGURES

CHAPTER 1

- Figure 1-1.* The water molecule on the left illustrates a bent hydrogen bond that forms high-density water (water_{HD}). The water molecule on the right illustrates a linear hydrogen bond, forming low-density water (water_{LD})..... 6
- Figure 1-2.* OH stretching band for HOD in 5% H₂O and 95% D₂O (solid line), a solution of KCl (■), TMAO (dashed line), and urea (●). 9
- Figure 1-3.* Intermolecular hydrogen bond angle distribution for pure water (solid line), the first hydration shell of TMAO (Δ) and and KCl (■)..... 9
- Figure 1-4.* A typical temperature excursion infrared spectra of the OH stretching in D₂O from 5oC to 80oC as is indicated on the graph. 11
- Figure 1-5.* Fit of the two Voigt functions to the 25°C OH stretch spectrum. The heavy line is the experimentally obtained spectra, while the faint lines are the two Voigt functions representing linear (left) and bent (right) hydrogen bonds and their sum. 11
- Figure 1-6.* Illustrative example of water molecules rearranging themselves to maximize their number of hydrogen bonds (red dotted lines) due to their inability to interact with the hydrophobe (grey circle). In comparison, the water molecules can interact with a hydrophilic moiety (white circle) and so maintain their optimal tetrahedral geometry. 13
- Figure 1-7.* a) Illustrative example of a water molecule potentially interacting with four neighbouring water molecules creating 6 possible conformations. b) Addition of a hydrophobic solute removes 3 possible conformations. 13
- Figure 1-8.* Proposed mechanism for the catalyzed transesterification of ApGpC and ApGpU. 22
- Figure 1-9.* Simplified schematic energy level diagram of a fluorescing molecule, known as a Jablonski diagram. 24
- Figure 1-10.* Absorbance (1st blue, green and yellow arrows) and emission spectrum (blue and red respectively) (2nd blue, green and yellow arrows) of anthracene..... 25
- Figure 1-11.* Absorbance (blue) and emission (red) spectrum of perylene (above) and quinine (below). 25
- Figure 1-12.* Typical arrangement of the basic components of a spectrofluorimeter. 27
- Figure 1-13.* The fluorescence spectrum of RNase t1 in the folded (solid line) and unfolded (dashed line) forms, showing the Raman peak at 320nm. 30

CHAPTER 2

Figure 2-1. Varian Cary Eclipse Fluorescence Spectrophotometer..... 50

Figure 2-2. Thermo Scientific Helios Zeta UV-Vis spectrophotometer..... 51

Figure 2-3. Fluorolog-3 Horiba Jobin Yvon Spectrofluorimeter.. 52

CHAPTER 3

Figure 3-1. The fluorescence spectrum of phenol in the presence of sodium acetate (a) and sodium formate (b). Quencher concentrations are 0M (black), 0.1M (red), 0.2M (green), and 0.4M (blue). 63

Figure 3-2. Stern-Volmer plots for the quenching of phenol by lithium acetate (a) and lithium formate (2). The concentration of lithium ions is kept constant at 1.5M (●) and 4M (○) by addition of LiCl. 63

Figure 3-3. Parameters *a* and *b* associated with equation 3-2, demonstrating the salt dependence of the Stern-Volmer constants obtained from the quenching of phenol by acetate and formate. 64

Figure 3-4. Salt concentration dependence of the $H_S - H_{S = 1.5 M}$ for LiCl (red), NaCl (black), KCl (blue) and RbCl (green). 76

CHAPTER 4

Figure 4-1. Illustration of a simple dipole. By convention the positive charge comprises the arrowhead, which indicates the direction of the dipole moment. 85

Figure 4-2. Dipole moment of the backbone amide group..... 86

Figure 4-3. Formation of induced surface charges at the edge of a protein in an electric field *E*. The electric field magnifies the intrinsic dipole of the backbone amides which cancel out except at the surface. 86

*Figure 4-4.*a) A charge located in a low dielectric medium is attracted to the induced surface charge, which can be represented by placing an opposite charge directly across the dielectric boundary in the high dielectric medium (red circle). b) Because of solvation effects, a charge located in a high dielectric medium will be repelled by a low dielectric medium. The effect of the charge can be represented by placing a mirror-image charge in the low dielectric medium (red circle). 87

Figure 4-5. Illustration representing the relative effect of induced point image charges on the folded and unfolded states of a protein. The folded state (left) of a protein will be stabilized relative to the unfolded state (right) since it has a smaller surface area and therefore fewer destabilizing interactions between the cations in solution and their induced point mirror-image charge..... 88

Figure 4-6. a) The fluorescence spectrum of RNase t1 in the folded (solid line) and unfolded (dashed line) forms, showing the Raman peak at 320nm. b) The fluorescence spectrum of the folded state of RNase t1 in the presence of 0 μ M ZnCl₂ (solid line), 50 μ M ZnCl₂ (dashed line) and 50 μ M ZnCl₂ and 100mM mgCl₂ (dotted line). The inset fits the data to a hyperbolic binding curve. c) The pH dependence of the dissociation constant, K_d, of the Zn²⁺ ligand concentration in μ M units. 90

Figure 4-7. The unfolding of RNase t1 dissolved in pH 7 buffer at low ionic strength. The solid line is the best fit to equation 4-1. 92

Figure 4-8. a) The unfolding profile of RNase t1 at increasing NaCl concentrations (0.05-1M). b) The dependence of $\Delta\Delta G_{\text{unfolding}}^{\circ}/RT$ on the ionic strength of the solvent. The solid line is the best fit to equation 4-2. c) The dependence of $\Delta\Delta G_{\text{unfolding}}^{\circ}/RT$ on the square root of the ionic strength of the solvent. The solid line is the best fit to equation 4-11. 95

Figure 4-9. a) The unfolding profile of RNase t1 at increasing KCl concentrations (0.1-1M). b) The dependence of $\Delta\Delta G_{\text{unfolding}}^{\circ}/RT$ on the ionic strength of the solvent. The solid line is the best fit to equation 3-2. c) The dependence of $\Delta\Delta G_{\text{unfolding}}^{\circ}/RT$ on the square root of the ionic strength of the solvent. The solid line is the best fit to equation 3-11. 96

Figure 4-10. a) The unfolding profile of RNase t1 at increasing LiCl concentrations (0.1-1M) b) The dependence of $\Delta\Delta G_{\text{unfolding}}^{\circ}/RT$ on the ionic strength of the solvent. The solid line is the best fit to equation 4-2. c) The dependence of $\Delta\Delta G_{\text{unfolding}}^{\circ}/RT$ on the square root of the ionic strength of the solvent. The solid line is the best fit to equation 4-11. 97

Figure 4-11. a) The unfolding profile of RNase t1 at increasing ZnCl₂ concentrations (100-600 μ M) b) The dependence of $\Delta\Delta G_{\text{unfolding}}^{\circ}/RT$ on the ZnCl₂ concentration. The solid line is the best fit to equation 4-3. 101

Figure 4-12. The unfolding profile of RNase t1 at increasing MgCl₂ concentrations (0.05-1M). 103

Figure 4-13. The dependence of $\Delta\Delta G_{\text{unfolding}}^{\circ}/RT$ on MgCl₂ concentration. The solid blue line is the best fit to equation 4-2 and the solid red line is the best fit to equation 4-18. 103

CHAPTER 5

Figure 5-1. Typical kinetic trace obtained after adding RNase t1 (final concentration of 2.98nM) to a solution containing 10 μ M GpC at pH 5.5, 10mM bis-tris buffer. 120

Figure 5-2. Effect of various chloride salts upon the k_{cat}/K_m parameter of RNase t1 obtained from the enzyme-catalyzed hydrolysis of GpC. The catalytic efficiency is reduced universally upon addition of various salts. 121

Figure 5-3. Dependence of the steady-state fluorescence of RNase t1 on 5'-GMP concentration. a) Steady-state fluorescence spectra of RNase t1 after addition of 0-200 μ M 5'-GMP, following the arrow, with excitation at 265nm. b) Fluorescence intensity maximum (330nm) of RNase t1 upon excitation at 265nm. c) Steady-state fluorescence spectra of RNase t1 after addition of 0-500 μ M 5'-GMP, following the arrow, with excitation at 290nm. d) Fluorescence intensity maximum (330nm) of RNase t1 upon excitation at 290nm. 125

Figure 5-4. Effect of salt concentration on the binding of 5'-GMP to RNase t1. The K_d values measured upon addition of NaCl (\square) and MgCl₂ (Δ) at the indicated concentrations. 127

Figure 5-5. Stern-Volmer plots of the quenching of RNase t1 (circles) and NATA (squares) in the absence (filled) and presence (open) of 1M MgCl₂. 127

Figure 5-6. a) Effect of NaCl concentration on the parameter k_{cat}/K_m obtained from the enzyme catalyzed hydrolysis of GpC by RNase t1. The solid line represents the best fit to equation 5-6. b) Effect of NaCl concentration on the K_d values obtained from the binding of 5'-GMP to RNase t1. 131

Figure 5-7. a) Dependence of the $K/(1 + K_0)$ parameter, obtained by plotting the data from Figure 5-2 to equation 5-9, as a function of the Jones-Dole B coefficient of various chloride salts. b) Dependence of the $K/(1 + K_0)$ parameter upon the cation hydration numbers of various salts. 138

Figure 5-8. Dependence of the $K/(1 + K_0)$ parameter of RNase t1 upon the amount of energy (ΔG°) needed to convert water_{HD} to water_{LD} of various 4.4 m salt solutions. 142

Chapter 1

Introduction

1.1 The importance of proteins

Proteins are an essential part of everyday life and are involved in every biological process in every living organism, whether it is a single-cell organism or a fully evolved mammal. They constitute half the dry weight of cells (1), more than any other biomolecule present in any given cell. The list of protein functions is long and continuously expanding: proteins act as cellular scaffolding (structural or cytoskeletal proteins) (2-4), they are used to carry other biomolecules from one area of the cell to another (transport proteins) (5-7), they make up muscle tissue (contractile proteins) (8-10), they alter/suppress the function of biomolecules (effector/repressor proteins) (11-13), they accelerate reactions within cells (enzymes or catalytic proteins) (14-16); to name just a few of their most prominent functions. It is of no surprise then that the research pertaining to proteins is a vast field with thousands of academic and industrial researchers working everyday to better understand a specific isolated protein system.

1.2 Protein structure and the folding process

To function properly, proteins need to adopt a specific 3D conformation, which is also known as the native folded state of the protein. In most biological cases, this requires that the folded state be more stable relative to the unfolded state (19, 20). Protein folding is driven by the need of the system to reach the lowest possible energy state. Generally, the folded state of the protein is 5-10 kcal/mol more stable than its unfolded state in vivo (19). There are a variety of interactions that favourably influence the folding process: the formation of hydrogen bonds, van der Waals interactions, hydrophobic interactions and entropy, disulfide bridges and electrostatic interactions are the most important (1, 20). The work presented here will focus on the contributions from hydrophobic and electrostatic interactions.

The cumulative effect of the above mentioned forces in folded proteins is that the strength of the favourable interactions outweighs the unfavourable ones. Conversely, in the case of unfolded proteins, the unfavourable interactions outweigh the favourable ones and cause the protein to denature.

The underpinning cause of this delicate balance can be found in the building blocks that make up proteins. Proteins are comprised of twenty unique amino acids having a variety of different properties; there are polar charged (e.g. arginine, aspartate) and polar uncharged (e.g. asparagine, serine), hydrophobic (e.g. methionine, leucine), cyclic (e.g. phenylalanine, proline), and aromatic (e.g. tyrosine, tryptophan) residues of varying sizes (1). These amino acids are connected by peptide bonds and comprise the primary structure of the protein which plays a determinant role in the folding process of the protein (21, 22). Briefly, the primary structure will reposition the amino acids locally according to the properties of the side-chain residues to give the secondary structure of the protein. Generally, the amino acids will position themselves so that the hydrophobic residues are in the interior of the protein, hidden away from the solvent, and the polar residues will face outward and be in contact with the solvent (22). Secondary structures include α -helices, β -strands and turns (1). The secondary structure will then reorganize itself to form larger groups, influenced to a large degree by the hydrophobic interactions present and the potential formation of disulfide bridges (22), to yield the tertiary structure of the protein, which is either the last step in the folding process, giving the final structure, or resulting in subunits that will interact with one another to then give the final structure of the protein (i.e. quaternary structure).

Therefore, the structure of a protein is of paramount importance for its proper function (23, 24). The mutation of a single residue can perturb the folding of the protein, which can lead

to the misfolding of the protein and subsequently to a defective performance (24). As an example, there are many prevalent neurodegenerative disorders that are thought to be caused by specific proteins that have not folded properly (25), Alzheimer's, Parkinson's, and Huntington's disease are thought to be caused by the death of nerves cells brought about by misfolded proteins (26, 27). This is brought about by the aggregation and deposition of misfolded proteins to form amyloid fibrils. These fibrillar aggregates form plaques and neurofibrillar tangles in the brain which are related to cellular toxicity and cellular decay, eventually leading to cell death (25, 26, 27).

While understanding the intramolecular forces that contribute to protein structure and its mechanisms of action is of course necessary, understanding the environmental interactions that affect the structure of the protein itself is also of the utmost importance. *In vivo* proteins are not created and do not perform their function in a dilute water environment; they reside in a crowded cellular environment which can contain genetic material, nutrients, various salts, and/or a plethora of cellular components. In this regard, the role of the environment is also of great importance. In this crowded environment, there are many external factors that can influence the stability of a protein, including metal binding, co-factor interactions, pH, temperature, and salts (28, 29). As an example, the pH of the environment of the apo trp repressor can modulate its ability to bind certain ligands (30): the binding of the ligands tryptamine and indole propionic acid is not affected by changes in pH, whereas the binding of trans- β -indole acrylic acid drops severely when the pH = 6-10 (30). Temperature will also have an impact on protein stability: the haemoglobin found in Antarctic fish needs a specific temperature range to function properly, and a deviation in temperature will change its structure and thus will be detrimental to its oxygen-carrying capability (31). The focus of this work will be the effect caused by co-solutes, i.e. salts,

on protein stability. However, before discussing the effect of salts, a firm understanding of the role of the solvent that contains both the protein and the salt is needed. Whether the *in vivo* protein is found in the cytosol, a mitochondria or the nucleus, it is always dissolved in a single universal solvent: water.

1.3 Water as a universal solvent and the hydrogen bond

Thales of Miletus was the first to recognize the importance of water over 2,500 years ago, stating that “*water constituted the principle of all things*” in his cosmological thesis. In the last century, the interest in water has been renewed with intense vigour. The longevity of the interest in water can be attributed to its many peculiar properties: abnormally high boiling, freezing and critical points for a small molecule, anomalously high surface tension and vaporizing enthalpy, increasing liquid fluidity with increasing pressure, high dielectric constant, and a high mobility of H^+ and OH^- ions (32, 33). What is perhaps the most paradoxical property of water is the fact that water is one of the most corrosive substances found in nature, yet it is physiologically harmless (33). This combination of peculiar properties is unique to water as it is very unusual to have so many oddities combined in one substance. It is this combination of physical properties which makes water a universal solvent and it is what has allowed life to develop and flourish in the last 3.5 billion years (32).

The key to understanding water and all or its peculiar properties lies in understanding the way by which water molecules interact with one another. Water is comprised of highly polar molecules that interact with each other through hydrogen bonds, with each water molecule able to both donate and receive hydrogen bonds. The study of the hydrogen bond has been ongoing for the better part of a century, with several books being written on the subject (34-37). Despite the intense research, it was only in 2007 that IUPAC formally defined the hydrogen bond as “*an*

attractive interaction between a group X-H and an atom or group of atoms Y in the same or different molecule(s), where there is evidence of bond formation” (38). A wide range of energies has been used to describe a hydrogen bond, from the linear symmetrical [H-F-H]⁺ (167 kJ/mol) to the van der Waals like Cl-H-Ne interaction (1.67 kJ/mol) (38); typically a hydrogen bond has a bond strength of ~5 kJ/mol in water (32).

1.4 Linear and bent hydrogen bonds

Theoretical work (39-41) on water-water interactions has shown that intermolecular hydrogen bonds occur in 2 modalities, either through high-angle, described as “bent” hydrogen bonds or low-angle, described as “linear” hydrogen bonds. The angle described as being either “high” or “low” is the smallest angle made between the H-O---O of two interacting water molecules (Figure 1-1). Modeling water as a two-state equilibrium was first postulated by Muller in the late 1980s (42) to explain the unusual thermodynamic properties of hydrophobic solutes dissolved in water. This model describes liquid water as an equilibrium between two populations of water: one population, or conformation, of water is participating in bent hydrogen bonds, leading to a high-density form of water (water_{HD}) at high concentrations. The second form of water is participating in linear hydrogen bonding, forming a tetrahedral network of low-density water (water_{LD}), often compared to the hydrogen bond network of solid water (ice). Muller concludes

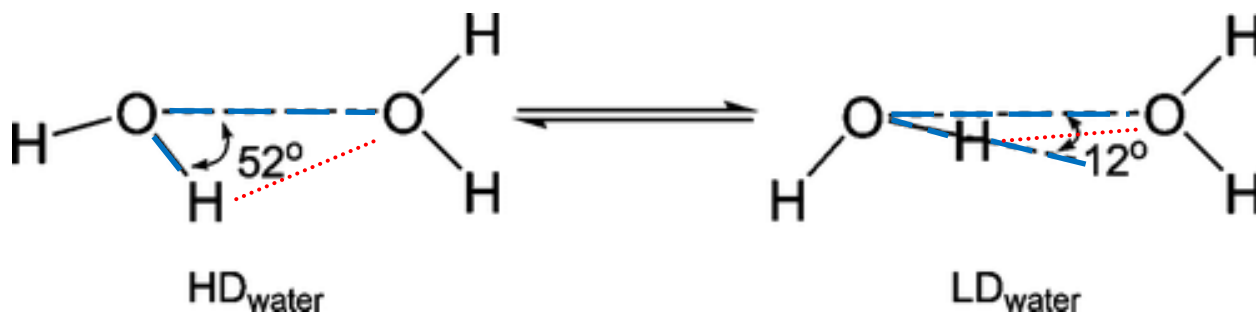


Figure 1-1. The water molecule on the left illustrates a bent hydrogen bond forming high-density water (water_{HD}). The water molecule on the right illustrates a linear hydrogen bond, forming low-density water (water_{LD}). The dashed blue lines indicate the lines used to obtain the angles shown and the dotted red lines are the hydrogen bonds.

that “the hydrogen bonds in the hydration shell of non-polar solutes are enthalpically stronger but more broken than those in bulk water” (43). Graziano et al. have used the two-state model extensively to study general theory of hydration of hydrophobic solutes (44). They found that the Muller model was more than adequate in explaining the experimental data for the solvation of alkanes (43), noble gases (45) and *n*-alcohols (46). However, this model is simplistic and requires arbitrarily chosen and/or empirically adjusted parameters (42, 47). Nevertheless, the two-state model effectively describes the fundamental process of the hydration of hydrophobic moieties (43, 47) and will be used in this work to qualitatively explain the different modes of hydrogen bonding.

1.5 Vibrational spectroscopy to study the hydrogen bond

The two types of hydrogen bonds have been studied extensively using vibrational spectroscopy. The first method of vibrational spectroscopy used (48-51) to study the hydrogen bond is Raman spectroscopy. The study of the temperature dependence of the intermolecular vibrational frequency region of water has shown that the hydrogen bonds between water molecules occur in two modalities (48). Also, changes in the OH stretching-mode regions spectrum of H₂O in D₂O at increasing temperatures have shown that there is a correlation between increasing temperature and decreasing strength of hydrogen bonds (51). The study of the Raman spectrum of water under high pressure conditions has also demonstrated that water undergoes a structural change, further supporting the hypothesis that water interacts through two distinct types of hydrogen bonds (49). These results are all consistent with results obtained by the second form of vibrational spectroscopy, infrared (IR) spectroscopy.

Specifically, IR spectroscopy studies the OH stretching band of HOD, typically 5% HOD is diluted in 95% D₂O. The OH stretching band is often referred to as an OH oscillator. An

example of an OH stretching band is shown in Figure 1-2 [obtained from (52)]. IR spectroscopy is sensitive to changes in the local environment of vibrating molecules and can be used to measure the strength of a hydrogen bond (53). An OH oscillator can be presumed to be completely decoupled from other OH oscillators since there are relatively few HOD molecules present in the D₂O solution (53), allowing researchers to use the OH stretch as a selective and independent probe of hydrogen bonding strength. Figure 1-2 depicts the effect of different solutes on the IR stretching frequency of water, originally centered at 3407 cm⁻¹. Solute that cause the peak to shift to lower frequencies, such as trimethylamine-N-oxide (TMAO), are often called kosmotropes and they have been shown to increase the strength of the intermolecular hydrogen bonding. Solute that cause a shift to higher frequencies, such as KCl, are often called chaotropes and they have been shown to weaken hydrogen bonding. The chemical denaturant urea has no measurable effect on the hydrogen bonding properties (52).

Theoretical work, supported by experimental observations, undertaken by the Sharp group (52) has shown that the observed shift in the IR spectrum of water upon addition of solute is due to a shift in the relative populations of linear and bent hydrogen bonds present in solutions. These simulations demonstrate that the hydrogen bond angle distributions are centered at peaks ~12° (linear hydrogen bonds) and ~52° (bent hydrogen bonds), as shown in Figure 1-3 [taken from (52)]. The addition of the hydrophobic solute TMAO increases the population of strong, linear hydrogen bonds, and the addition of the ionic species KCl increases the population of weak, bent hydrogen bonds in their first hydration shells. It is important to note that the addition of solute changes the population distribution of the hydrogen bonds but not the angle of the hydrogen bond themselves, i.e. the H-O---O angle distributions remain centered at ~12° or ~52°. Vanderkooi et al. expanded their use of IR spectroscopy and utilized a technique called

OH stretch (5% HOH in DOD)

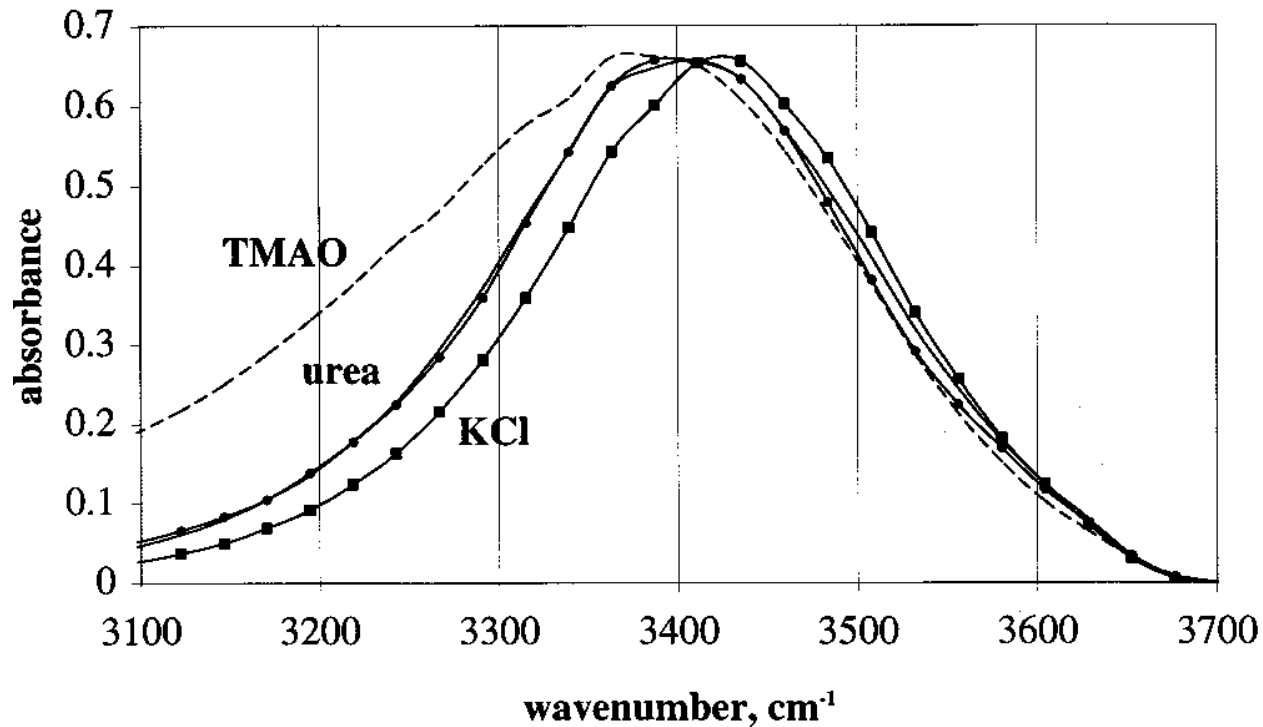


Figure 1-2. OH stretching band for HOD in 5% H₂O and 95% D₂O (solid line), a solution of KCl (■), TMAO (dashed line), and urea (●). Obtained from (52) and used with permission.

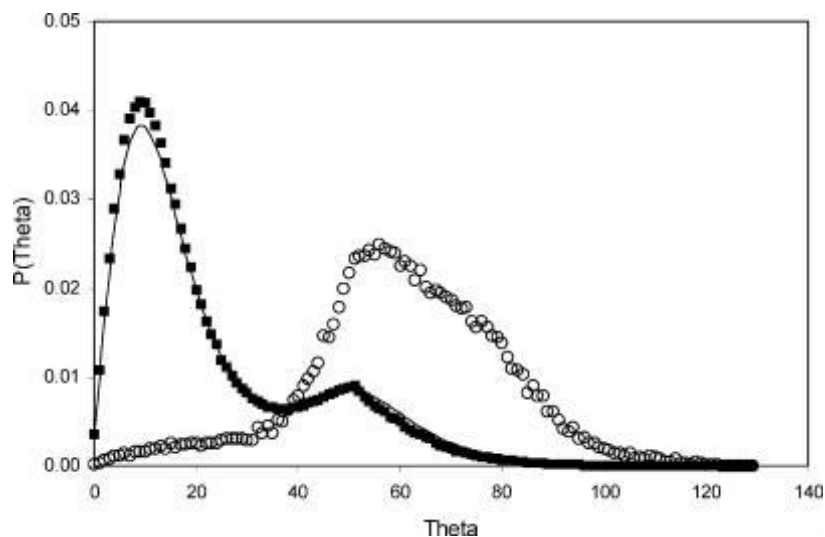


Figure 1-3. Intermolecular hydrogen bond angle distribution for pure water (solid line), the first hydration shell of TMAO (Δ) and KCl (■). Obtained from (52) and used with permission.

temperature-excursion infrared (TEIR) spectroscopy (54). TEIR measures the effect of temperature on the IR absorption of the OH stretching frequency. The OH stretching frequency of HOD will decrease as temperature increases. The increase in temperature will increase the population of strong, linear hydrogen bonds. Since linear hydrogen bonds are stronger than bent hydrogen bonds, this will enable the hydrogen to stretch away from the oxygen atom to a greater extent. This is then reflected in the OH stretching frequency which can be measured by TEIR (41, 52, 54). A characteristic TEIR spectrum is shown in Figure 1-4 [taken from (41)]. Each individual spectrum is fit to two Voigt functions to determine the relative populations of linear and bent hydrogen bonds. The areas under each Voigt fit (Figure 1-5 [taken from (41)]) are then used to calculate the relative populations, of which ratios are subsequently used to obtain the effective equilibrium constant, $K_{b \rightarrow l} = A_l/A_b$, for the transition of an OH bond from a bent hydrogen bond to a linear hydrogen bond. Finally, the effective equilibrium constant was used by Vanderkooi et al. to quantify the effective energy required to transition between a bent hydrogen bond to a linear hydrogen bond ($\Delta G_{b \rightarrow l}$) using the Boltzmann relationship to free energy. Tabulation of these results showed a strong correlation between the ($\Delta G_{b \rightarrow l}$) of salts and their ordering in the Hofmeister series, as well as with the Jones-Dole β viscosity parameter (41). The significance of the $\Delta G_{b \rightarrow l}$ parameter in relation to this work will be discussed in the final chapter.4

1.6 The hydrophobic effect

In a biological setting, the main difference between bent and linear hydrogen bonds is their effect on the solubility of hydrophobes. Hydrophobes require a large population of bent hydrogen bonds available to be dissolved (55). This is a result of the geometry of the hydrogen bond network of water. Since non-polar solutes cannot interact with water molecules directly, they

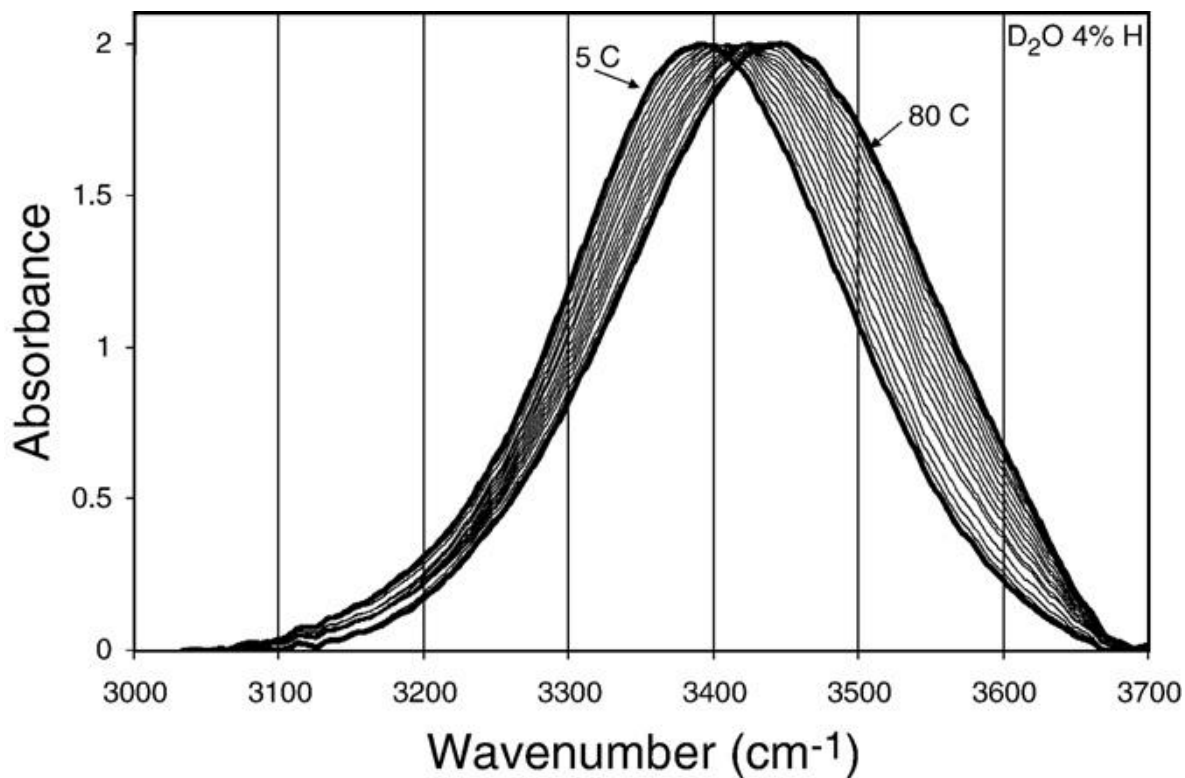


Figure 1-4. A typical temperature excursion infrared spectrum of the OH stretching in D_2O from $5^\circ C$ to $80^\circ C$ as is indicated on the graph. Obtained from (52) and used with permission.

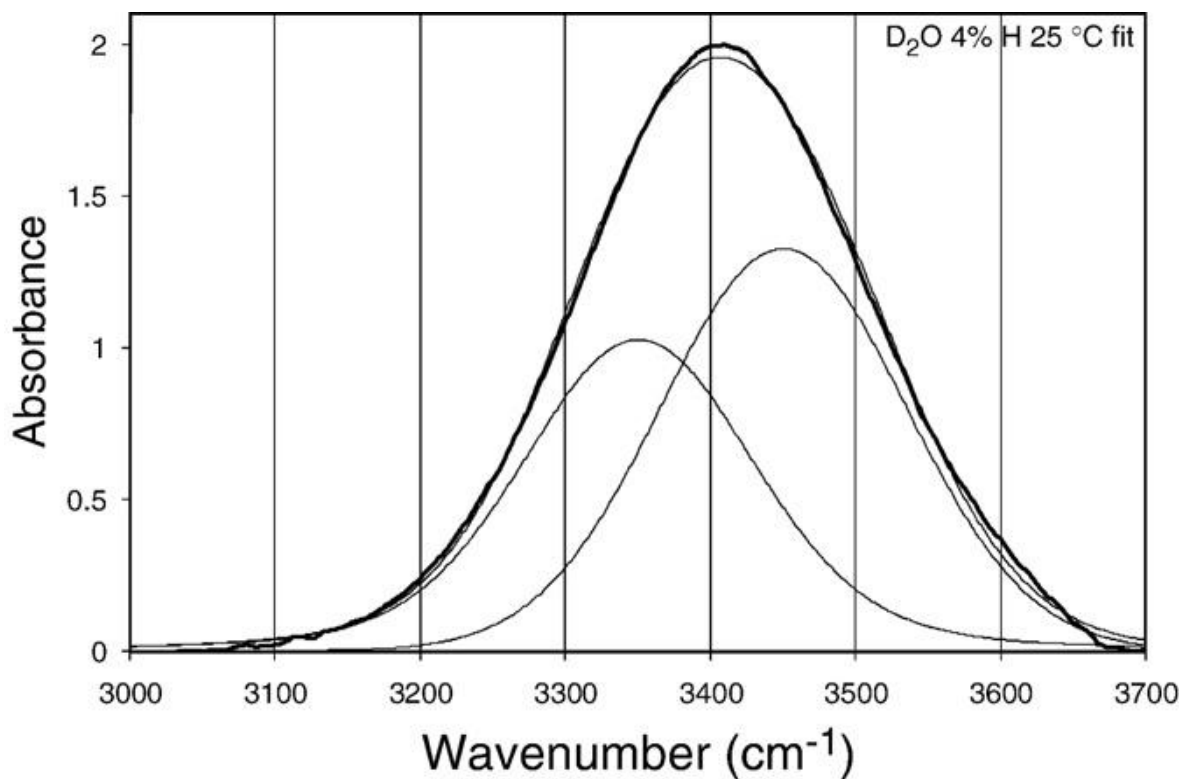


Figure 1-5. Fit of the two Voigt functions to the $25^\circ C$ OH stretch spectrum. The heavy line is the experimentally obtained spectra, while the faint lines are the two Voigt functions representing linear (left) and bent (right) hydrogen bonds and their sum. Obtained from (52) and used with permission.

need to break or displace hydrogen bonds; the bent hydrogen bonds form weaker interactions than linear hydrogen bonds, therefore bent hydrogen bonds are easier to perturb than their linear counterparts (39). And so to minimize the hydrophobic effect, hydrophobes need a population of water_{LD} available to be converted to water_{HD} (39, 55). The hydrophobic effect is the term given to the interaction, or force, of the phenomenon observed when non-polar solutes aggregate after being transferred to water. Non-polar molecules are insoluble in water because they do not have a charged region that can interact with the dipole of the solvent water molecules (33). The hydrophobic effect manifests itself when non-polar moieties are dissolved in water and there is disruption of the hydrogen bond network of the bulk solvent (56). The effect of transferring a non-polar solute to water is best described in thermodynamic terms by the change in the water's heat capacity (C_p) which relates the changes in entropy, enthalpy and free energy to the change in the temperature of the system (40, 57). The addition of a non-polar solute will result in a positive change of C_p , whereas the addition of a polar solute will net a negative change of C_p . This provides a simple and straightforward way to differentiate between the hydration of non-polar solutes ($+\Delta C_p$) and polar solutes ($-\Delta C_p$), whereas the study of the ΔS and ΔH only provides a negative result for both non-polar and polar solutes at room temperature (57). Sharp et al. (39) have proposed that the change in the water's heat capacity is due primarily to the change of the relative populations of strong, linear hydrogen bonds and weak, bent hydrogen bonds in the first hydration shell of the solute. Polar solutes will have a strong electrostatic interaction with the solvent water molecules, causing them to form bent non-polar solutes, it is the entropic interactions in the solutes first hydration shell (39, 57, 58). The increase in the population of strong, linear hydrogen bonds by the solvation of hydrophobic moieties forces water into a more structured/organized conformation around the hydrophobe, thereby decreasing the overall

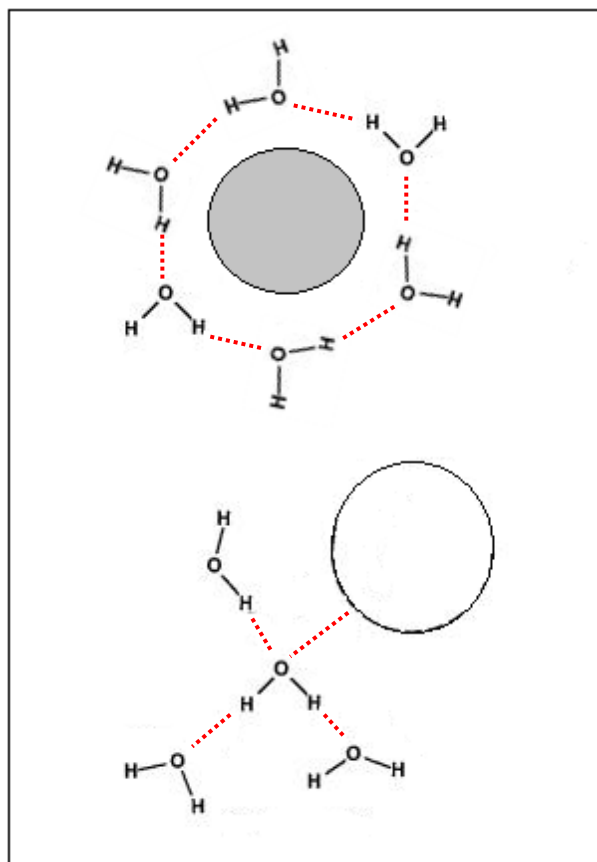


Figure 1-6. Illustrative example of water molecules rearranging themselves to maximize their number of hydrogen bonds (red dotted lines) due to their inability to interact with the hydrophobe (grey circle). In comparison, the water molecules can interact with a hydrophilic moiety (white circle) and so maintain their optimal tetrahedral geometry.

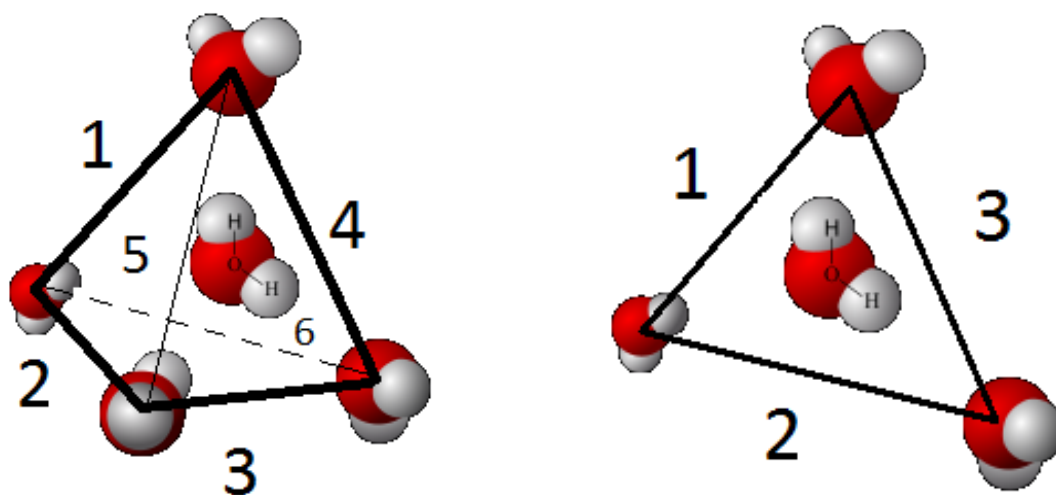


Figure 1-7. Illustrative example of a water molecule potentially interacting with four neighbouring water molecules creating 6 possible conformations (left). b) Addition of a hydrophobic solute removes 3 possible conformations (right).

entropy of the system, which results in a positive change in the water's heat capacity (57). The loss of entropy stems from the fact that a portion of the water molecules around the hydrophobe lose a hydrogen bond (pointing towards the hydrophobe) since they cannot interact directly with the hydrophobe, the water molecules must rearrange themselves in a more structured manner to maximize hydrogen bonding with neighbouring water molecules (Figure 1-6) (32, 56). The loss of entropy can be best visualized by considering a single water molecule as being in the middle of a tetrahedron with the four corners being neighbouring water molecules (Figure 1-7). The primary water molecule can form hydrogen bonds with two neighbouring water molecules at any given time, resulting in six possible conformations. Figure 1-7 depicts the formation of two hydrogen bonds between the central water molecule and the top and bottom right neighbours, a unique configuration would be identified by forming a triangle between the central water molecule, the two neighbouring water molecules (top and bottom right) and the edge number 4 of the tetrahedron; repeating this process yields six possible hydrogen bond configurations. Now if the scenario where the central water molecule is placed next to a hydrophobic moiety is considered, a single neighbouring water molecule would be removed. Removing one water molecule in this simple model results in the loss of three potential hydrogen bond configurations. In other words, the conformational entropy of the central water molecule has been reduced by half. I can now crudely approximate the entropic loss of adding a mole of hydrophobes to the solution by calculating the Boltzmann entropy:

$$\Delta S^{\circ} = S_{in\ water}^{\circ} - S_{on\ hydrophobic\ surface}^{\circ} = N_A(k \ln W_{in\ water} - k \ln W_{on\ hydrophobic\ surface}) \quad (1-1)$$

$$\Delta S^{\circ} = N_A(k \ln 6 - k \ln 3) = N_A k \ln 6/3 = N_A k \ln 2 \quad (1-2)$$

$$T\Delta S^{\circ} = RT \ln 2 = 0.42\ kcal/mol \quad (1-3)$$

where N_A is the Avogadro number, k is the Boltzmann constant and W is the maximal number of configurations that can be attained by the system. From the result in equation 1-3, the entropic cost of dissolving a mole of hydrophobic solutes in water can be crudely approximated to be 0.42 kcal/mol. And so it can be concluded that the hydrophobic effect is driven by the system trying to minimize the loss of entropy that occurs upon the transfer of a hydrophobic solute. To accomplish this, hydrophobic solutes will aggregate in solution to minimize the surface area that is exposed to solvent. This reduces the total surface area of the hydrophobic moieties and minimizes contact with the polar water molecules, thereby decreasing the total loss of entropy by the system (40, 56). While the ordering of hydrophobic moieties to reduce the loss of entropy might seem paradoxical, it must be remembered that the entropic cost of ordering the hydrophobes to form aggregates is considerably smaller than the entropic cost of ordering water molecules around the entire surface of the hydrophobe.

In 1959, Kauzmann first postulated (59) that the hydrophobic effect was a major contributing factor to the folding process of proteins. In the half-century since, experimental and theoretical work has reinforced this idea and today it is generally accepted that the hydrophobic effect is a major force behind protein folding (19, 60-62). However, as mentioned above, there are numerous interactions that drive the proper folding of a protein. The driving forces behind protein folding that will be studied in this work are the hydrophobic effect, described above, and electrostatic interactions, described in the following section.

1.7 *Electrostatic interactions and salt effects*

Salt effects on electrostatic interactions are the sum of three separate effects: charge solvation, charge screening, and induced point image charges. The first salt effect is the result of the individual charges, located on or in a protein, inducing a counter-ion cloud in the near vicinity of

the protein (63). The induced counter-ion cloud will help to solvate the point charges via direct electrostatic interactions; this has an overall stabilizing effect on the protein. As the solvent exposed surface area of the charged residue increases, so does the charge solvation. Therefore salts will stabilize the unfolded state of a protein to a greater extent than the folded state, since the charged residues will be completely exposed in the unfolded state. This can be rationalized using a generalized Born model (64) which characterizes the solvation energy of a charged group:

$$\frac{Aq^2}{r} \left(1 - \frac{e^{-\kappa r}}{\epsilon_s}\right) * f \quad (1-4)$$

κ is the Debye screening parameter, ϵ_s is the dielectric constant of the water, A is a unit dependent constant, q is the magnitude of the charge, r is the Born radius of the charge, and f is the fraction of the area of the charged group that is accessible by the solvent. The charged residues will interact favourably with the induced solvent counter-ion cloud, however, an unfolded protein will make the charged residues more accessible to the solvent ($f_{\text{unfolded}} > f_{\text{folded}}$), thereby strengthening their interaction with the counter-ion cloud and lowering the free energy of the unfolded state of the protein (63). While this effect will be present in the folded state as well, it will not be as strong since the exposed surface area of the charges will be much smaller, therefore it is the unfolded state that will be stabilized (63).

The second manner in which salts influence electrostatic interactions is via the dampening of charge-charge interactions between two residues, known as charge screening (65). When a pair or a group of charged residues are within a certain distance to one another, they will interact via a charge-charge interaction (65). When the residues are of a similar charge, there will be repulsion between the mirror charges. The extent of folding of a protein will influence the magnitude of the charge screening. In the case of highly charged proteins, charge screening will

stabilize the folded state of the protein to a greater extent than the unfolded state (66, 67). This is due to the fact that the charged residues are in closer proximity in the folded state than the same charged residues in the unfolded state, therefore the charge repulsion will be greater in the folded state and the dampening of the charge interactions will be more significant (67). This can be rationalized using the following formula which characterizes the strength of a charge-charge interaction:

$$B \frac{q_1 q_2}{d} \left(1 - \frac{e^{-\kappa d}}{\epsilon_s} \right) \quad (1-5)$$

where B is a constant, q_1 and q_2 are the magnitude of each charge, κ is the Debye screening parameter, ϵ_s is the dielectric constant of the water, and d is the distance between the charges (63). As the distance between the charges (d) increases, the strength of the charge-charge interaction decreases. Therefore as the protein unfolds, the distance between amino acids increases, the charge-charge interactions weaken concomitantly and so the stabilizing effect of the charge screening by the induced solvent counter-ion cloud will also diminish accordingly.

On the other hand, when a protein is neutral or has a small net charge, the charge screening will destabilize the folded state of a protein. This is because the counter-ion cloud will screen the favourable charge-charge interactions between oppositely charged residues. In other words, the favourable charge-charge interactions will be diminished and so the unfolded state will be stabilized to a greater extent than the folded state. Therefore the overall effect of charge screening is dependent on the charge distribution of the protein in question; charge screening can stabilize either the folded or unfolded state of a protein.

This is not the case for the final effect of salts on electrostatic interactions. Induced point image charges will exclusively stabilize the folded state of a protein relative to the unfolded state. Induced point image charges were first introduced in a model by Kirkwood and Tanford

(71). In this model, proteins are modeled as low-dielectric spheres with fixed embedded charges in the center. The presence of a salt on the surface of a protein will have the following effect on the electrostatics: a charge placed in a high dielectric medium (i.e. water) will induce an image charge of the same sign in a low dielectric medium (i.e. proteins). The induced mirror-image charge will destabilize the system via repulsion and adding more salt will increase this destabilization, eventually destabilizing the protein enough to cause precipitation. However, the induced mirror-image charges will destabilize both the folded state and unfolded state of a protein but to different extents (63, 72). The surface area of a protein in its unfolded state will be much larger than its folded state which will increase the destabilizing salting-out effect (72). Since the folded state of a protein has a smaller surface area, the destabilizing salting-out effect will be smaller relative to the destabilizing salting-out effect on the unfolded state (72). Hence the folded state of a protein will effectively be stabilized by induced mirror-image charges. This interaction will be explained further in chapter 4. And so electrostatic effects are simultaneously stabilizing and destabilizing, and a large portion of the work presented here investigates the different effects of various salts on protein stability via point induced image charges.

1.8 Model systems

The work presented here has made use to two separate models to study the influence of salts on the hydrophobic effect and on the conformational stability of proteins and subsequently on their combined effect on enzyme catalysis. The first model is a simple system that utilizes the quenching of the tyrosine analog phenol by the amino acid mimics acetate and formate to study salt effects on hydrophobicity. There are many distinct advantages to using these analogs over a protein as the fluorophore and an amino acid as the quencher, which will be discussed in the following section. The second model used in this work is the model enzyme ribonuclease t1

(RNase t1), whose extensive study and characterization of structure, kinetics, stability and folding pathway make it an ideal protein to study the effect of induced image charges on protein stability and activity.

1.9 Contact pair formation of phenol and acetate/formate as a simple model.

To study the effect of salts on the hydrophobic effect, I have used a simple model of two molecules whose mode of interaction is well understood. By using this simple model, I hope to eliminate any potential complicating factors that would occur if I had used proteins as the fluorophore which would have distorted the interpretation of the experimental data. The model used in this work is the contact pair formed between a phenol molecule and either an acetate or a formate molecule. A distinct advantage offered by this simple model is the fact that the fluorescent and quencher molecules do not self-associate. Acetate and formate are negatively charged and therefore any self-association is naturally ruled out. Phenol is used in very small (micromolar) concentrations, which minimizes self-association (74). Another advantage is that phenol shows considerable fluorescence at micromolar concentrations, making it an ideal substrate for quenching studies since the low concentrations make it both easy to prepare and manipulate while exhibiting a high quantum yield that makes any quenching quite evident.

The quenching of phenol by acetate/formate was first introduced by Scheraga et al. (74, 75) to determine association constants of weakly binding complexes that employed hydrogen bonding and/or hydrophobic interactions (74, 75). In their introduction of the phenol-acetate system, Scheraga et al. show that it is possible to obtain association constants for weakly associating systems using fluorescence quenching. In this work, they propose that the quenching of phenol by acetate is a diffusion-controlled mechanism due to the experimentally obtained values of the activation energy and the magnitude of the quenching rate constant (75). The

process of quenching will be discussed later in this introduction.

This model is a useful because it outlines a method to isolate the hydrophobic contribution to the standard free energy of association between a phenol molecule and a quencher. This is accomplished by subtracting the experimentally obtained free energy of association between a carboxylate acid and the free energy of association between a phenol and a formate ion. The association of acetate (and higher homologs) with phenol presumably has contributions from both a hydrogen bond between the OH group on the phenol and the carboxylate ion, and a hydrophobic interaction between the non-polar parts of phenol and the carboxylate compound. Since formate does not contain a non-polar area, it cannot interact with phenol via a hydrophobic bond. Therefore by subtracting the free energy of association of formate, which is purely due to a hydrogen bond, from that of a carboxylate homolog, which has contributions from both a hydrogen bond and a hydrophobic bond, I am able to isolate the hydrophobic contribution to the contact-pair formation. The work presented here will utilize this system to isolate the hydrophobic contribution to the association of phenol and acetate/formate in solutions of increasing concentrations of alkali chloride salts to determine the effect of salt on hydrophobicity.

1.10 Ribonuclease t1 as a model enzyme

To study the effect of salts on the conformational stability of proteins, the well understood and extensively characterized enzyme ribonuclease t1 (RNase t1) was used. RNase t1 is a globular protein made up of 104 amino acids (M_r 11,085) which was originally isolated from the bacterium *Aspergillus oryzae* (76, 77). X-ray crystallography has established that the tertiary structure of RNase t1 consists of an α -helix of 4.5 coils, three long and two short β -sheets forming an extended anti-parallel β -sheet, an additional short two-stranded anti-parallel β -sheet,

four wide loops, a dozen different turns and two disulfide bridges that connect the C- and N-terminal regions (78).

The catalytic properties of RNase t1 have also been established. It hydrolyzes phosphate diester bonds at the 3'-side of guanosine residues in single-stranded RNA molecules (77). RNase t1 preferentially cleaves at guanine residues, with nearly 1 million fold selectivity over other residues (79). A number of studies using a variety of techniques (80-83) have shown that the residues His40, His92, Glu58 and an unknown carboxylic residue are necessary for the enzyme to function properly. These key amino acids contribute to hydrolysis by using general acid-base catalysis during the two step hydrolysis of single-stranded RNA; the first step is the transesterification of a 5'-phosphoester bond to form guanosine 2'3'- phosphate terminus followed its hydrolysis to give the final 3'-phosphate product (84). The proposed mechanism of RNase t1 is shown in Figure 1-8. The enzymatic activity of RNase t1 has been extensively studied by the Steyaert (86-88) and Walz groups (79, 84, 85, 89, 90), and the kinetic parameters of this enzyme are well-established, making it an ideal model enzyme for study. Another contributing factor to RNase t1 as an ideal model enzyme is its high thermal stability. IR spectroscopy (91) along with X-ray crystallography (77), calorimetric techniques (92), and UV-vis absorbance (93) have thoroughly investigated the thermal properties of RNase t1 and the enzyme was found to be very stable, having a melting point ~50 – 60°C. documented folding pathway (94-99). The folded state of RNase t1 is stabilize by 86 intramolecular hydrogen bonds (96), a hydrophobic core that is enclosed between a long 4.5 turn.

1.11 The folding of ribonuclease t1

Perhaps the greatest advantage that RNase t1 offers as a model system is its extremely-well characterized structure, which contains an α -helix and central antiparallel β -sheet which hides

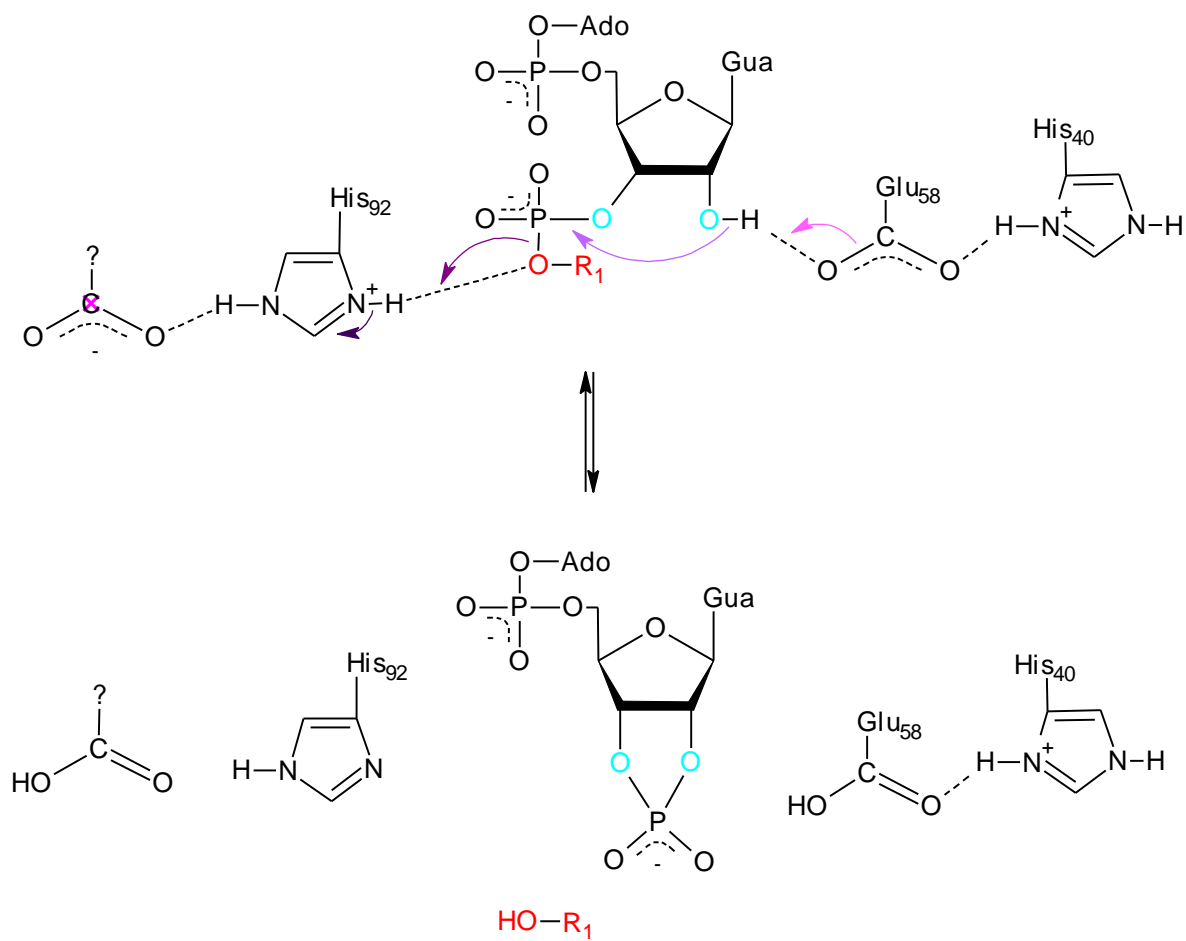


Figure 1-8. Proposed mechanism for the catalyzed transesterification of ApGpC and ApGpU.

away 85% of the hydrophobic residues (100), and two disulfide bridges (99). The intramolecular hydrogen bonds each contribute ~1.3 kcal/mol for an estimated total of 112 kcal/mol (96) to the folded state of the protein, which is very similar to the rough estimate of 98 – 132 kcal/mol contribution made by the hydrophobic effect (96). RNase t1 has two disulfide bonds linking the 2 and 10 residues, and the 6 and 103 residues which contribute a combined 7.2 – 9.3 kcal/mol contribution to the conformational stability of RNase t1 (101). Even though the melting temperature is drastically diminished (to 30 – 40°C) upon reduction of the disulfide bonds (92, 101), it is interesting to note that the enzyme retains some of its activity even when all of its disulfide bonds are reduced (101).

The folded form of the protein is more stable by 5.6 kcal/mol than the unfolded form at 25°C and pH 7.0 (97). It has been definitively shown, with the use of multiple spectroscopic techniques, that the unfolding thermodynamics of RNase t1 follows a simple two-state pathway which is completely reversible (94, 97). There are many techniques available to monitor the unfolding of RNase t1, including IR difference spectroscopy used in conjunction with FTIR (98), circular dichroism (103), differential scanning calorimetry (104) and optical rotary dispersion (97). Yet perhaps the most commonly used technique to monitor the unfolding of RNase t1 is steady-state fluorescence spectroscopy, which is the technique used in this work.

1.12 Fluorescence spectroscopy

Steady-state fluorescence spectroscopy has been used extensively to characterize the folding pathway of ribonuclease t1 (105-108). Fluorescence is one of the two types of luminescence, which describes the emission of light from any substance via an electronically excited state (20). Fluorescence is the process by which electronically excited molecules return to their original ground state by the emission of a photon, without any change in spin multiplicity (1, 109). When

a change in the spin of an excited electron is necessary to return to the ground state, the process is called phosphorescence, the second type of luminescence, which will not be discussed in this work (20).

Fluorescence is most often explained using a Jablonski diagram (Figure 1-9) which is a schematic representation of different energy levels for absorption and subsequent fluorescence or phosphorescence of any given excited molecule. The Jablonski diagram in Figure 1-9 shows three distinct electronic energy levels, S_0 (ground state), S_1 , and S_2 (excited states) each with three individual vibrational energy levels (0, 1, and 2). The vibrational energy levels are due to the vibrations of individual atoms within a molecule and are much more closely spaced than the different electronic energy levels (20, 109). Generally, molecules in their ground state (S_0) will have electrons in their lowest electronic energy level and the molecule as a whole will be located in its lowest vibrational energy level (0) (109). Electrons can be excited by light to the next

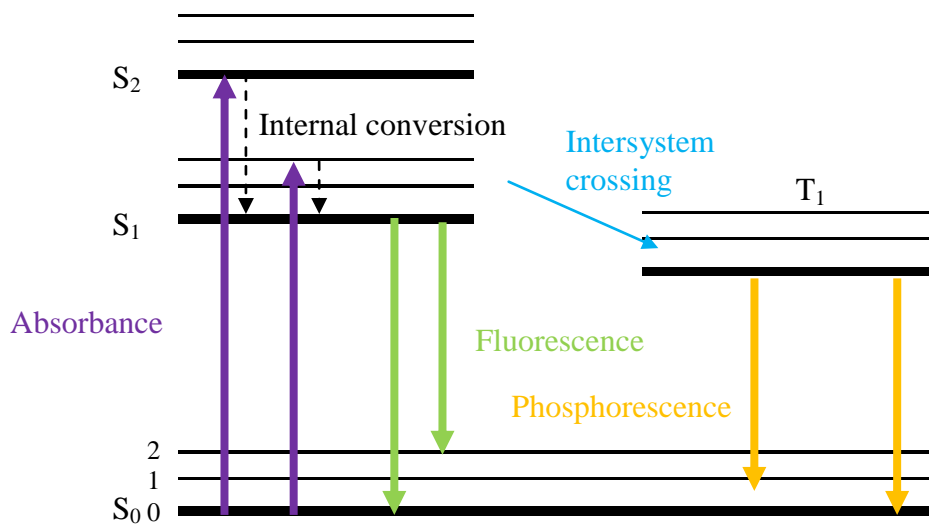


Figure 1-9. Simplified schematic of the different energy levels of a fluorescent molecule, known as a Jablonski diagram.

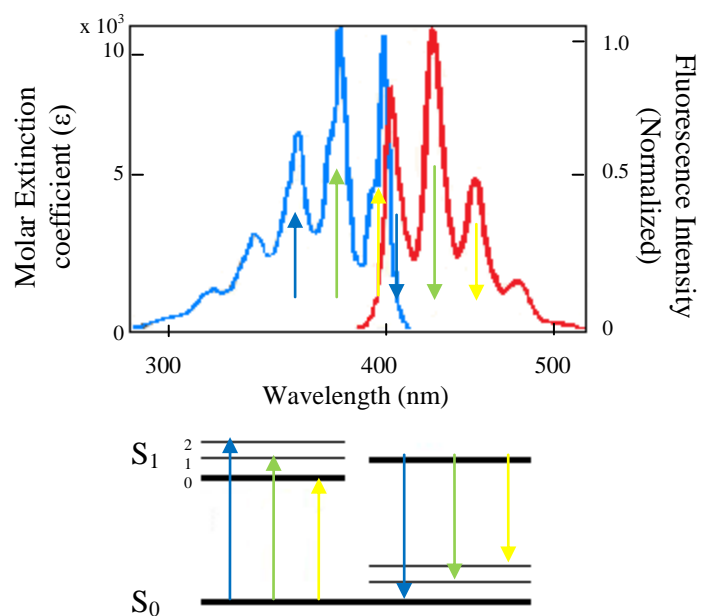


Figure 1-10. Absorbance (1st blue green and yellow arrows) and emission spectrum (blue and red respectively) (2nd blue, green and yellow arrows) of anthracene.

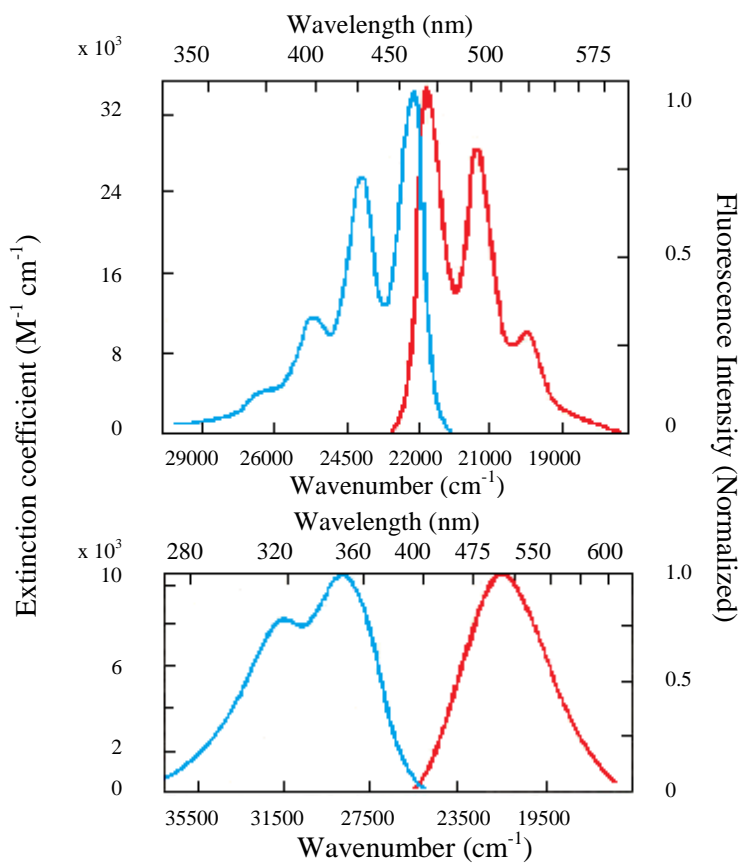


Figure 1-11. Absorbance (blue) and emission (red) spectrum of perylene (above) and quinine (below).

electronic energy level (S_1) and can then be in any of the S_1 vibrational states (20, 109).

Generally, the excited electrons will first relax to the lowest vibrational energy level very rapidly ($< 10^{-13}$ s), known as internal conversion, through the production of heat (109), and subsequently the electrons in the excited electronic energy state will relax to the ground state ($\sim 10^{-12}$ s) by emitting a photon, which is the process of fluorescence (1, 20, 109). In the majority of cases, molecules emit from their S_1 state; although there are known examples of molecules emitting from their S_2 state, they are rare and generally not found in biological settings (20). As a general example, I will compare the absorption and emission spectra of perylene and quinine, shown in Figure 1-10. The absorbance spectrum of quinine has two peaks, located at ~ 315 nm and ~ 340 nm, while the emission spectrum has only one peak at ~ 470 nm. The absorbance peak at ~ 315 nm is the quinine absorbing in the S_2 state, but there is rapid internal conversion from the excited S_2 state to the excited S_1 state and subsequent emission occurs solely from the S_1 state (20). In the case of perylene, absorbance occurs in various vibrational energy states within the S_1 state exclusively, which is why the emission spectrum is a mirror image of the absorbance spectrum (20).

The individual peaks seen in the absorbance and emission spectra of perylene are due to the excitation and subsequent relaxation of individual vibrational energy states of the molecule. This process is also illustrated by the absorbance and emission spectra of anthracene (Figure 1-11), where symmetry between the absorbance and emission spectra of anthracene is observed. Anthracene is a classic example of the mirror-image rule, which states that emission spectrum of any given molecule is typically the mirror-image of its absorption spectrum (20). This occurs because the electronic excitation does not change the nuclear geometry of an excited molecule. Therefore the spacing between the vibrational energy levels will be nearly identical in the S_0 and

S_1 states. Consequently, if the excitation of an electron from one electronic energy level to the next has a certain probability, the relaxation from said excited state to the ground state will have the same probability (20). And so the absorbance and emission spectra will be mirror-images since the probability of an electron being excited to a certain vibrational energy level is the same as that electron relaxing to its original vibrational state. The excitation of electrons to different vibrational states in different molecules and subsequent relaxations will create the individual peaks that make up the absorption and emission spectra.

To characterize the emission fluorescence of a molecule, the number of photons emitted is counted by a spectrofluorimeter, or fluorimeter. The basic layout of a fluorimeter is shown in Figure 1-12. All fluorimeters start with a lamp, usually deuterium or xenon based, to generate light at a wide range of wavelengths, followed by a monochromator which selects for light at the desired excitation wavelength. A beam splitter follows which splits the beam of light in two to

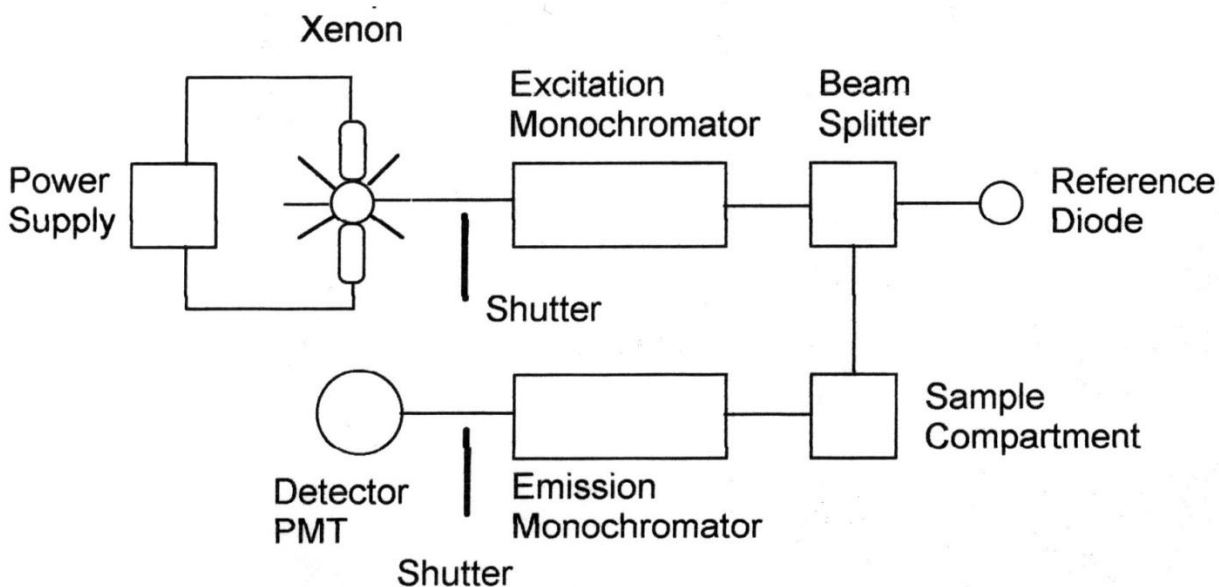


Figure 1-12. Typical arrangement of the basic components of a spectrofluorimeter.

provide a reference before the light hits the sample. Typically, the sample chamber is located at a right angle to the incident beam to minimize the amount of light detected that originated from the lamp. Once the sample fluoresces, the light travels through an emission monochromator to filter out any stray radiation and is finally registered by a detector, which is typically a photomultiplier tube (PMT) (1). The efficiency of fluorescence will be quantified by a computer system with specialized software and be converted to give the quantum yield.

The efficiency of a fluorophore is characterized mainly by two parameters, the quantum yield, (109) and the lifetime (τ) of the excited state (1, 20). The quantum yield is the fraction of photons emitted relative to the number of photons absorbed, depicted by equation 1-9a (1).

$$Q.Y. = \frac{\text{number of photons emitted}}{\text{number of photons absorbed}} \quad (1-9a)$$

$$Q.Y. = \frac{\Gamma}{\Gamma + k_{nrd}} \quad (1-9b)$$

where $Q.Y.$ is the quantum yield, Γ is the emissive rate of the fluorophore and k_{nrd} is the rate of non-radiative decay. Theoretically, the maximal quantum yield would be equal to 1, but practically most quantum yields are somewhere between 0.3 and 0.7 (109). It must be noted that most biological molecules that absorb light do not produce measurable fluorescence, they simply release their excess energy through the production of heat; this is known as non-radiative decay (20). A more accurate description of the quantum yield is shown above (equation 1.9b). In this description, all the processes responsible for the return of the molecule from the excited state to the ground state are accounted for: the emissive rate of the fluorophore (Γ) and the rate of non-radiative decay (k_{nrd}), encompassing all processes that are not the emission of photons (20). A bright fluorophore having a significant $Q.Y.$ will relax to the ground state mainly by emitting photons, i.e. $\Gamma > k_{nrd}$ (20). The quantum yield of an excited fluorophore is directly proportional to the time it spends in the excited state. The average time a fluorophore spends in the excited

state is described by the fluorescence lifetime of the fluorophore, typically denoted τ . The fluorescence lifetime can theoretically be calculated using the absorbance, extinction coefficient, and emission spectra of a fluorophore (20), or it can be measured experimentally with a sensitive photon-counting fluorimeter by exciting the molecule with short pulses of light and measuring the decay of fluorescence (1, 109). Generally, fluorescence lifetimes are on the order of 10 ns (20), but they can range from a few picoseconds to hundreds of nanoseconds (1). Measurements of fluorescence lifetimes can yield valuable information on molecular motion and the environment of the fluorophore (1).

1.13 Fluorescence in proteins

For biochemists studying proteins, the only amino acids that produce significant fluorescence are tyrosine, phenylalanine and tryptophan (1, 109). Tryptophan is the most useful fluorescent probe as it dominates the fluorescence spectrum of any given protein in the 300 – 400 nm range and its emission spectrum is extremely sensitive to the local environment (1, 20, 109). RNase t1 has a single tryptophan at the 59 position located within the protein's hydrophobic core (111), as evidenced by its crystal structure (100) and reactivity experiments (112, 113). The degree of folding of RNase t1 can be directly determined by noting the maximal emission wavelength of the fluorescence spectrum. The fluorescence spectrum of the lone tryptophan exhibits a red shift, that is to say the maximal emission peak shifts from ~320 nm to ~355 nm (Figure 1-13), upon unfolding of RNase t1. This is a result of the W59 residue leaving the hydrophobic core and being exposed to the polar solvent (114). When the W59 residue is exposed to solvent water molecules, the residue's environment becomes much more polar, which affects the fluorescence properties of the protein (115). The maximal emission wavelength of a tryptophan residue is determined by the local electric field projection along the long axis of its

indole moiety, and an increase in the local dipole of the tryptophan's environment (i.e. exposure to solvent water molecules) forces the electrons away from the pyrrole towards the benzene ring, resulting in an increase in the maximal emission wavelength (116). The work carried out here takes advantage of the enzyme's lone tryptophan and its unique fluorescence properties to examine the effect of salts on the conformational stability of RNase t1 by monitoring its unfolding via fluorescence.

1.14 Collisional quenching

Another technique often employed with the use of a fluorimeter is the phenomenon of quenching. Any process which decreases the intensity of fluorescence of any given fluorophore

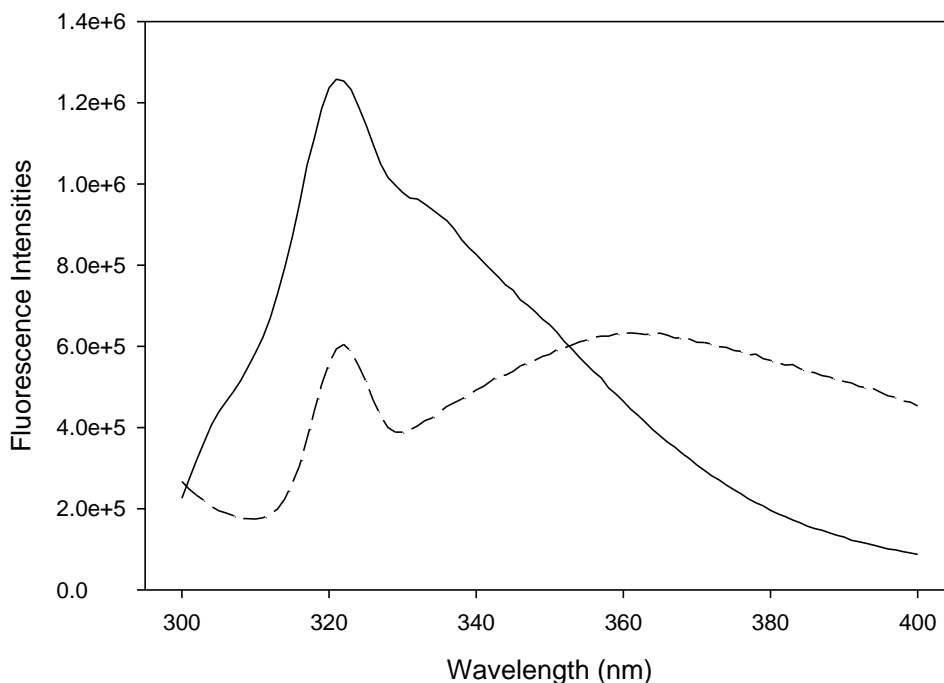


Figure 1-13. The fluorescence spectrum of RNase t1 in the folded (solid line) and unfolded (dashed line) forms, showing the Raman peak at 320nm.

is called quenching (20). Quenching occurs through two molecular mechanisms, either collisional quenching or static quenching. Collisional quenching occurs when an excited fluorophore comes into contact with a random solvent molecule (a.k.a. quencher molecule) via a diffusion-controlled encounter which subsequently returns the excited fluorophore to its ground state (1, 20). This depopulation of excited-state fluorophore decreases the emission intensity of the solution in a quencher-concentration dependent manner, shown in equation 1-10b (1). To quantify the dependence of the fluorescence on the quencher concentration, Stern-Volmer equation will be defined. This is done by dividing the quantum yields in the absence of quencher ($Q.Y._o$) and by the quantum yield in the presence of quencher ($Q.Y._q$).

$$Q.Y._o = \frac{\Gamma}{\Gamma + k_{nrd}} = \frac{\Gamma}{\frac{1}{\tau}} = \tau * \Gamma \quad (1-10a)$$

$$Q.Y._q = \frac{\Gamma}{\Gamma + k_{nrd} + k_q[Q]} = \frac{k_f}{\frac{1}{\tau} + k_q[Q]} \quad (1-10b)$$

$$\frac{Q.Y._o}{Q.Y._q} = \frac{F_0}{F} = \frac{\frac{\Gamma}{\frac{1}{\tau}}}{\frac{\Gamma}{\Gamma + k_{nrd} + k_q[Q]}} = 1 + k_q\tau[Q] = 1 + K_{SV}[Q] \quad (1-10c)$$

The relationship between the concentration of the quencher and the extent of fluorescence quenching can now be characterized by the Stern-Volmer equation:

$$\frac{F_0}{F} = (1 + K_{SV}[Q]) \quad (1-10)$$

where F_0 and F are the initial fluorescence in the absence of quencher and in any given quencher concentration respectively, K_{SV} is the Stern-Volmer constant, and $[Q]$ is the concentration of the

quencher. The Stern-Volmer constant describes the accessibility of a fluorophore to the solvent (1, 20). In the case of proteins, a low Stern-Volmer constant is indicative of a fluorophore that is buried in the core of the macromolecule and cannot be reached by polar quenchers. Conversely, a high Stern-Volmer constant indicates a fluorophore that is located on or near the surface of the macromolecule (1, 20). A linear Stern-Volmer plot is typical for collisional quenching, and the presence of non-linearity is indicative of a contribution from static quenching (110).

1.15 Static quenching

Static quenching occurs when there is a quencher molecule close to the fluorophore prior to excitation (20, 110). After excitation, the fluorophore will rapidly exchange energy with the quencher and thus immediately return to its ground state without emission of a photon (20). A nearly identical version of the Stern-Volmer equation can be obtained in the following manner to characterize static quenching. If it is assumed that the fluorophore and the quencher form a ground-state complex, the association constant for the formation of the ground-state complex will be:

$$K_a = \frac{[F-Q]}{[F][Q]} \quad (1-11a)$$

where $[F-Q]$ is the concentration of the ground-state complex, $[F]$ is the concentration of free fluorophore and $[Q]$ is the quencher concentration. The total concentration of fluorophore $[F]_o = [F] + [F-Q]$, and so it can be rearranged and inserted into equation 1-11a to obtain:

$$K_a = \frac{[F]_o - [F]}{[F][Q]} = \frac{[F]_o}{[F][Q]} - \frac{1}{[Q]} \quad (1-11b)$$

The fluorophore concentrations can be substituted for fluorescence intensities and rearranged to give equation 1-11b:

$$\frac{F_0}{F} = 1 + K_a[Q] \quad (1-11c)$$

In this case the Stern-Volmer constant is replaced by the association constant, K_a , of the ground-state complex. As is the case for collisional quenching, purely static quenching yields a linear plot (20). To distinguish between pure collisional quenching and pure static quenching, additional measurements of the fluorescence lifetimes, quenching dependence on temperature, or examination of the absorption spectra are needed (20).

1.16 Deviations from linear Stern-Volmer plots

In most cases, static quenching will contribute alongside collisional quenching. This usually results in a non-linear Stern-Volmer plot due to the fraction of fluorescence remaining (F/F_0) which is not quenched by collisional encounters and is not bound to a quencher which can be represented by:

$$\frac{F}{F_0} = f \frac{\gamma}{\gamma + k_q[Q]} \quad (1-12a)$$

Insertion of the Stern-Volmer equation ($f^{-1} = (1 + K_{SV}[Q])$) and rearrangement yields:

$$\frac{F_0}{F} = (1 + K_{SV}[Q])(1 + K_a[Q]) \quad (1-12b)$$

This modified Stern-Volmer equation now accounts for the curvature which is typically seen in Stern-Volmer plots with a significant contribution from static quenching. However, a departure from linearity does not necessarily indicate the formation of a ground-state complex. At high quencher concentrations ($> 0.25M$), there is a finite possibility that a quencher will be in the near vicinity of a fluorophore prior to excitation and if the quencher and fluorophore are not interacting directly, the following equation is needed to describe this situation (20):

$$\frac{F_0}{F} = (1 + K_{SV}[Q])\exp(V[Q]) \quad (1-13)$$

in which V is the volume of the sphere of action. When a quencher is within the sphere of action of a fluorophore during excitation, quenching will occur before the molecules can drift apart (20).

1.17 Contributions brought by thesis

The work presented here offers several conclusions that have contributed to the general knowledge of the scientific community through the publication of journal articles. These published papers were written by Dr. Mazdak Khajehpour and the author of this thesis and the content of the published papers make up the bulk of the thesis presented here. The format of this work will be a “sandwich” thesis; chapters 3, 4, and 5 are respectively based on the following published papers: “*The effect of lithium ions on the hydrophobic effect: does lithium affect hydrophobicity differently than other ions?*” (Figures are reprinted with permission from Biophysical Chemistry available online 14 February 2012. Copyright 2012 Elsevier), “*Studying salt effects on the protein stability using ribonuclease t1 as a model system*”, (Figures are reprinted with permission from Biophysical Chemistry, 2012; 161:29-38. Copyright Elsevier) and “*Probing the effects of water-water interactions on enzyme activity with salt gradients: a case study using ribonuclease t1*” (Figures are reprinted with permission from Journal of Physical Chemistry B, 2010; 114(50): 16918-28. Copyright 2010 American Chemical Society).

The conclusions presented are as follows: first, strong evidence is offered that shows that lithium does indeed affect the hydrophobic effect as should an ion with a high charge density. I propose that the lithium anomaly observed in more complex systems is due to specific interactions between lithium and hydrophobic moieties located on large macromolecules (p. 44 – 68). Second, the importance of induced point image charges when considering the effect of salt

on electrostatic interactions and how they affect the conformational stability of proteins is clearly demonstrated (p. 72 – 104). And finally, for the first time, the observed loss of enzyme activity upon addition of chloride salts is correlated with a salts ability to induce linear hydrogen bonds in the enzyme's hydration shell. This highlights the importance of the intermolecular hydrogen bonding between water molecules in the protein's hydration shell and the ability of water to influence the conformational stability of proteins (p 109 – 135).

References

1. David Whitford. Proteins structure and function. West Sussex, England: John Wiley and Sons Ltd.; 2008.
2. Mathias Gautel. The sarcomeric cytoskeleton: Who picks up the strain? *Current Opinion in Cell Biology*. 2011;23(1):39-46.
3. Hugh Kim, Christopher A. McCulloch. Filamin A mediates interactions between cytoskeletal proteins that control cell adhesion. *Federation of European Biochemical Scientists Letters*. 2011;585(1):18-22.
4. Andreea E. Radulescu, Don W. Cleveland. NuMA after 30 years: The matrix revisited. *Trends in Cell Biology*. 2010;20(4):214-22.
5. Yves Gouriou, Nicolas Demaurex, Philippe Bijlenga, Umberto De Marchi. Mitochondrial calcium handling during ischemia-induced cell death in neurons. *Biochimie*. 2011;93(12):2060-7.
6. Nicolas Tournier, Xavier Decleves, Bruno Saubamea, Jean-Michel Schermann, Salvatore Cisternino. Opioid transport by ATP-binding cassette transporters at the blood-brain barrier: Implications for neuropsychopharmacology. *Current Pharmaceutical Design*. 2011;17(26):2829-42.
7. G. Zifarelli MP. CLC transport proteins in plants. *Federation of European Biochemical Scientists Letters*. 2010;584(10):2122-7.
8. Angel Zarain-Herzberg, Jorge Fragosó-Medina, Rafael Estrada-Aviles. Calcium-regulated transcriptional pathways in the normal and pathologic heart. *International Union of*. 2011;63(10):847-55.
9. Shin'ichi Ishiwata, Yuta Shimamoto, Madoka Suzuki. Molecular motors as an auto-oscillator. *Human Frontier Science Program Journal*. 2010;4(3-4):100-4.
10. David W. Maughan. Kinetics and energetics of the crossbridge cycle. *Heart Failure Reviews*. 2005;10(3):175-85.
11. Markus Koeck, Adrienne R. Hardham, Peter N. Dodds. The role of effectors of biotrophic and hemibiotrophic fungi in infection. *Cellular Microbiology*. 2011;13(12):1849-57.
12. Tamara Hewavitharana, Philip B. Wedegaertner. Non-canonical signalling and localizations of heterotrimeric G proteins. *Cellular Signalling*. 2012;24(1):25-34.
13. Laurens Pauwels AG. The JAZ proteins: A crucial interface in the jasmonate signalling cascade. *Plant Cell*. 2011;23(9):3089-100.
14. Thomas Christian, Georges Lahoud, Cuiping Liu, Ya-Ming Hou. Control of catalytic cycle by a pair of analogous tRNA modification enzymes. *Journal of Molecular Biology*. 2010;400(2):204-17.
15. Wei-chung Liu, Wen-hsien Lin, Andrew J. Davis, Ferenc Jordan, Hsihte Yang, Ming-jing Hwang. A network perspective on the topological importance of enzymes and their phylogenetic conservation. *BMC Bioinformatics*. 2007;8.

16. Susan M. Aitken, Jack F. Kirsch. The enzymology of cystathionine biosynthesis: Strategies for the control of substrate and reaction specificity. *Archives of Biochemistry and Biophysics*. 2005;433(1):166-75.
17. Amroyan E., Gabrielian E., Panossian A., Wilkman G., Wagner H. Inhibitory effect of andrographolide from *andrographis paniculata* on PAF-induced platelet aggregation. *Phytomedicine: international journal of phytotherapy and phytopharmacology*. 1999;6(1):27-31.
18. Liqun Huang, Gerardo G. Mackenzie, Yu Sun, Nengtai Ouyang, Gang Xie, Kvetoslava Vrankova, Despina Komninou, Basil Rigas. Chemotherapeutic properties of phospho-nonsteroidal anti-inflammatory drugs, a new class of anticancer compounds. *Cancer Research*. 2011;71(24):7617-27.
19. Nick C Pace, Bret A Shirley, Marsha Mcnutt, Ketan Gajiwala. Forces contribution to the conformational stability of proteins. *The Journal of the Federation of American Societies for Experimental Biology*. 1996;10(1):75.
20. Joseph R. Lakowicz. Principles of fluorescence spectroscopy, 3rd edition. *Analytical and Bioanalytical Chemistry*. 2008;390(5):1223-4.
21. Jia-Feng Yu, Xiao Sun, Ji-Hua Wang. A novel 2D graphical representation of protein sequence based on individual amino acid. *International Journal of Quantum Chemistry*. 2011;111(12):2835-43.
22. Christian B. Anfinsen. Principles that govern the folding of protein chains. *Science*. 1973;181(4096):223-30.
23. D. Philippe, A. Ababou, X. Yang, R. Ghosh, T. Daviter, J.E. Ladbury, M. Pfuhl. Making ends meet: The importance of the N- and C- termini for the structure, stability, and function of the third SH3 domain of CIN85. *Biochemistry*. 2011;50(18):3649-59.
24. Matthew J. Whitley, Jun Zhang, Andrew L. Lee. Hydrophobic core mutations in CI2 globally perturb fast side-chain dynamics similarly without regard to position. *Biochemistry*. 2008;47(33):8566-76.
25. A.R. Lam, J. Jiang, S. Mukamel. Distinguishing amyloid fibril structures in Alzheimer's disease (AD) by two-dimensional (2DUV) spectroscopy. *Biochemistry*. 2011;50(45):9809-16.
26. Jan Bieschke, Jenny Russ, Ralf P. Friedrich, Dagmar E. Ehrnhoefer, Heike Wobst, Katja Neugebauer, Erich E. Wanker. EGCG remodels mature α -synuclein and amyloid- β fibrils and reduces cellular toxicity. *Proceedings of the National Academy of Sciences of the United States of America*. 2010;107(17):7710-5.
27. Cristina Airoidi, Erika Sironi, Barbara La Ferla, Francisco Cardona, Francesco Nicotra. A β monomers, oligomers and fibrils: Structural features. *Current Bioactive Compounds*. 2011;7(3):198-213.
28. Bruno Berra SR. Carbohydrate, protein and lipid metabolism in the skin; biochemical and molecular aspects. *NATO ASI Series*. 1990;181:37-52.
29. Rong-Jin Guan, Ye Xiang, Xiao-Lin He, Chun-Guang Wang, Miao Wang, Ying Zhang, Eric J. Sundberg, Da-Cheng Wang. Structural mechanism governing the cis and trans isomeric states and an

intramolecular switch for cis/trans isomerization of a non-proline peptide bond observed in crystal structures of scorpion toxins. *Journal of Molecular Biology*. 2004;341(5):1189-204.

30. Mythrei Kavanoor, Maurice R. Eftink. Characterization of the role of side-chain interactions in the binding of ligands to apo trp repressor: PH dependence studies. *Biophysical Chemistry*. 1997;66(1):43-55.

31. Guido di Prisco, Joseph T. Eastman, Daniela Giordano, Elio Parisi, Cinzia Verde. Biogeography and adaptation of notothenioid fish: Hemoglobin function and globin-gene evolution. *Gene*. 2007;398(1-2):143-55.

32. Frank H. Stillinger. Water revisited. *Science*. 1980;209(4455):4455-457.

33. Ken A. Dill, Thomas M. Truskett, Vojko Valchy, Barbara Hribar-Lee. Modeling water, the hydrophobic effect, and ion solvation. *Annual Review of Biophysics and Biomolecular Structur*. 2005;34:173-99.

34. S. Scheiner. Hydrogen bonding. A theoretical perspective. Oxford University Press; 1997.

35. G.A. Jeffrey. An introduction to hydrogen bonding. Oxford University Press; 1997.

36. G.R. Desiraju TS. The weak hydrogen bond. Oxford University Press; 1999.

37. G.C. Pimentel ALM. The hydrogen bond. San Fransisco: W.H. Freeman and Co.; 1960.

38. A.D. Buckingham, J.E. Del Bene, S.A.C. McDowell. The hydrogen bond. *Chemical Physics Letters*. 2008;463(1-3):1-10.

39. Kim A. Sharp, J.M. Vanderkooi. Water in the half shell: Structure of water, focusing on angular structure and solvation. *Accounts of Chemical Research*. 2010;43:231-9.

40. Kim A. Sharp, Bhupinder Madan. Hydrophobic effect, water structure, and heat capacity changes. *The Journal of Physical Chemistry B*. 1997;101:4343.

41. Nathaniel V. Nucci, Jane M. Vanderkooi. Effects of salt on the Hofmeister series on the hydrogen bond network of water. *Journal of Molecular Liquids*. 2008;143:160-70.

42. Norbert Muller. Is there a region of highly structured water around a nonpolar solute molecule? *Journal of Solution Chemistry*. 1988;17(7):661-72.

43. Giuseppe Graziano BL. On the intactness of hydrogen bonds around nonpolar solutes dissolved in water. *Journal of Physical Chemistry*. 2005;109:8103-7.

44. B. Lee GG. A two-state model of hydrophobic hydration that produces compensating enthalpy and entropy changes. *Journal of the American Chemical Society*. 1996;118(22):5163-8.

45. Giuseppe Graziano. On the temperature dependence of hydration thermodynamics for noble gases. *Physical Chemistry Chemical Physics*. 1999;1(8):1877-86.

46. Giuseppe Graziano. Hydration thermodynamics of aliphatic alcohols. *Physical Chemistry Chemical Physics*. 1999;1(15):3567-76.
47. Giuseppe Graziano. On the heat-capacity change of pairwise hydrophobic interactions. *Journal of Chemical Physics*. 2005;123(3):034509/1,034509/4.
48. George E. Walrafen. Raman spectral studies of the effects of temperature on water structure. *Journal of Chemical Physics*. 1967;47(1):114-26.
49. Tatsujiko Kawamoto, Shukichi Ochiai, Hiroyuki Kagi. Changes in the structure of water deduced from the pressure dependence of the raman OH frequency. *Journal of Chemical Physics*. 2004;120(13):5867-70.
50. S.A. Corcelli JLS. Infrared and raman line shapes of dilute HOD in liquid H₂O and D₂O from 10 to 90°C. *Journal of Physical Chemistry A*. 2005;109(28):6154-65.
51. C.I. Ratcliffe DEI. Vibrational spectral studies of solutions at elevated temperatures and pressures. 5. raman studies of liquid water up to 300°C. *Journal of Physical Chemistry*. 1982;86(25):4897-905.
52. Kim A. Sharp, Bhupinder Madan, Eric Manas, Jane M. Vanderkooi. Water structure changes induced by hydrophobic and polar solutes revealed by simulations and infrared spectroscopy. *Journal of Phy*. 2001;114(4):1791-6.
53. Nathan J. Scott, Nathaniel V. Nucci, Jane M. Vanderkooi. Changes in water structure induced by the guanidinium cation and implications for protein denaturation. *The Journal of Physical Chemistry A*. 2008;112(43):10939-48.
54. Jane M. Vanderkooi, Jennifer L. Dashnau, Bogumil Zelent. Temperature excursion infrared (TEIR) spectroscopy used to study hydrogen bonding between water and biomolecules. *Methods in Protein Structure and Analysis*. 2007;Pt. B:248-.
55. G. Wilse Robinson, C.H. Cho. Role of hydration water in protein unfolding. *Biophysical Journal*. 1999;77:3311-8.
56. Philippa M. Wiggins. Hydrophobic hydration, hydrophobic forces and protein folding. *Physica A: Statistical Mechanics and Its Applications*. 1997;238(1-4):113-28.
57. Kelly R. Gallagher, Kim A. Sharp. A new angle on heat capacity changes in hydrophobic solvation. *Journal of the American Chemical Society*. 2003;125(23):9853-60.
58. Barbara Hribar, Noel T. Southhall, Vojko Vlachy, Ken A. Dill. How ions affect the structure of water. *Journal of the American Chemical Society*. 2002;124(41):12302-11.
59. W. Kauzmann. Some factors in the interpretation of protein denaturation. *Advances in Protein Chemistry*. 1959;14:1-63.
60. Ken A Dill. Dominant forces in protein folding. *Biochemistry*. 1990;29(31):7133.
61. T. E. Creighton. *Proteins, structure and molecular principles*. New York: W.H. Freeman; 1984.

62. Charles Tanford. How protein chemists learned about the hydrophobic factor. *Protein Science*. 1997;6:1358-66.
63. Daniel S. Spencer, Ke Xu, Timothy M. Logan, Huan-Xing Zhou. Effects of pH, salt and macromolecular crowding on the stability of KF506-binding protein: An integrated experimental and theoretical study. *Journal of Molecular Biology*. 2005;351(1):219-32.
64. Jayashree Srinivasan, Megan W. Trevathan, Paul Beroza, David A. Case. Application of a pairwise generalized born model to proteins and nucleic acids. inclusion of salt effects. *Theoretical Chemistry Accounts*. 1999;101(6):426-34.
65. Raul Perez-Jimenez, Raquel Godoy-Ruiz, Beatriz Ibarra-Molero, Jose M Sanchez-Ruiz. The efficiency of different salts to screen charge interactions in proteins: A hofmeister effect? *Biophysical Journal*. 2004;86(4):2414-29.
66. C. Nick Pace, Roy W. Alston, Kevin L. Shaw. Charge-charge interactions influence the denatured state ensemble and contribute to protein stability. *Protein Science*. 2000;9(7):1395-8.
67. S. Dao-pin, E. Soderlind, W.A. Baase, J.A. Wozniak, U. Sauer, B.W. Matthews. Cumulative site-directed charge-change replacements in bacteriophage T4 lysozyme suggest that long-range electrostatic interactions contribute little to protein stability. *Journal of Molecular Biology*. 1991;221(3):873-87.
68. Vakhtang V. Loladze, George I. Makhatadze. Energetics of charge-charge interactions between residues adjacent in sequence. *PROTEINS: Structure, Function, and Bioinformatics*. 2011;79(12):3494-9.
69. Saul R. Trevino, Kuppan Gokulan, Stephanie Newsom, Richard L. Thurlkill, Kevin L. Shaw, Vladimir A. Mitkevich, Alexander A. Makarov, James C. Sacchettini, J. Martin Scholtz, C. Nick Pace. Asp79 makes a large, unfavourable contribution to the stability of RNase sa. *Journal of Molecular Biology*. 2005;354(4):967-78.
70. Alexey V. Gribenko, Mayank M. Patel, Jiajing Liu, Scott A. McCallum, Chunyu Wang, George I. Makhatadze. Rational stabilization of enzymes by computational redesign of surface charge-charge interactions. *Proceedings of the National Academy of Sciences of the United States of America*. 2009;106(8):2601-6.
71. John G. Kirkwood. Acid-base equilibrium in solutions of ampholytes. *Annals of the New York Academy of Sciences*. 1941;41:321-8.
72. Huan-Xiang Zhou. Interactions of macromolecules with salt ions: An electrostatic theory for the Hofmeister effect. *Proteins: Structure, Function, and Bioinformatics*. 2005;61:69-78.
73. Charles Tanford, John G. Kirkwood. Theory of protein titration curves. I. general equations for impenetrable spheres. *Journal of the American Chemical Society*. 1957;79(20):5333-9.
74. Donald K. Kunimitsu, Young A. Woody, Evelyn R. Stimson, Harold A. Scheraga. Thermodynamic data from fluorescence spectra. II. hydrophobic bond formation in binary complexes. *Journal of Physical Chemistry*. 1968;69(9):2960-866.

75. A. Young Moon, Douglas C. Poland, Harold A. Scheraga. Thermodynamic data from fluorescence spectra. I. the system phenol-acetate. *Journal of Physical Chemistry*. 1965;69(9):2960-6.
76. C. Nick Pace, Gerald R. Grimsley. Ribonuclease t1 is stabilized by cation and anion binding. *Biochemistry*. 1988;27:3242-6.
77. Kohki Ishikawa, Ei-ichiro Suzuki, Masaru Tanokura, Kenji Takahashi. Crystal structure of ribonuclease t1 carboxymethylated at Glu58 in complex with 2'-GMP. *Biochemistry*. 1996;35(25):8329-34.
78. José Martinez-Oyanedel, Hui-Woog Choe, Udo Heinemann, Wolfram. Ribonuclease t1 with free recognition and catalytic site: Crystal structure analysis at 1.5 Å resolution. *Journal of Molecular Biology*. 1991;222:335-52.
79. Charissa Libertin, Harry L. Osterman, Frederick G. Walz Jr. Base-group specificity at the primary recognition site of ribonuclease t1 for minimal RNA substrates. *Archives of Biochemistry and Biophysics*. 1979;195(1):95-102.
80. K. Takahashi SM. *The enzymes*. New York: Academic Press Inc.; 1982.
81. S. Nishikawa, H. Morioka, H.J. Kim, K. Fuchimura, T. Tanaka, S. Uesugi, T. Hakoshima, K. Tomita, E. Ohtsuka, M. Ikehara. Two histidine residues are essential for ribonuclease T1 activity as is the case for ribonuclease A. *Biochemistry*. 1987;26(26):8620-4.
82. Fuyuhiko Inagaki, Yoshi Kawano, Ichio Shimada, Kenji Takahashi, Tatsuo Miyazawa. Nuclear magnetic resonance study on the microenvironments of histidine residues of ribonuclease t1 and carboxymethylated ribonuclease t1. *Journal of Biochemistry*. 1981;89(4):1185-95.
83. Udo Heinemann WS. Specific protein-nucleic acid recognition in ribonuclease t1-2'-guanylic acid complex: An x-ray study. *Nature*. 1982;299(5878):27-31.
84. Kapil Kumar, Frederick G. Walz Jr. Probing functional perfection in substructure of ribonuclease t1: Double combinatorial random mutagenesis involving Asn43, Asn44, and Glu46 in the guanine binding loop. *Biochemistry*. 2001;40(12):3748-57.
85. Harry L. Osterman, Frederick G. Walz Jr. Subsite interactions and ribonuclease t1 catalysis: Kinetic studies with ApGpC and ApGpu. *Biochemistry*. 1979;18(10):1984-8.
86. Jan Steyaert, Abdel Fattah Haikal, Lode Wyns, Patrick Stanssens. Subsite interactions of ribonuclease t1: Viscosity effects indicate that the rate-limiting step of GpN transesterification depends on the nature of N. *Biochemistry*. 1991;30(35):8661-5.
87. Jan Steyaert, Chris Opsomer, Lode Wyns, Patrick Stanssens. Quantitative analysis of the contribution of Glu46 and Asn98 to the guanosine specificity of ribonuclease t1. *Biochemistry*. 1991;30(2):494-9.
88. Jan Steyaert, Klaas Hallenga, Lode Wyns, Patrick Stanssens. Histidine-40 of ribonuclease t1 acts as base catalyst when the true catalyst base, glutamic acid-58, is replaced by alanine. *Biochemistry*. 1990;29(38):9064-72.

89. Frederick G. Walz Jr. Studies on the nature of guanine nucleotide binding with ribonuclease t1. *Biochemistry*. 1977;16(25):5509-15.
90. Michael Zabinski, Frederick G. Walz Jr. Subsites and catalytic mechanism of ribonuclease t1: Kinetic studies using GpC and GpU as substrates. *Archives of Biochemistry and Biophysics*. 1976;175(2):558-64.
91. Heinz Fabian, Christian Schultz, Jan Backman, Ulrich Hahn, Wolfram Saenger, Henry H. Mantsch, Dieter Naumann. Impact of point mutations on the structure and thermal stability of ribonuclease t1 in aqueous solution probed by fourier transform infrared spectroscopy. *Biochemistry*. 1994;33(35):10725-30.
92. Matthias F. Haun, Matthias Wirth, Heinz Rueterjans. Calorimetric investigation of thermal stability and ligand-binding characteristics of disulfide-bond-cleaved ribonuclease t1. *European Journal of Biochemistry*. 1995;227(1/2):516-23.
93. Thomas Kiefhaber, Franz Xaver Schmid, Michael Renner, Hans Juergen Hinz, Ulrich Hahn, Rainer Quaas. Stability of recombinant lys-25 ribonuclease t1. *Biochemistry*. 1990;29(36):8250-7.
94. Thomas Kiefhaber, Rainer Quaas, Ulrich Hahn, Franz X. Schmid. Folding of ribonuclease t1. 1. existence of multiple unfolded states created by proline isomerization. *Biochemistry*. 1990;29:3053-61.
95. Thomas Kiefhaber, Rainer Quaas, Ulrich Hahn, Franz X. Schmid. Folding of ribonuclease t1. 2. kinetic models for the folding and unfolding reactions. *Biochemistry*. 1990;29:3061-70.
96. Bret A. Shirley, Patrick Stanssens, Ulrich Hahn, C. Nick Pace. Contribution of hydrogen bonding to the conformational stability of ribonuclease t1. *Biochemistry*. 1992;31:725-32.
97. James A. Thomas, Bret A. Shirley, Gerald R. Grimsley, C. Nick Pace. Conformational stability and mechanism of folding of ribonucleae t1. *Journal of Biological Chemistry*. 1989;264(20):11614-20.
98. Ralf Moritz, Diane Reinstäler, Heinz Fabian, Dieter Naumann. Time-resolved FTIR difference spectroscopy as tool for investigating refolding reactions of ribonuclease T1 synchronized with trans-cis prolyl isomerization. *Biopolymers*. 2002;67(3):145-55.
99. C. Nick Pace, T.E. Creighton. The disulphid folding pathway of ribonuclease t1. *Journal of Molecular Biology*. 1986;188:477-86.
100. Arni Raguvir, Udo Heinemann, Ryoji Tokuoka, Wolfram Saenger. Three-dimensional structure of the ribonuclease t1*2'-GMP complex at 1.9-Å resolution. *Journal of Biological Chemistry*. 1988;263(30):15358-68.
101. C. Nick Pace, Gerald R. Grimsley, James A. Thomson, Ben J. Barnett. Conformational stability and activity of ribonuclease t1 with zero, one, and two intace disulfide bonds. *Journal of Biological Chemistry*. 1988;24(25):11820-5.
102. Thmoas Schindler, Lorenz M. Mayr, Olfert Landt, Ulrich Hahn, Franz X. Schmid. The role of a *trans*-proline in the folding mechanism of ribonuclease t1. *European Journal of Biochemistry*. 1996;241:516-24.

103. Motohisa Oobatake, Sho Takahashi, Tatsuo Ooi. Conformational stability of ribonuclease t1. II. salt-induced renaturation. *Journal of Biochemistry*. 1979;86(1):65-70.
104. I.M. Plaza del Pino, C. Nick Pace, E. Freire. Temperature and guanidine hydrochloride dependence of the structural stability of ribonuclease t1. *Biochemistry*. 1992;31(45):11196-202.
105. Lorenz M. Mayr, Olfert Landt, Ulrich Hahn, Franz X. Schmid. Stability and folding kinetics of ribonuclease t1 are strongly altered by the replacement of cis-proline 39 with alanine. *Journal of Molecular Biology*. 1993;231(3):897-912.
106. Margherita Ruoppolo, Robert B. Freedman. Refolding by disulfide isomerization: The mixed disulfide between ribonuclease t1 and glutathione as a model refolding substrate. *Biochemistry*. 1995;34(29):9380-8.
107. Jason L. Johnson, Frank M. Raushel. Influence of primary sequence transpositions on the folding pathways of ribonuclease t1. *Biochemistry*. 1996;35(31):10223-33.
108. Cui-Qing Hu, Julian M. Sturtevant, James A. Thomson, Rick E. Erickson, C. Nick Pace. Thermodynamics of ribonuclease t1 denaturation. *Biochemistry*. 1992;31(20):4876-82.
109. Gordon G. Hammes. *Physical chemistry for the biological sciences*. Hoboken, New Jersey: John Wiley and Sons, Inc.; 2007.
110. S.E. Webber. The role of time-dependent measurements in elucidating static versus dynamic quenching processes. *Photochemistry and Photobiology*. 1997;65(1):33-8.
111. M.C. Shastry MRE. Reversible thermal unfolding of ribonuclease t1 in reverse micelles. *Biochemistry*. 1996;35(13):4094-101.
112. Kenji Takahashi. Structure and function of ribonuclease t1. VIII. reaction of 2-hydroxy-5-nitrobenzyl bromide with the single tryptophan residue in ribonuclease t1. *Journal of Biochemical and Biophysical Methods*. 1970;67(4):541-7.
113. Seiichi Kawashima TA. Oxidation with N-bromosuccinimide of the single tryptophan residue in ribonuclease t1. *International Journal of Protein Research*. 1969;1(3):185-92.
114. Thomas Kiefhaber, Franz Xaver Schmid, Kathrien Willaert, Yves Engelborghs, Alain Chaffotte. Structure of a rapidly forming intermediate in ribonuclease t1 folding. *Protein Science*. 1992;1(9):1162-72.
115. Daniel W. Pierce, Steven G. Boxer. Stark effect spectroscopy of tryptophan. *Biophysical Journal*. 1995;68(4):1583-91.
116. Patrik R. Callis, Berit K. Burgess. Tryptophan fluorescence shifts in proteins from hybrid simulations: An electrostatic approach. *Journal of Physical Chemistry B*. 1997;101(46):9429-32.

Chapter 2

Materials and Methods

2.1 Chapter 3

2.1.1 Materials. Lithium chloride and sodium acetate were purchased from Fisher Scientific (Fair Lawn, NJ); lithium formate was purchased from GFS Chemicals Inc. (Columbus, OH); lithium acetate, sodium formate and sodium chloride were purchased from Sigma (St-Louis, MO); rubidium chloride, rubidium acetate and rubidium formate were respectively purchased from Alfa Aesar (Ward Hill, MA), Strem Chemicals (New Bury Port, MA) and Science Lab Inc. (Houston, TX). Phenol was purchased from Baker Chemical Co. (Phillipsburg, NJ).

2.1.2 Methods. All experiments were performed in 10 mM bis-tris purchased from Sigma (St-Louis, MO) at pH 7.0. The concentration of phenol in all samples is 200 μ M. Steady-state fluorescence measurements were carried out on a Varian Cary Eclipse Fluorescence Spectrophotometer (Figure 2-1) in a in a 10 x 3 mm² quartz cuvette at room temperature (23.5°C).

A series of samples for one cation (i.e. lithium, sodium, potassium, or rubidium) was prepared in triplicate in the morning and data was collected in the afternoon of the same day. To prepare the 1 mL samples, a concentrated stock solution of phenol, a concentrated stock solution of the acetate salt and a concentrated stock solution of the formate salt were all prepared on the day of the experiment and mixed to give the final concentrations shown (Table 2-1). The same stock solutions were used for the preparation of all the samples in a single series and fresh phenol stock solutions were prepared for every cation. All 1 mL samples were prepared in triplicate.

The fluorescence data were collected using an excitation wavelength set to 270 nm, and the excitation and emission slits were set to 5 nm band pass resolution. Quenching studies were performed by monitoring the changes in fluorescence intensity at the maximum emission of 297

nm as a function of quencher concentration and fitting to the linear Stern-Volmer equation.

2.2 Chapter 4

2.2.1 Materials. Ribonuclease t1 (RNase t1) solution in 2.8M ammonium sulfate was purchased from Worthington Biochemical Corporation (Lakewood, NJ). Guanylyl-5'-monophosphate (5'-GMP), guanylyl-3'-5'-cytidine (GpC), acrylamide and *N*-acetyl-L-tryptophanamide (NATA) were purchased from Sigma (St. Louis, MO). All experiments were performed in pH 5.5 bis-tris buffer from Sigma (St. Louis, MO). All of the salts were purchased from Fisher Scientific (Fair Lawn, NJ).

2.2.2 Dialysis. To eliminate the effect of the ammonium sulfate in the storage solution, the RNase t1 was dialyzed prior to use for kinetic and fluorimetric assays. To begin, the dialysis tape (MWCO= 6,000- 8,000), purchased from Spectrum Laboratories, Inc. (Rancho Dominguez, CA), was boiled in two separate 500 mL volumes of ddH₂O for 5 minutes each to remove any impurities present on the tape. The dialysis tape was finally rinsed in fresh ddH₂O. To determine the appropriate length to use, the ruler on the package of the dialysis tape was used and ~5 cm was added to allow room for the clips. One side of the tape was closed with a clip and the sample of RNase t1 was added using the 5 mL pipette. The second end of the dialysis tape was then closed with a second clip making sure to leave enough tape past the clip to be able to open the bag at the end of the dialysis without spilling any of the enzyme solution.

The RNase t1 solution was placed in 1L of a dialysis buffer (10mM bis-tris, 10mM NaCl pH 5.5) for 1 hour at 4°C. This was repeated twice in fresh buffer each time for a total of 3 x 1 hour of dialysis in 3 x 1 L volumes of buffer. To ensure that the clips held throughout the dialysis, the dialysis tape was checked on periodically. If the clips released or the dialysis tape tore, re-concentration of the protein through centrifugation would be necessary to recover the

enzyme. To verify the effect of dialysis on enzyme activity, kinetic measurements were taken prior to use as described in the next paragraph, the results were then compared to fresh, non-dialyzed enzyme, which was used as a standard. Dialysis had no deleterious effect on enzyme activity.

2.2.3 UV-vis Spectroscopy. Kinetic measurements were performed using a Thermo Scientific Helios Zeta UV-Vis spectrophotometer (Dubuque, IA) in a 10 x 10mm² quartz cuvette (Figure 2-2). The samples were thermostatically controlled at 25°C by a Jeio-Tech refrigerating bath circulator (Des Plaines, IL). The specificity constant was determined according to the Walz methodology (1). Specifically, RNase t1 was added to a 2.5mL sample containing 10µM GpC at pH 5.5, the solution was mixed by using a pipette set to 100 uL, and the change in absorbance was monitored at 280nm. The enzyme solution and all GpC solutions were kept on ice throughout the entire experiment until needed. The enzyme cleaves the dinucleotide causing an increase in absorbance at 280nm. The trace was then plotted to equation 2-1 using Sigma Plot (Point Richmond, CA) software.

Since the concentration of GpC used is 1/20th that of its K_M value (220µM) (2), the Michaelis-Menton equation can be reduced to the mono-exponential equation 2-1 (3):

$$k = \frac{V_{max} [S]}{K_M + [S]}$$

Since $[S] \ll K_M$

$$k = \frac{V_{max}}{K_M}$$

And $V_{max} = \{E\}k_{cat}$, we can rewrite the Michaelis-Menten equation as the following mono-exponential:

$$A = A_0 + B(1 - e^{-kt}); \quad k = \frac{\{E\}k_{cat}}{K_M} \quad (2 - 1)$$

where k_{cat} and K_M are the Michaelis-Menton parameters, and A_0 and B are fitting constants.

2.2.4 Fluorescence Spectroscopy. Steady-state fluorescence spectra were measured on a Fluorolog-3 Horiba Jobin Yvon spectrofluorimeter (Edison, NJ) in a 10 x 10mm² quartz cuvette (Figure 2 – 3). The samples were thermostatically controlled at 25°C by a Jeio-Tech refrigerating bath circulator (Des Plaines, IL). The data were analyzed using Sigma Plot (Point Richmond, CA) software. Since the 5'-GMP has significant absorbance at high concentrations (4), fluorescence spectra reported have been corrected for inner filter effects (5) using the following equation:

$$F_{\text{corr}} = 10^{\frac{\text{OD}_{x\text{nm}}}{2}} * F_{x\text{nm}} \quad (2-2)$$

where $F_{x\text{nm}}$ is the fluorescence obtained from a given excitation wavelength, $\text{OD}_{x\text{nm}}$ is the optical density of the solution at the excitation wavelength, and F_{corr} is the corrected fluorescence (5).

2.3 Chapter 5

2.3.1 Materials. RNase t1 solution in 2.8M ammonium sulfate was purchased from Worthington Biochemicals Corporation (Lakewood, NJ). Urea (ultragrade) was purchased from Sigma (St-Louis, MO). All experiments were performed at pH 7.0 in 10mM bis-tris purchased from Sigma (St-Louis, MO). All salts were purchased from Fisher Scientific (Fair Lawn, NJ). To eliminate the effect of the ammonium sulfate in the storage solution, the enzyme was dialyzed as described previously. To verify the quality of the enzyme, activity measurements were made prior to its use, as described previously, the results were then compared to fresh non-dialyzed enzyme which was used as a standard.

2.3.2 Fluorescence spectroscopy. Steady-state fluorescence spectra were measured on a

Fluorolog-3 Horiba Jobin Yvon spectrofluorometer (Edison, NJ) in a 10 x 3 mm² quartz cuvette at room temperature (Figure 2-3). All measurements were made at pH 7.0 in 10mM bis-tris buffer. The data was analyzed with Sigma Plot (Point Richmond, CA). The samples were excited at 290nm, the excitation and emission slits were set to a 4nm bandpass.

2.3.3 Measurements of protein unfolding free energy. The unfolding free energy was measured by urea denaturation following the technique of Pace et al (6). A separate series of 1mL samples with a final concentration of 0.2 uM RNase t1, were prepared individually for each concentration of urea and salt. Every sample was prepared in triplicate for each given concentration of urea and salt. To prepare the 1 mL samples, concentrated stock solution of urea, salt, and enzyme were prepared individually in 10 mM bis-tris buffer at pH 7.0. The stock urea was prepared by adding the urea to a specific amount of water using the following ratio (6):

$$V_{ddH_2O} = \frac{mass_{urea}}{1.103 \text{ g}_{urea}/\text{ml}_{water}} \quad (2-3)$$

To facilitate the dissolution of urea, the solution was heated lightly until clear. The concentration of the stock urea was measured by its refractive index on an 115V Refractometer from Fisher Scientific (6). The final 1 mL samples were then allowed to stand overnight to allow adequate time for protein unfolding.

The extent of protein unfolding was measured by fluorescence, specifically by monitoring the change in the ratio of the emission intensities at 350nm (F_{350}) and 330nm (F_{330}). This ratio was then plotted as a function of the urea concentration to yield protein unfolding curves. The thermodynamic folding parameters were determined using the method of Bolen and Santoro (7), by fitting the data via a non-linear square minimization using the software Curve Expert (Chattanooga, TN) to equation 2-4:

$$\frac{F_{330}}{F_{350}} = y = \frac{y_f + m_f[\text{urea}] + (y_u + m_u[\text{urea}]) \exp\left(\frac{\Delta G_{\text{unfolding}}^0 - m[\text{urea}]}{RT}\right)}{1 + \exp\left(\frac{\Delta G_{\text{unfolding}}^0 - m[\text{urea}]}{RT}\right)} \quad (2-4)$$

Where y_f and m_f , y_u and m_u are the slope and intercept of the pre- and post-transitional baselines, $[\text{urea}]$ is the urea concentration and $\Delta G_{\text{unfolding}}^0$ is the standard free energy of unfolding in the absence of urea and m is a measure of the dependence of $\Delta G_{\text{unfolding}}^0$ on urea concentration.



Figure 2 – 1. Varian Cary Eclipse Fluorescence Spectrophotometer.



Figure 2 – 2. Thermo Scientific Helios Zeta UV-Vis spectrophotometer.

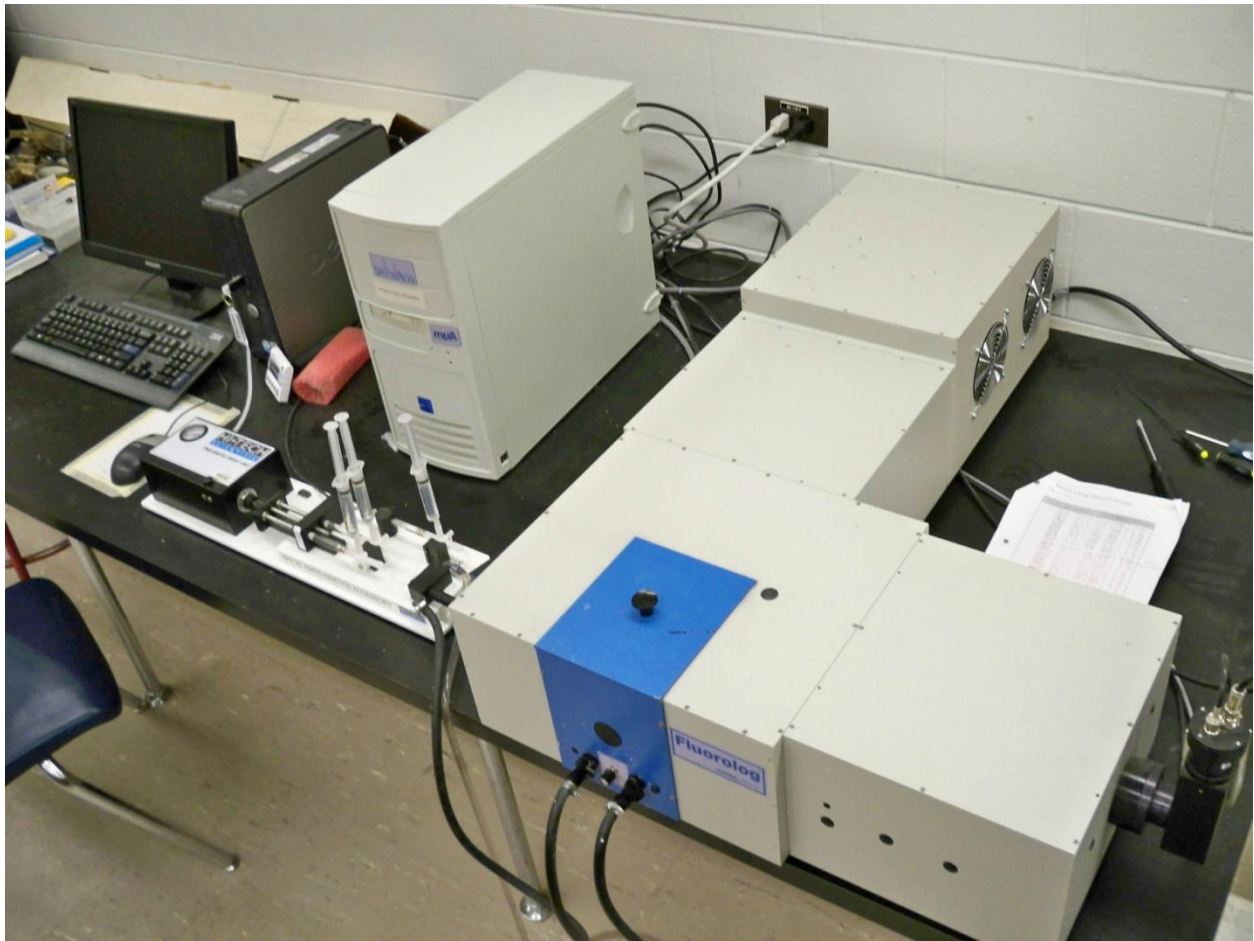


Figure 2 – 3. Fluorolog-3 Horiba Jobin Yvon Spectrofluorimeter.

References

1. Kapil Kumar, Frederick G. Walz Jr. Probing functional perfection in substructure of ribonuclease t1: Double combinatorial random mutagenesis involving Asn43, Asn44, and Glu46 in the guanine binding loop. *Biochemistry*. 2001;40(12):3748-57.
2. Jan Steyaert, Abdel Fattah Haikal, Lode Wyns, Patrick Stanssens. Subsite interactions of ribonuclease t1: Viscosity effects indicate that the rate-limiting step of GpN transesterification depends on the nature of N. *Biochemistry*. 1991;30(35):8661-5.
3. Jan Steyaert, Chris Opsomer, Lode Wyns, Patrick Stanssens. Quantitative analysis of the contribution of Glu46 and Asn98 to the guanosine specificity of ribonuclease t1. *Biochemistry*. 1991;30(2):494-9.
4. Hai By Du, Amy Ru-Chun Fuh, Junzhong Li, Andrew L. Corkan, Jonathan S. Lindsey. Photochem CAD: A computer-aided design and research tool in photochemistry. *Photochemistry and Photobiology*. 1998;68(2):141-2.
5. Joseph R. Lakowicz. Principles of fluorescence spectroscopy, 3rd edition. *Analytical and Bioanalytical Chemistry*. 2008;390(5):1223-4.
6. C. Nick Pace. Determination and analysis of urea and guanidine hydrochloride denaturation curves. *Methods in Enzymology*. 1986;131:266-80.
7. Marcelo M. Santoro, D.W. Bolen. Unfolding free energy changes determined by the linear extrapolation method. 1. unfolding of phenylmethanesulfonyl alpha- chymotrypsin using different denaturants. *Biochemistry*. 1988;27(21):8063-8.

Chapter 3

The effect of lithium ions on the hydrophobic effect: is the lithium anomaly a real anomaly?

3.1 The hydrophobic effect and hydrogen bonding

In the introductory chapter of this work, I saw a general overview of the hydrophobic effect and a separate overview of the effect of salts on protein stability. In this chapter, the effect of salts on the hydrophobic effect itself will be investigated. During the introduction, I saw that the hydrophobic effect is the manifestation of non-polar solutes aggregating in an effort to minimize the loss of entropy upon transfer to an aqueous environment (1-4). I discussed how the structure of water can influence the solubility of hydrophobes; the solubility of non-polar solutes is significantly higher in water with a high population of bent hydrogen bonds versus water that has a high population of linear hydrogen bonds (5). This is because bent hydrogen bonds are weaker than linear hydrogen bonds, and since the hydrophobic effect is in essence the disruption of hydrogen bonds, non-polar solutes will more easily disrupt the weak hydrogen bonds (5). Given that the hydrophobic effect is the disruption of the hydrogen bond network of water, it is reasonable to assume that the magnitude of the hydrophobic effect will depend on the strength of the hydrogen bonds between the water molecules. One approach to verify this hypothesis is to change the relative populations of linear and bent hydrogen bonds by the addition of co-solutes and to then correlate any change in the hydrophobic effect to the average strength of the hydrogen bonds (6, 7).

3.2 The effect of salts on the hydrophobic effect

Theoretical and experimental work (6, 8, 9) has shown that solutes like salts or osmolytes can shift the equilibrium between strong, linear hydrogen bonds and weak, bent hydrogen bonds. It has been shown that ions with a high charge density promote linear hydrogen bonds while ions with a low charge density promote bent hydrogen bonds in their hydration spheres (1, 2, 9). The promotion of linear or bent hydrogen bonds is the result of two competing interactions: the

charge-charge interaction between the dipole of the water molecule and the charge of the ion, and the contribution of entropy to the free energy of the system (1). When an ion has a small radius, the distance between the dipole of the water and the charge of the ion is small, leading to a strong charge-charge interaction (10). This leads to a dense packing of the water molecules in the ion's first hydration shell and hence to the formation of bent hydrogen bonds immediately around the ion (2, 10). However, to satisfy the equilibrium between bent and linear hydrogen bonds, subsequent hydration shells of the hydrated ion will have a large population of linear hydrogen bonds; this will increase the overall population of linear hydrogen bonds (2, 10). On the other hand, when an ion has a large radius, the distance between the charge of the ion and the dipole of the water will be greater, leading to a weak charge-charge interaction (10). Therefore the water molecules in the first hydration shell of a low charge density ion will arrange themselves in a cage-like structure to minimize the loss of entropy, thereby causing an increase in the population of bent hydrogen bonds (1). Therefore, knowing that salts with a high charge density promote linear hydrogen bonds, and that bent hydrogen bonds are necessary for the optimal solvation of hydrophobes, an inverse correlation between the charge density of a co-solute and the solubility of a hydrophobic moiety would be expected (10).

3.3 The lithium anomaly

However, experimental results do not always conform to the above prediction. The addition of lithium chloride often ameliorates the solubility of hydrophobic compounds. This is best exemplified by the changing solubility of aliphatic and aromatic compounds in aqueous solutions with varying concentration of different salts (11, 12). These studies utilize the Setschenow constant, also known as the salting-out constant (11), to quantitatively determine the effect of a co-solute on the solubility of a non-electrolyte solute. The Setschenow constant describes the

change in the solubility of a certain molecule due to the addition of a co-solute, typically a salt (11). These studies (11, 12) demonstrate that the Setschenow constant of various chloride salts decreases from NaCl to CsCl. This indicates that the strength of the salting out effect decreases from NaCl to CsCl; i.e. the strength of the hydrophobic effect diminishes as the size of the cation co-solute increases (11, 12). This trend follows the expected result, except for LiCl, whose Setschenow constant is similar to KCl or RbCl (12). Even though lithium is a small ion with a high charge density, it breaks the expected trend and behaves like a much larger cation with a much smaller charge density.

This departure of lithium from theoretical expectations also manifests itself in biophysical phenomena. In a study of salt effects on the formation of micelles, it was shown that the efficiency of micelle formation increases with the addition of cations with increasing charge density (from CsCl to NaCl), but abruptly drops when LiCl is added (13). Protein unfolding studies have also shown that unlike potassium and sodium chloride, who strongly promote protein structure, lithium chloride only modestly promotes protein structure (14, 15). Due to its high charge density, lithium should promote protein structure to an even greater extent than either potassium or sodium. Therefore, although the lithium cation has a high charge density, it behaves like a much larger ion. Such experimental results involving a variety of complex systems have shown that lithium enhances hydrophobicity much less than is predicted by theory, thus giving rise to the “lithium anomaly”.

2.4 Potential explanations of the lithium anomaly

Recent experimental work and theoretical calculations have offered plausible explanations for the lithium anomaly. Resonance Raman results demonstrate that lithium ions can interact directly with amides by polarizing the peptide bond carbonyls, thereby strengthening the polypeptide

backbone carbonyl dipole-dipole interaction (16). Other theoretical work has shown that lithium ions can interact with non-polar moieties such as methyl groups through a novel interaction that appears to be half-way between a van der Waals contact and a solvent-separated interaction (17). It has also been shown that lithium ions can bind to benzene via s - π and p - π orbital interactions, forming bonds that are of comparable strength to those of normal chemical bonds (18).

Therefore it appears that lithium ions contribute favourably to the solvation of these groups in aqueous solutions through direct interactions. This seems to indicate that previous systems used to study the effect of ions on hydrophobicity are too complicated since most of these models could include moieties that would interact directly with lithium ions. In other words, the observed lithium anomaly may be the result of contributions from interactions other than the hydrophobic effect. The work presented here aims to determine whether a) the lithium anomaly is a result of lithium ions diminishing the hydrophobic effect directly or b) lithium ions interacting directly with specific segments of molecules, solubilizing the entire molecule and thereby counteracting the hydrophobic effect.

3.5 Contact pair formation of phenol and acetate or formate as a simple model

To distinguish between these two possibilities, a simple system comprised of two moieties whose modes of interaction are well understood has been used. By using a simple model which includes only two molecules, any complicating factors that could distort the interpretation of the effect of lithium ions on the hydrophobic effect have been eliminated. As was discussed in the introductory chapter, the hydrophobic effect is one of the main driving forces in protein folding (1, 4, 26). Since salts are ubiquitous in biological settings, it is crucial to understand their effect on the hydrophobic effect and subsequently on protein folding. However, using proteins to study

the effect of salts on the hydrophobic effect leads to complications and misinterpretation, and so to minimize the complications brought about by using proteins as the model system, a simple model to study the effect of salts on the hydrophobic effect has been used. The simple model system used in this work is the contact pair formation between a phenol molecule and a formate or an acetate ion acting as a quencher, first introduced by Scheraga in 1965 (19). There are many advantages to using this contact pair formation as a simple model: there is no self-association of the acetate or formate molecules since they are negatively charged, and the phenol concentration used is very small, which eliminates self-association but still allows for remarkable fluorescence in the excited state (20). In this system the lithium ions can interact with the benzene ring of the phenol molecules on one side of the ring, however the opposite side is presumably free to interact with the quencher molecule without interference from the interacting lithium ion (18). Also, potential methyl-lithium interactions occur over a distance of $\sim 4.5 - 4.6 \text{ \AA}$ (17), which is within a typical reaction sphere of a proton transfer of $5 - 8 \text{ \AA}$ (21). Thus the formation of the contact pair does not perturb the methyl-lithium or the benzene-lithium interaction, thus the contribution of that specific interaction to the solubility is negligible.

3.6 Mechanism of phenol quenching by acetate and formate

The formation of contact pairs between phenol and acetate/formate can be easily monitored via fluorescence quenching experiments (19, 20). Acetate and formate quench excited phenols via a reaction controlled mechanism; that is to say the quenching of phenol by acetate/formate begins with the formation of an encounter complex, followed by rearrangement of the encounter complex to facilitate quenching via a proton transfer mechanism (20, 22). Proton transfer is an extremely fast process due to hydrogen's ability to act as both a particle and a wave (23). This allows hydrogen to tunnel through the energy barrier between the potential energy minima in the

hydrogen bond (23). However, this extremely fast process is entirely dependent on the orientation of the donor species relative to that of the acceptor (23). This suggests that the energy transfer rate of the quenching process represents the time necessary for the encounter complex to adopt the optimal geometry, rather than the time it takes for the proton transfer itself (21). The initial formation of the encounter complex between the phenol fluorophore and the acetate/formate quencher is mainly dependent on two types of interactions: the hydrophobic interaction between the non-polar regions of the quencher and the phenyl ring, and the hydrogen bonding between the phenol OH group and the carboxylate ion (20). The work presented here lays out a technique to isolate the hydrophobic contribution to the formation of the phenol-acetate encounter complex.

The work presented in this chapter aims to resolve the debate concerning the observed lithium anomaly by utilizing a simple model first introduced by Scheraga et al. (19, 20). Building on their work, a method of isolating the hydrophobic contribution to the formation of the phenol-acetate contact pair is presented here. Using this simple model, many problems faced by more complex systems (11-15) can be avoided completely. The data presented here will show that the hydrophobic contribution to the formation of the contact pair is salt dependent and that lithium enhances the hydrophobic contribution in the methyl-benzene interaction to a greater extent than other alkali-chlorides, as predicted by theory. I propose that the observed lithium anomaly in more complex systems is a result of direct interactions between the lithium cation and specific moieties, rather than a direct modification of the hydrophobic effect.

3.7 Fluorescence quenching and the Stern-Volmer equation

To understand the effects of alkali salts on the magnitude of the hydrophobic effect, I have monitored the fluorescence spectrum of phenol in increasing concentrations of acetate and

formate salts, acting as the quencher. The fluorescence spectra of phenol in the presence of increasing concentrations of sodium acetate and sodium formate are shown in Figure 3-1. The resulting Stern-Volmer plots (Figure 3-2) show a high degree of linearity, indicative of collisional quenching. Nevertheless I have checked for static quenching using the modified Stern-Volmer equation (equation 3-1b), where V is the action-sphere, or volume of action, or the fluorophore. Equation 3-1b describes a quenching process that has contributions from both collisional and static quenching in which the quencher exists in close proximity to the excited fluorophore (24). The exponential factor describes the quenching contribution of the quencher molecules located within the volume of action (V) of the fluorophore (24) prior to excitation.

$$\frac{F_0}{F} = (1 + K_{SV}[Q]) \quad (3-1a)$$

$$\frac{F_0}{F} = (1 + K_{SV}[Q])\exp(V[Q]) \quad (3-1b)$$

By fitting the obtained data to equation 3-1b, I have found that the modified Stern-Volmer equation does not significantly improve the fits. In fact, a large variance in the value of V , between 0.2 – 0.3 for acetate and 0.1 – 0.2 for formate was observed. Therefore, I can conclude that the contribution from the exponential factor to the quenching process is negligible and the classic Stern-Volmer equation will be used in this work. To characterize the influence of salts on the hydrophobic effect, I will be measuring the effect of alkali chloride salts on the quenching of phenol fluorescence by acetate and formate. The effect of cesium has not been investigated due to its strong intrinsic quenching capacity.

The Stern-Volmer constants obtained from the Stern-Volmer plots are shown in Table 3-1 and plotted against the concentration of the chloride salts, shown in Figure 3-3. As can be seen in Table 3-1, the obtained Stern-Volmer constants are entirely dependent on the alkali cation. To elucidate the nature of the dependence of the Stern-Volmer constant on the alkali cation, I have fit the plots in Figure 3-3 to the following equation:

$$K_{SV} = a + b[S] \quad (3-2)$$

where a and b are constants that depend on the nature of the co-solute and $[S]$ is its concentration; these values have been tabulated in Table 3-2. As a control I have also investigated the effect of alkali chlorides on the fluorescence spectrum of phenol (data not shown). The addition of lithium, sodium, and potassium only slightly increased the maximal emission of phenol. However the fluorescence of phenol is quenched by the presence of rubidium. This quenching is the reason for the large deviation in the b values of RbCl from the b values of the other alkali metals. Equation 3-2 will be used later on in this work to calculate the Stern-Volmer constant at any given salt concentration.

3.8 Collisional quenching vs static quenching in the phenol-acetate system

As was seen in the introductory chapter, fluorescence quenching can occur via two distinct molecular mechanisms: collisional and static (26). Collisional quenching is a diffusion-controlled process that results when the quencher enters the action-sphere of the fluorophore while it is in the excited state and results in linear Stern-Volmer plots (26). Static quenching, on the other hand, is caused by the formation of a stable complex prior to excitation of the fluorophore, and typically results in non-linear Stern-Volmer plots (26). The formation of the ground-state complex will have an association constant, K_a , which necessitates the modification of the Stern-Volmer equation to the following (24, 26):

$$\frac{F_0}{F} = (1 + K_{SV}[Q])(1 + K_a[Q]) \quad (3-3)$$

Equation 3-3 describes a quenching process that contains contributions from both dynamic and static quenching (26) and was used by Scheraga et al. (19, 20) to define the quenching process of

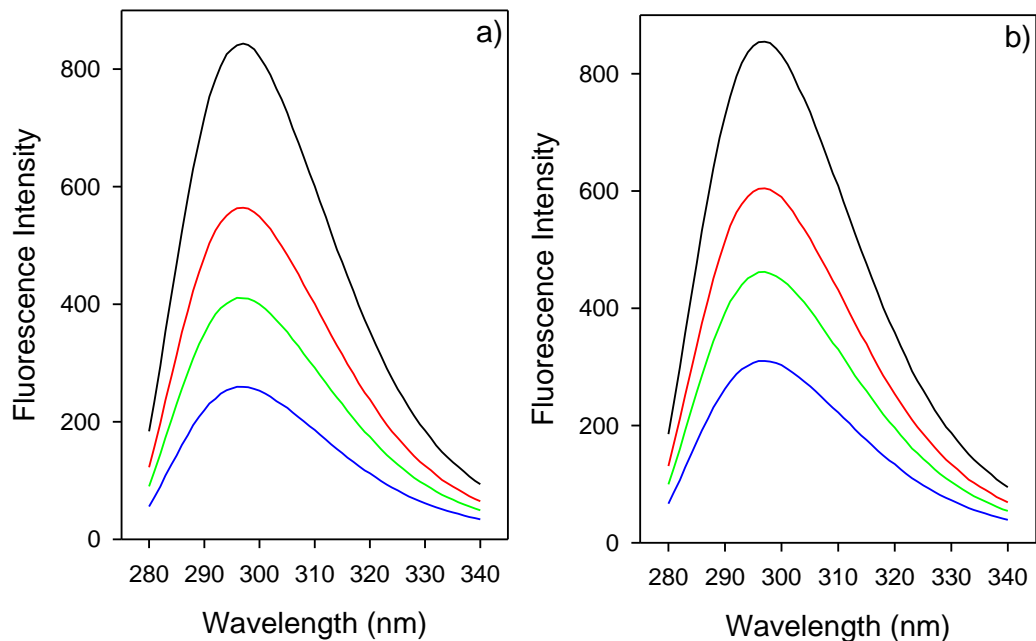


Figure 3-1. The fluorescence spectrum of phenol in the presence of sodium acetate (a) and sodium formate (b). Quencher concentrations are 0M (black), 0.1M (red), 0.2M (green), and 0.4M (blue).

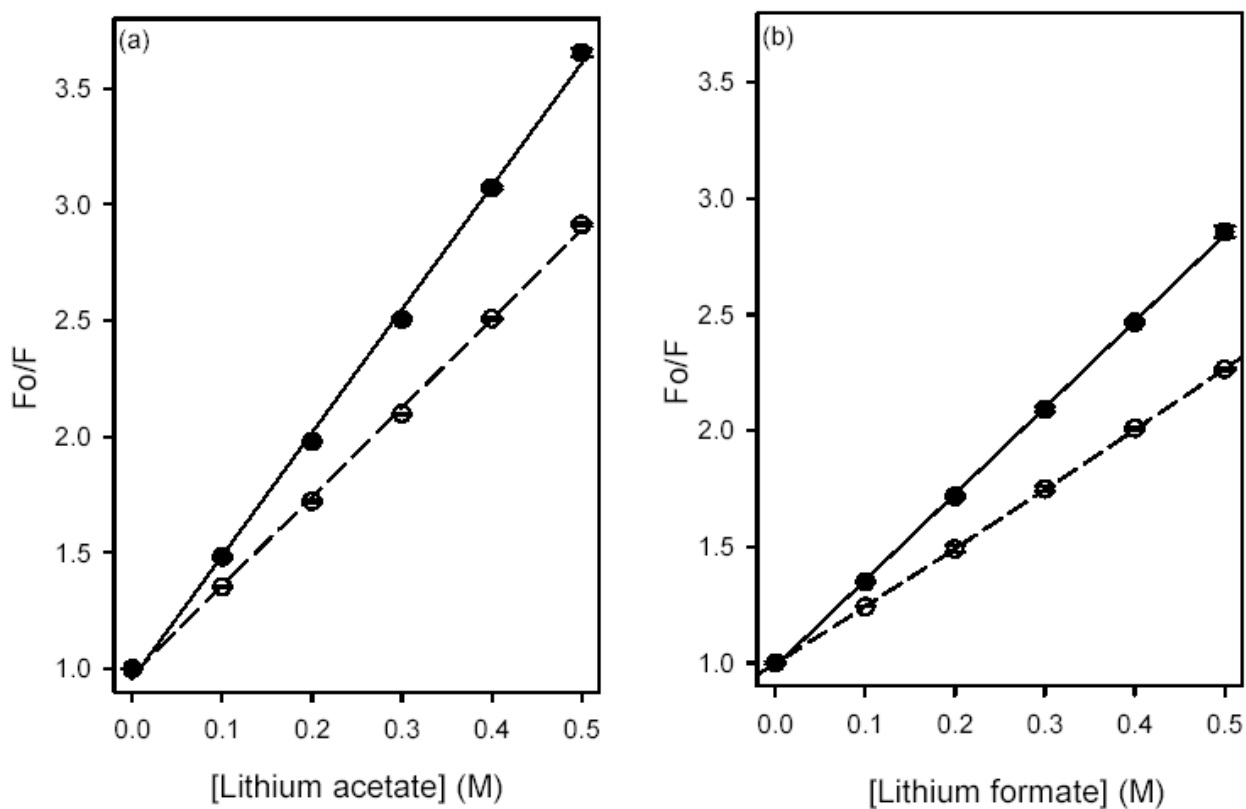


Figure 3-2 Stern-Volmer plots for the quenching of phenol by lithium acetate (a) and lithium formate (b). The concentration of lithium ions is kept constant at 1.5M (●) and 4M (○) by addition of LiCl.

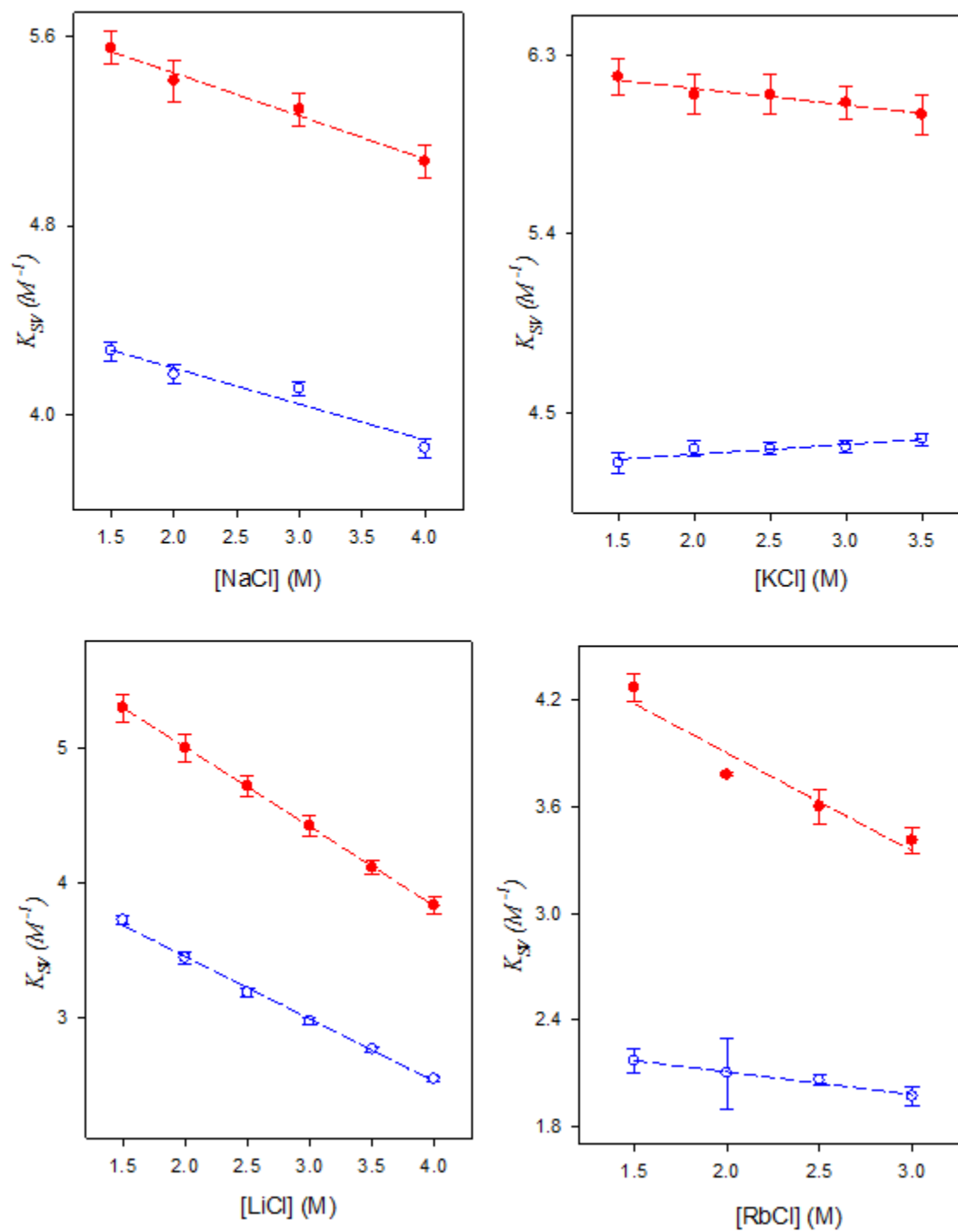


Figure 3-3. Parameters a and b associated with equation 3-2, demonstrating the salt dependence of the Stern-Volmer constants obtained from the quenching of phenol by acetate and formate.

Table 3-1. Stern-Volmer constants measured for the quenching of phenol fluorescence by acetate and formate ions in alkali chloride solutions at various concentrations.

(M)	K_{sv} (acetate) M^{-1}	K_{sv} (formate) M^{-1}
[NaCl]		
1.5	5.55 ± 0.07	4.27 ± 0.04
2.0	5.41 ± 0.09	4.17 ± 0.04
3.0	5.29 ± 0.07	4.11 ± 0.03
4.0	5.07 ± 0.07	3.86 ± 0.04
[KCl]		
1.5	6.19 ± 0.09	4.25 ± 0.05
2.0	6.10 ± 0.1	4.32 ± 0.04
2.5	6.1 ± 0.1	4.32 ± 0.03
3.0	6.06 ± 0.08	4.33 ± 0.03
3.5	6.0 ± 0.1	4.37 ± 0.01
[LiCl]		
1.5	5.3 ± 0.1	3.72 ± 0.03
2.0	5.0 ± 0.1	3.44 ± 0.04
2.5	4.72 ± 0.08	3.18 ± 0.03
3.0	4.42 ± 0.08	2.97 ± 0.03
3.5	4.11 ± 0.05	2.76 ± 0.02
4.0	3.83 ± 0.06	2.54 ± 0.02
[RbCl]		
1.5	4.27 ± 0.08	2.17 ± 0.07
2.0	3.78 ± 0.01	2.1 ± 0.2
2.5	3.6 ± 0.1	2.06 ± 0.03
3.0	3.41 ± 0.07	1.97 ± 0.05

Table 3-2. Parameters associated with equation 3-2, demonstrating the salt dependence of the Stern-Volmer constants obtained from the quenching of phenol by acetate and formate.

Quencher co-solute	a	b	R^2
Na ⁺ (acetate)	-0.18 ± 0.02	5.81 ± 0.05	0.982
Na ⁺ (formate)	-0.15 ± 0.03	4.50 ± 0.08	0.934
K ⁺ (acetate)	-0.08 ± 0.01	6.30 ± 0.04	0.919
K ⁺ (formate)	0.05 ± 0.01	4.19 ± 0.03	0.836
Li ⁺ (acetate)	-0.590 ± 0.004	6.19 ± 0.02	0.999
Li ⁺ (formate)	-0.47 ± 0.01	4.38 ± 0.04	0.996
Rb ⁺ (acetate)	-0.6 ± 0.1	5.01 ± 0.02	0.932
Rb ⁺ (formate)	-0.13 ± 0.01	2.36 ± 0.03	0.980

phenol by carboxylates. However, equation 3-3 does not apply to the instances where a high concentration (> 0.25 M) of quencher is used (20, 24). The non-linearity observed in the Stern-Volmer plots in this case is actually due to the finite probability of finding a quencher in the action-sphere of a fluorophore during excitation, rather than to the formation of a ground-state complex. Therefore, the application of equation 3-3 by Scheraga (19, 20) to measure the phenol-carboxylate contact pair is erroneous and an alternative mathematical description is needed and proposed in the following section.

3.9 Defining the phenol-carboxylate system

The linearity of the experimentally obtained Stern-Volmer plots indicates that the major contribution to the quenching of phenol is collisional quenching. In the case of collisional quenching, the Stern-Volmer constant is defined as the product of the rate of quenching, k_q , and the fluorescence lifetime, τ , shown below in equation 3-4

$$K_{SV} = k_q * \tau \quad (3-4)$$

The rate of quenching, k_q , depends on the extent of the interaction and the distance between the electron clouds of the fluorophore and the quencher (27). The quenching process can be represented by the following scheme (21):



in which F^* is the fluorophore in the excited state, Q is the quencher, $[F^* \bullet Q]$ is the encounter complex formed between the excited fluorophore and the quencher, k_{et} is the rate of energy transfer between the excited fluorophore and the quencher, F is the ground-state fluorophore and K_{ec} is the equilibrium constant for the formation of the encounter complex. Previous studies on the phenol-acetate system have shown that the quenching process is reaction controlled (19, 20).

In this case, equation 3-4 can be rewritten as:

$$K_{SV} = k_q * \tau = K_{ec} * k_{et} * \tau \quad (3-5)$$

A reaction controlled mechanism implies that the rate of energy transfer, k_{et} , is much faster than the formation of the encounter complex between the fluorophore and the quencher. This is due to the nature of the quenching of phenol by a carboxylate ion, which is the transfer of a proton (28). Proton transfer is an extremely fast process due to hydrogen's ability to act as both a wave and a particle. This allows a hydrogen atom to tunnel through the energy barrier between the potential energy minima in the hydrogen bond (23). The proton transfer process, which quickly follows the formation of a hydrogen bond, is entirely dependent on the orientation of the donor species relative to that of the acceptor species. And so the time-dependent search for the optimal conformation can be considered the rate-limiting step (21). Therefore, the K_{ec} can be considered as the contribution of the contact pair formation to the quenching process.

3.10 Isolating the hydrophobic contribution to the contact pair formation

To determine the hydrophobic contribution to the contact pair formation of phenol with acetate/formate, I will analyze the thermodynamic properties of the encounter complex. The first step is to define the standard free energy of formation of the encounter complex with equation 3-6:

$$\Delta G_{ec}^o = -RT \ln K_{ec} \quad (3-6)$$

The standard free energy of formation at any given salt concentration ($\Delta G_{ec}^o[S]$) is also the sum of three distinct contributions:

$$\Delta G_{ec}^o[S] = \Delta G_{sol}^o + \Delta G_{es}^o + \Delta G_{hydrophobic}^o \quad (3-7)$$

The first term is the contribution from the free energy of solvation of free phenol, quencher and the encounter complex. The second term is the contribution of electrostatic interactions between phenol and quencher in the encounter complex. The final term is the contribution of the hydrophobic interaction to the association of phenol and acetate/formate. As can be seen in equation 3-7, the contribution from the hydrogen bond is not considered. As was discussed in the previous paragraph, the formation of a hydrogen bond is a time-dependent search for the optimal conformation that, once established, quickly leads to the quenching of phenol (24). Therefore the formation of the hydrogen bond is better reflected in the rate of energy transfer (k_{et}) rather than the formation of the encounter complex (K_{ec}).

To isolate the effect of the salts on the formation of the encounter complex, equation 3-7 must be expanded in the following manner:

$$\Delta G_{ec}^o[S] = \{\Delta G_{sol}^o(0) + \Delta G_{sol}^o[S]\} + \Delta G_{es}^o + \{\Delta G_{hydrophobic}^o(0) + \Delta G_{hydrophobic}^o[S]\} \quad (3-8)$$

The first and third terms have been expanded to include the contribution of the solvation energy and the hydrophobic contribution in pure water $\Delta G_{sol}^o(0)$ and $\Delta G_{hydrophobic}^o(0)$, and in the presence of a given concentration of salt $\Delta G_{sol}^o[S]$ and $\Delta G_{hydrophobic}^o[S]$. The contribution of the electrostatic interaction between the carboxylate ion and the phenol molecule is not expanded because it is unlikely that the addition of salt will significantly affect the electrostatic contribution. This is because the distance between the reactants is very small, therefore no solvent molecules will be able to occupy the space within the solvent cage and influence the electrostatic interaction.

3.11 Contribution of the solvation energy to the formation of the contact pair

In contrast, the solvation energies ΔG_{sol}^o of acetate, formate and phenol are highly dependent on the ionic strength of the solvent. The contribution of salt to the solvation energy can be estimated using a generalized Born model that models the ionic species (salt, phenol and quencher) as point charges embedded in the middle of a sphere (29):

$$\Delta G_{sol}^o = \Delta G_{sol}^o(0) + \frac{Aq}{R_{ec}\epsilon_w} \left(1 - e^{-0.3R_{ec}\sqrt{I}}\right) - \left(\phi + \frac{Aq}{r_q\epsilon_w} \left(1 - e^{-0.3r_q\sqrt{I}}\right)\right) \quad (3-9)$$

where A is a conversion constant, ϵ_w is the dielectric constant of water, I is the ionic strength (which is equal to $[S]$), ϕ is the change in phenol solvation due to salt effects, q is the electron charge, r_q is the radius of the quencher, and R_{ec} is the radius of the solvent cage which is larger than the sum of the radius of phenol and the diameter of acetate/formate. The method of Bondi (30) will allow us to determine r_q and R_{ec} by estimating the van der Waals radii of phenol, acetate and formate to be 2.73 Å, 2.0 Å and 2.4 Å respectively. The first term of equation 3-9 is the solvation energy of the encounter complex in pure water, $\Delta G_{sol}^o(0)$, the second term, $\frac{Aq}{R_{ec}\epsilon_w} \left(1 - e^{-0.3R_{ec}\sqrt{I}}\right)$, is the solvation energy of the encounter complex in any given salt concentration and the final term, $\left(\phi + \frac{Aq}{r_q\epsilon_w} \left(1 - e^{-0.3r_q\sqrt{I}}\right)\right)$, is the solvation energy of the individual phenol and acetate/formate molecules. Thus the contribution of the solvation energy to the formation of the encounter complex can be estimated by adding the solvation energy of the encounter complex in pure water (first term) to the difference between the solvation energies of the encounter complex (second term) and the free phenol and quencher molecules (third term). However, equation 3-9 has too many variables to solve. Therefore equation 3-9 can be expanded in a linear fashion using a Taylor series at 1.5M salt around the second exponent, $e^{-0.3r_q\sqrt{I}} = 1$, by ignoring the

first exponent $e^{-0.3R_{ec}\sqrt{I}}$ since $-0.3r_q\sqrt{I}$ is significantly larger than $-0.3R_{ec}\sqrt{I}$ (values of $\approx 0.7 - 0.9 \gg 0.1$). Thus equation 3-9 can be rewritten as follows:

$$\Delta G_{sol}^o = \Delta G_{sol}^o(0) + \phi + \frac{Aq}{R_{ec}\epsilon_w} (1 - \dots) - \frac{Aq}{r_q\epsilon_w} (1 - 2e^{-1} + e^{-1}(0.3r_q\sqrt{I}) + \dots) \quad (3-10a)$$

$$\Delta G_{sol}^o = \Delta G_{sol}^o(0) + \phi + \frac{Aq}{R_{ec}\epsilon_w} - \frac{Aq}{r_q\epsilon_w} (1 - 2e^{-1}) - \frac{Aq}{\epsilon_w} (e^{-1}(0.3\sqrt{I}) + \dots) \quad (3-10b)$$

3.12 Introducing the H parameter

Now that a method to isolate the contribution of the solvation energy to the formation of the encounter complex has been established, the parameter “H” can be introduced and defined as:

$$H = -RT \ln \left(\frac{(K_{sv})_{acetate}}{(K_{sv})_{formate}} \right)_{[S]} \quad (3-11)$$

If equation 3-5 is inserted into the above definition:

$$H = -RT \ln \left(\frac{(K_{ec})_{acetate-phenol} * \tau_{phenol} * (k_{et})_{acetate-phenol}}{(K_{ec})_{formate-phenol} * \tau_{phenol} * (k_{et})_{formate-phenol}} \right)_{[S]} \quad (3-11a)$$

As can be seen, the H parameter corrects for variations in the fluorescence lifetime of phenol. If equation 3-6 is taken into account, equation 3-11a can be rewritten as:

$$H = \Delta G_{acetate-phenol}^o - \Delta G_{formate-phenol}^o - RT \ln \left(\frac{(k_{et})_{acetate-phenol}}{(k_{et})_{formate-phenol}} \right)_{[S]} \quad (3-11b)$$

We now obtain the following by inserting equation 3-7 into equation 3-11b:

$$H = (\Delta G_{sol}^o + \Delta G_{es}^o + \Delta G_{hydrophobic}^o)_{\text{acetate-phenol}} - (\Delta G_{sol}^o + \Delta G_{es}^o + \Delta G_{hydrophobic}^o)_{\text{phenol-acetate}} - RT \ln \left(\frac{(k_{et})_{\text{acetate-phenol}}}{(k_{et})_{\text{formate-phenol}}} \right)_{[S]} \quad (3-11c)$$

Since formate ions lack a non-polar region, they participate minimally in hydrophobic interactions, therefore $(\Delta G_{hydrophobic}^o)_{\text{phenol-acetate}} = 0$ and equation 3-11c becomes:

$$H = \left((\Delta G_{hydrophobic}^o)_{\text{acet.-phe.}} \right)_{[S]} - RT \ln \left(\frac{(k_{et})_{\text{acetate-phenol}}}{(k_{et})_{\text{form.-phe.}}} \right)_{[S]} + \left((\Delta G_{sol}^o)_{\text{acet.-phe.}} - \Delta G_{sol}^o_{\text{form.-phe.}} + \Delta G_{es}^o_{\text{acet.-phe.}} - \Delta G_{es}^o_{\text{form.-phe.}} \right) \quad (3-11d)$$

Applying equation 3-10b accounts for the contribution of the solvation energy at any given salt concentration to the formation of the encounter complex:

$$H_{[S]} = \left((\Delta G_{hydrophobic}^o)_{\text{acet.-phe.}} \right)_{[S]} - RT \ln \left(\frac{(k_{et})_{\text{acet.-phenol}}}{(k_{et})_{\text{form.-phenol}}} \right)_{[S]} + \left(\left(\Delta G_{sol}^o(0) + \phi - \frac{Aq}{Rec\epsilon_w} + Aqrq\epsilon_w 1 - 2e - 1 + \dots \right)_{\text{acet.-phe.S}} - \left(\Delta G_{sol}^o(0) + \phi - \frac{Aq}{Rec\epsilon_w} + Aqrq\epsilon_w 1 - 2e - 1 + \dots \right)_{\text{form.-phe.S}} + \Delta G_{es}^o_{\text{acet.-phe.}} - \Delta G_{es}^o_{\text{form.-phe.S}} \right) \quad (3-12)$$

As can be seen in equation 3-12, the contribution of the solvation energy from the formate-phenol mixture negates the contribution from the acetate-phenol solution at any salt concentration. Keeping this in mind, the H parameter at $[S] = 1.5$ M can be calculated:

$$H_{[S]} =$$

$$\left((\Delta G_{hydrophobic}^o)_{acet.-phe.} \right)_{[S]=1.5M} - RT \ln \left(\frac{(k_{et})_{acet.-phenol}}{(k_{et})_{form.-phenol}} \right)_{[S]=1.5M} + \left((\Delta G_{es}^o)_{acet.-phe.} - \Delta G_{esoform.-phe.S=1.5M} \right) \quad (3-13)$$

Now if $H_{[S]=1.5M}$ is subtracted from $H_{[S]}$:

$$H_{[S]} - H_{[S]=1.5M} = \Delta G_{ec}^o[S]_{acet.} - \Delta G_{ec}^o[S]_{form.} + \Delta G_{ec}^o[1.5M]_{acet.} - \Delta G_{ec}^o[1.5M]_{form.} - RT \ln \left(\frac{\left(\frac{(k_{et})_{acet.-phenol}}{(k_{et})_{form.-phenol}} \right)_{[S]}}{\left(\frac{(k_{et})_{acet.-phenol}}{(k_{et})_{form.-phenol}} \right)_{[S]=1.5M}} \right) \quad (3-14)$$

If the definition $\Delta \Delta G_{hydrophobic}^o = \Delta G_{hydrophobic}^o[S] - \Delta G_{hydrophobic}^o[1.5M]$ is inserted into equation 3-14, since ΔG_{es}^o is not salt dependent and the contribution from the solvation energy cancels-out, equation 3-14 can be rewritten to give the following:

$$H_{[S]} - H_{[S]=1.5M} = -RT \ln \left(\frac{\left(\frac{(K_{SV})_{acet.}}{(K_{SV})_{form.}} \right)_{[S]}}{\left(\frac{(K_{SV})_{acet.}}{(K_{SV})_{form.}} \right)_{[S]=1.5M}} \right) \approx \Delta \Delta G_{hydrophobic}^o - RT \ln \left(\frac{\left(\frac{(k_{et})_{acet.}}{(k_{et})_{form.}} \right)_{[S]}}{\left(\frac{(k_{et})_{acet.}}{(k_{et})_{form.}} \right)_{[S]=1.5M}} \right) \quad (3-15)$$

The rate constant k_{et} is a conformation search within the encounter complex for the optimal geometry to establish a hydrogen bond which is quickly followed by quenching via a proton transfer. According to the Arrhenius equation:

$$k = A \exp(-E_a/RT) \quad (3-16a)$$

the activation energy (E_a) of a process with a rate (k) is not dependent on the solvent but rather depends on the energy distribution of the different conformations that the encounter complex adopts during its search to overcome the hydrogen bond energy barrier. However, according to

Kramers' theory, which describes internal friction effects on rate constants, the pre-exponential factor can be influenced by the local viscosity (η) of the system (31, 32). Therefore the pre-exponential factor, where A is a constant, will be affected by the local viscosity, which allows us to define the rate constant with equation 3-16b:

$$k_{et} = A * \eta * \exp\left(\frac{E_a}{RT}\right) \quad (3-16b)$$

Therefore, substituting equation 3-16b into equation 3-15 and rearranging will yield:

$$-RT \ln(H) \approx \Delta\Delta G_{hydrophobic}^o - RT \ln \left(\frac{\left(\frac{A_{acet.} \eta_{acet.} \exp\left(\frac{E_a}{RT}\right)_{acet.}}{A_{form.} \eta_{form.} \exp\left(\frac{E_a}{RT}\right)_{form.}} \right)_{[S]}}{\left(\frac{A_{acet.} \eta_{acet.} \exp\left(\frac{E_a}{RT}\right)_{acet.}}{A_{form.} \eta_{form.} \exp\left(\frac{E_a}{RT}\right)_{form.}} \right)_{[S]=1.5M}} \right) \quad (3-17a)$$

Given that the constant A and the activation energies are practically identical at different salt concentrations, equation 3-17a can be reduced to give:

$$-RT \ln(H) \approx \Delta\Delta G_{hydrophobic}^o - RT \ln \left(\frac{\left(\frac{\eta_{acet.}}{\eta_{form.}} \right)_{[S]}}{\left(\frac{\eta_{acet.}}{\eta_{form.}} \right)_{[S]=1.5M}} \right) \quad (3-17b)$$

Since the solvent cage will be nearly identical whether it is acetate or formate forming the encounter complex with phenol, the local viscosities will be nearly identical as well. Therefore equation 3-15 can be simplified to the following polynomial expansion:

$$H_{[S]} - H_{[S]=1.5M} = RT \ln \left(\frac{\left(\frac{(K_{SV})_{acet.}}{(K_{SV})_{form.}} \right)_{[S]}}{\left(\frac{(K_{SV})_{acet.}}{(K_{SV})_{form.}} \right)_{[S]=1.5M}} \right) \approx \frac{\Delta\Delta G_{hydrophobic}^o}{RT} = \alpha * ([S] - 1.5) + \beta * ([S] - 1.5)^2 + \dots \quad (3-18)$$

The constants α and β are specific to each salt studied and can be used to characterize how each

individual salt influences the hydrophobic contribution to the formation of the encounter complex. In addition, equation 3-2 and the interpolated K_{SV} values displayed in Figure 3-3 will be used to analyze the experimental results.

3.13 Influence of salts on the hydrophobic contribution to the formation of the encounter complex

Using equation 3-2 to construct the correlation lines shown in Figure 3-3, the K_{SV} values of the alkali salts can easily be determined at any concentration. The interpolated K_{SV} values are used to determine $H_{[S]} - H_{[S]=1.5M}$, which is then plotted against $([S] - 1.5)$ in Figure 3-4. If I base my observations on the initial slope α of each plot, I can see that each salt has a unique influence on the hydrophobicity of the contact pair. Lithium (red) enhances the hydrophobic effect, sodium (black) has a negligible impact on the hydrophobic effect, while potassium (blue) diminishes the hydrophobic effect modestly and rubidium (green) significantly reduces the hydrophobic effect. Since the counterion is kept constant throughout these experiments, the observed effect on the hydrophobicity is due solely to the cation. The increased hydrophobicity induced by lithium will reduce the solubility of hydrophobic moieties while the easing of the hydrophobic effect by potassium and rubidium will alleviate the energetic cost of solubilizing hydrophobic moieties.

This is the trend predicted by theory, which states that ions with a high charge density will enhance the hydrophobic effect through the ordering of hydration shell water molecules and ions with a low charge density will relieve the hydrophobic effect (1, 2, 6, 33). The most noteworthy aspect of the results is the absence of the so-called lithium anomaly. In the simple model, lithium has the expected effect on the hydrophobic contribution to the phenol-acetate encounter complex; the hydrophobicity is enhanced.

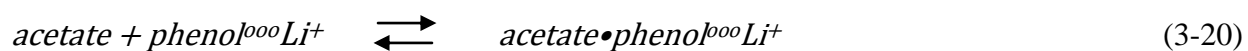
3.14 Alternative explanation for the observed lithium anomaly

I propose here that the observed lithium anomaly is a result of specific interactions between lithium and certain moieties in solution since my data demonstrates that lithium influences the hydrophobic effect according to its charge density, as expected by theory. As was discussed earlier in this chapter, recent work has shown that lithium can interact directly with a variety of moieties which are present in commonly studied systems (16, 18). As a general example, the case of the formation of a drop of liquid benzene in an aqueous lithium chloride solution will be considered. Since the benzene molecule has a strong interaction with lithium, stronger than a self-interaction (18), the following equilibrium can be written as:



where n is the number of benzene molecules and $\textit{benzene}_{\textit{drop}}$ is the drop formed. The forming of a benzene drop will necessitate the breakage of a large number of interactions between lithium and benzene. This will be highly unfavourable since the benzene-lithium interaction is much stronger than the benzene-benzene interaction (18). Therefore, the experimentally observed increase in benzene solubility in lithium chloride solutions is actually due to the specific benzene-lithium interactions and not a lessening of the hydrophobic effect.

This is not the case in the formation of the acetate-phenol encounter complex. The encounter complex is a molecular entity and the interaction between a quencher and the phenol does not preclude the lithium-phenol interaction:



Consequently the simple model used in this work has the distinct advantage of being insensitive

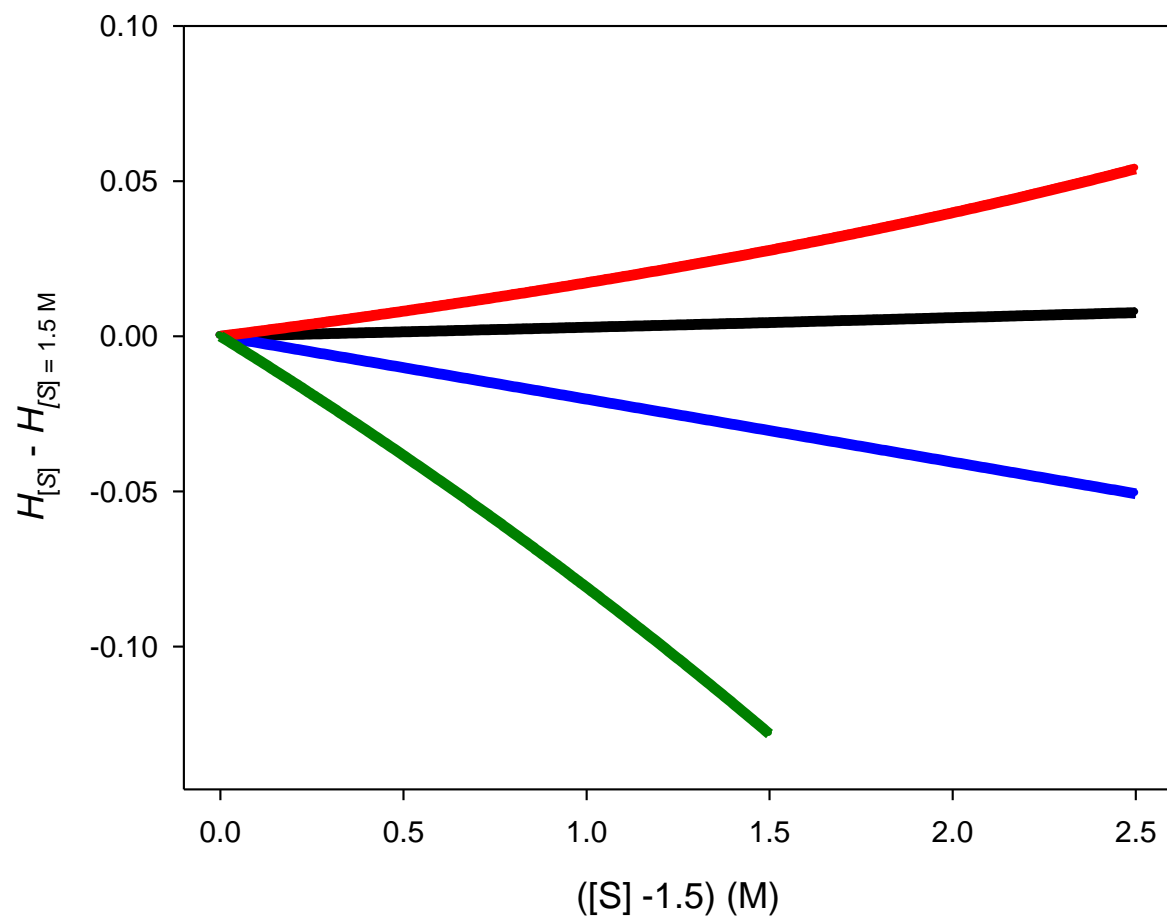


Figure 3-4. Salt concentration dependence of the $H_{[S]} - H_{[S]=1.5M}$ parameter for LiCl (red), NaCl (black), KCl (blue) and RbCl (green).

to specific interactions and so only measures the influence of salts on hydrophobicity.

3.15 Conclusions

The addition of lithium chloride to many systems has the peculiar effect of enhancing their solubility, i.e. of lowering the hydrophobic effect. This is in stark contrast to other cations and anions that all influence the hydrophobic effect in proportion to their charge density: ions with a high charge density order water molecules around themselves in such a fashion as to enhance the hydrophobic effect, while ions with a low charge density alleviate the hydrophobic effect. However, recent work has shown that lithium can uniquely interact with different hydrophobic moieties, and these interactions can compensate for the hydrophobic effect. Therefore the aim of this study was to ascertain whether lithium did indeed reduce the hydrophobic effect, or whether specific lithium interactions were overcoming the theoretical strengthening of the hydrophobic effect that should occur in the presence of lithium. To solve the lithium anomaly, I employed a simple model to characterize the hydrophobic contribution to the formation of the contact pair between acetate and phenol.

The data presented here demonstrates that salts influence the hydrophobic effect according to their charge density and the extent to which they can order water molecules in their hydration shell. Most importantly, no lithium anomaly is observed in the results. Therefore I propose that the observed lithium anomaly in more complex systems is in fact due to lithium interacting specifically with hydrophobic moieties, which then compensates for the enhanced hydrophobic effect. This counteraction of the enhanced hydrophobic effect is not due to the rearrangement of solvent molecules, but rather is due to specific interactions in which lithium solubilises hydrophobic moieties.

References

1. Ken A. Dill, Thomas M. Truskett, Vojko Valchy, Barbara Hribar-Lee. Modeling water, the hydrophobic effect, and ion solvation. *Annual Review of Biophysics and Biomolecular Structur.* 2005;34:173-99.
2. Barbara Hribar, Noel T. Southhall, Vojko Vlachy, Ken A. Dill. How ions affect the structure of water. *Journal of the American Chemical Society.* 2002;124(41):12302-11.
3. A.D. Buckingham, J.E. Del Bene, S.A.C. McDowell. The hydrogen bond. *Chemical Physics Letters.* 2008;463(1-3):1-10.
4. Kim A. Sharp, Bhupinder Madan. Hydrophobic effect, water structure, and heat capacity changes. *The Journal of Physical Chemistry B.* 1997;101:4343.
5. G. Wilse Robinson, C.H. Cho. Role of hydration water in protein unfolding. *Biophysical Journal.* 1999;77:3311-8.
6. Nathaniel V. Nucci, Jane M. Vanderkooi. Effects of salt on the Hofmeister series on the hydrogen bond network of water. *Journal of Molecular Liquids.* 2008;143:160-70.
7. Nathan J. Scott, Nathaniel V. Nucci, Jane M. Vanderkooi. Changes in water structure induced by the guanidinium cation and implications for protein denaturation. *The Journal of Physical Chemistry A.* 2008;112(43):10939-48.
8. Kim A. Sharp, J.M. Vanderkooi. Water in the half shell: Structure of water, focusing on angular structure and solvation. *Accounts of Chemical Research.* 2010;43:231-9.
9. Nathaniel V. Nucci, Jane M. Vanderkooi. Temperature excursion infrared spectroscopy. *Methods in Protein Structure and Analysis.* 2007:231-48.
10. Andrew S. Thomas, Adrian H. Elcock. Molecular dynamics simulations of hydrophobic association in aqueous salt solutions indicate a connection between water hydrogen bonding and the Hofmeister effect. *Journal of the American Chemical Society.* 2007;129:14887-98.
11. Wen-Hui Xie, Wan-Ying Shiub, Donald Mackay. A review of the effect of salts on the solubility of organic compounds in seawater. *Marine Environ.* 1997;44(4):429-44.
12. Miklos Gorgenyi, Jo Dewulf, Herman Van Langenhove, Karoly Heberge. Aqueous salting-out effect of inorganic cations and anions on non-electrolytes. *Chemosphere.* 2006;65(5):802-10.
13. Ashoka Ray GN. Effects of ionic protein denaturants on micelle formation by nonionic detergents. *Journal of the American Chemical Society.* 1971;93(25):6787-93.
14. Christine Ebel, Pierre Faou, Blandine Kernel, Giuseppe Zacca. Relative role of anions and cations in the stabilization of halophilic malate dehydrogenase. *Biochemistry.* 1999;38:9039-47.

15. Kristina Borén, Hannah Grankvist, Per Hammarström, Uno Carlsson. Reshaping the folding energy landscape by chloride salts: Impact on molten-globule formation and aggregation behavior of carbonic anhydrase. *Federation of European Biochemical Scientists*. 2004;566(1-3):95-9.
16. Sanford Asher SB. Raman studies of solution polyglycine conformations. *The Journal of Physical Chemistry B*. 2010;114:6636-41.
17. Adrian H Elcock, Andrew S Thomas. Molecular dynamics simulations predict a favorable and unique mode of interaction between lithium (Li⁺) ions and hydrophobic molecules in aqueous solutions. *Journal of Theory and Chemical Computation*. 2011;7(4):828-4.
18. Jian Tan Xiao, Liang Zhu Wei, Meng Cui, Min Luo Xiao, De Gu Jian, Israel Silman, Joel L. Sussman, Liang Jiang Hua, Yun Ji Ru, Kai Xian Chen. Noncovalent interaction or chemical bonding between alkaline earth cations and benzene? A quantum chemistry study using MP2 and density-functional theory methods. *Chemical Physics Letters*. 2001;349(1,2):113-22.
19. A. Young Moon, Douglas C. Poland, Harold A. Scheraga. Thermodynamic data from fluorescence spectra. I. the system phenol-acetate. *Journal of Physical Chemistry*. 1965;69(9):2960-6.
20. Donald K. Kunimitsu, Young A. Woody, Evelyn R. Stimson, Harold A. Scheraga. Thermodynamic data from fluorescence spectra. II. hydrophobic bond formation in binary complexes. *Journal of Physical Chemistry*. 1968;69(9):2960-866.
21. Matteo Rini, Dian Pines, Ben-Zion Magnes, Ehud Pines, Erik T.J. Nibbering. Bimodal proton transfer in acid-base reactions in water. *Journal of Chemical Physics*. 2004;121(19):9593-610.
22. Young A. Moon, Douglas C. Poland, Harold A. Scheraga. Thermodynamics data from fluorescence spectra. I. the system phenol-acetate. *Journal of Physical Chemistry*. 1965;69(9):2960-6.
23. *Comprehensive chemical kinetics: Proton transfer of related reactions*. C.H Bamford CFHT, editor. Amsterdam: Elsevier Scientific Publication Company; 1977.
24. S.E. Webber. The role of time-dependent measurements in elucidating static versus dynamic quenching processes. *Photochemistry and Photobiology*. 1997;65(1):33-8.
25. C. Nick Pace, Gerald R. Grimsley. Ribonuclease t1 is stabilized by cation and anion binding. *Biochemistry*. 1988;27:3242-6.
26. Joseph R. Lakowicz. *Principles of fluorescence spectroscopy*, 3rd edition. Analytical and Bioanalytical Chemistry. 2008;390(5):1223-4.
27. Bogumil, Zelent, Jozef Kusba, Ignacy Gryczynski, Michael L. Johnson, Joseph R. Lakowicz. Distance-dependent fluorescence quenching of p-bis[2-(5-phenyloxazolyl)] benzene by various quenchers. *Journal of Physical Chemistry*. 1996;100(47):18592-602.
28. Audrey White. Effect of pH on fluorescence of tyrosine, tryptophan, and related compounds. *Biochemical Journal*. 1959;71:217-20.

29. Jayashree Srinivasan, Megan W. Trevathan, Paul Beroza, David A. Case. Application of a pairwise generalized born model to proteins and nucleic acids. inclusion of salt effects. *Theoretical Chemistry Accounts*. 1999;101(6):426-34.
30. A. Bondi. Van der waals volumes and radii. *Journal of Physical Chemistry*. 1966;70(9):3006-7.
31. Julia Toth, Zoltan Simon, Peter Medveczky, Linda Gombos, Balazs Jelinek, Laszlo Szilagy, Laszlo Graf, Andras Malnasi-Csizmadia. Site directed mutagenesis at position 193 of human trypsin 4 alters the rate of conformational change during activation: Role of local internal viscosity in protein dynamics. *PROTEINS: Structure, Function, and Bioinformatics*. 2007;67(4):1119-27.
32. Linlin Qiu, Stephen J. Hagen. A limiting speed for protein folding at low solvent viscosity. *Journal of the American Chemical Society*. 2004;126(11):3398-9.
33. Kim A. Sharp, Bhupinder Madan, Eric Manas, Jane M. Vanderkooi. Water structure changes induced by hydrophobic and polar solutes revealed by simulations and infrared spectroscopy. *Journal of Phy.* 2001;114(4):1791-6.

Chapter 4

Studying salt effects on protein stability using ribonuclease t1 as a model system

4.1 Overview

The work presented in this chapter utilizes the model developed by Zhou (1) to evaluate the influence of various chloride salts on the conformational stability of RNase t1, an extremely well-characterized model protein (see Introduction). The results presented in this chapter demonstrate that the addition of chloride salts significantly stabilizes the folded form of RNase t1 to varying extents, depending on the nature of the salt. I go on to show that while salts uniformly increase the conformational stability of RNase t1, it is not always due to cation binding. In fact, the increase in stability caused by non-binding salts at high salt concentrations can be explained via salting-out effects which closely follow the expected results predicted by Zhou's model. The work presented in this chapter further confirms the theoretical model presented by Zhou and highlights the importance of considering induced point image charges when studying protein conformational stability.

Salts are an essential component of living systems, most biological systems contain ionic species that vary in concentration from 1 to 200 mM (2, 3). At these concentrations salts can have a sizable impact on the stability of biomolecules. As an example, the presence of salts can screen repulsive electrostatic interactions created by the highly negative net charge of nucleic acids. Positive counterions screen the negatively charged phosphate groups that are located along the DNA backbone (4). However, the building blocks of proteins are much more diverse than those of nucleic acids, leading to a protein with a significantly lower net charge than a strand of nucleic acids of comparable size. The effect of salts on protein conformation and stability is therefore much more complex and differs from protein to protein.

The first systematic study of the effect of salts on proteins was done by Hofmeister in 1888 (5). In these studies, Hofmeister observed that the addition of salts decreases the solubility

of proteins (i.e. salts-out), and that the efficacy of the salting-out depends on the nature of the salt (5). The tabulation of their results is now known as the Hofmeister series, whose study remains widespread due to its applicability to a broad range of fields: including the study of enzyme activity (6), protein-protein interactions (7), the crystallization of proteins (8) and the study of protein stability (9).

Another reason for the endurance of the Hofmeister series is that no one has been able to comprehensively explain the observed salting-out effect. In the mid-twentieth century, Kirkwood and Tanford contributed to the discussion and developed a model to explain the observed salting-out effect (10, 11). To develop this model, they applied a rigorous statistical mechanical analysis to explain the observed salting-out problem (10, 11). They proposed a method to calculate the solvation energy of charged residues located on a protein by modeling the charged residues as spheres at fixed locations on the protein. This was a more realistic representation of charged residues than the previous models which had represented proteins as spheres with a continuous and uniform charge (11). According to their work, the existence of the charges present in the protein and the ions in the solvent will have the following effects on the protein-water system (11).

First, a charge placed in a high dielectric medium, such as water, will induce an image charge of the same sign in the low dielectric medium, such as proteins. The interaction between the charge in the high dielectric medium and the induced mirror image charge in the low dielectric medium is unfavourable, and is therefore destabilizing. Increasing the amount of salt will increase this destabilization, leading to the observed “salting-out” phenomenon. According to the Kirkwood model, a point charge located in a low dielectric medium (i.e. charged residue in a protein) will induce an image charge of the opposite sign in the neighbouring high dielectric

medium (i.e. water), causing a favorable interaction. Therefore, the net effect of the addition of salts will be an initial increase in the favorable interaction between the charged residues and their induced image charges in the solvent, leading first to an increase in protein stability. This effect is called “salting-in” and the salting-in effect will stabilize the protein until the number of ions overwhelms the limited number of charges present in the protein. These unfavorable interactions will then cause a net destabilization of the protein. The unfavorable interactions will then be minimized by protein aggregation and precipitation, thus causing the protein molecule to “salt-out” of solution.

Salts can also stabilize the folded state versus the unfolded state or vice versa by the same interaction principles. Increasing the concentration of salt increases the salting-out interactions for both states. However, since the unfolded state has a larger surface area than the folded state, salting-out interactions will destabilize the unfolded state to a greater extent than the folded state, which leads to a net stabilization of the folded state. In other words, the increase in salt increases the amount of energy needed to unfold the protein (i.e. leads to an increase in the folding free energy of the protein). Increasing the salt concentration will also increase the salting-in stabilization of both the folded and unfolded states. Since the charged residues in the unfolded state are more solvent accessible, the charged residues in the unfolded state will have a larger solvation energy and be stabilized to a greater extent than the folded state. Conversely, the folded state will also be stabilized since the charged residues in the folded state are in closer proximity to each other than in the unfolded state, which leads to greater charge screening and a net stabilizing of the folded state. Therefore at low salt concentrations both the folded and unfolded states of the protein will be stabilized by salting-in effects.

To understand the underlying mechanism of induced point charges, I will begin by

defining a simple dipole moment. A dipole moment is the separation of charge within an atom or molecule in any given direction (Figure 4-1). A dipole can be an intrinsic property of a molecule (e.g. water or proteins), or it can be induced by an external electric field originating from a charge (i.e. a cation).

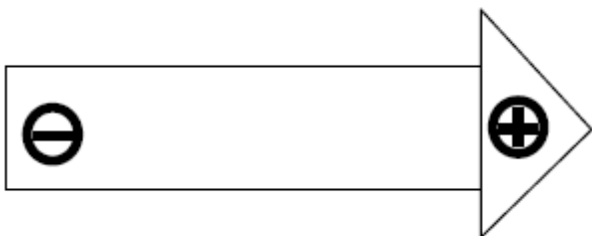


Figure 4-1. Illustration of a simple dipole. By convention the positive charge comprises the arrowhead, which indicates the direction of the dipole moment.

The measure of a dipole moment is the measure of the charge separation within the molecule. An atom or molecule can develop a dipole in two ways; 1) electronic polarization: an electrical field will induce a shift of the positive nucleus in one direction, while simultaneously pushing the electron cloud in the opposite direction, thereby creating charge separation. 2) orientational polarization (limited to molecules with an intrinsic dipole moment): molecules with a dipole moment will tumble freely due to thermal motion, netting a time averaged dipole moment of zero. However, when an electrical field is applied, the tumbling will be biased in the direction of the field, leading to a non-zero time-averaged dipole moment. In the case of proteins, it is not appropriate to consider orientational polarization unless you are measuring the overall change of the dielectric constant of a solution containing solubilised proteins.

The dominant force to consider when analyzing dielectric constants of proteins are their main chain amides, which have a relatively strong dipole moment (Figure 4-2). The presence of an electric field will magnify the intrinsic dipole moment of the protein, yet for the most part this enlargement will cancel out. Only at the edges of the protein will the inducing electric field have

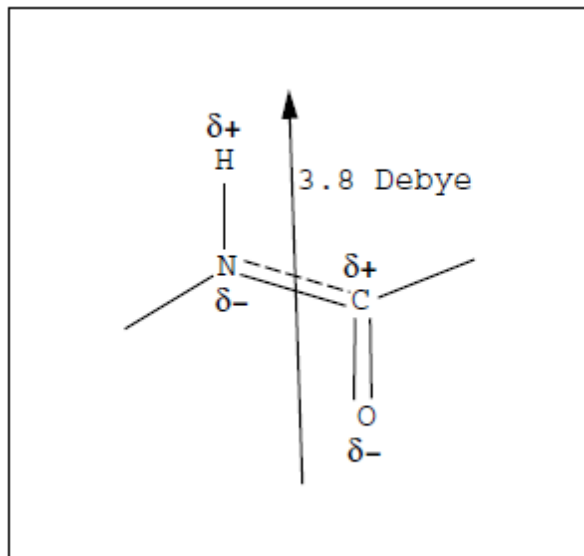


Figure 4-2. Dipole moment of the backbone amide.

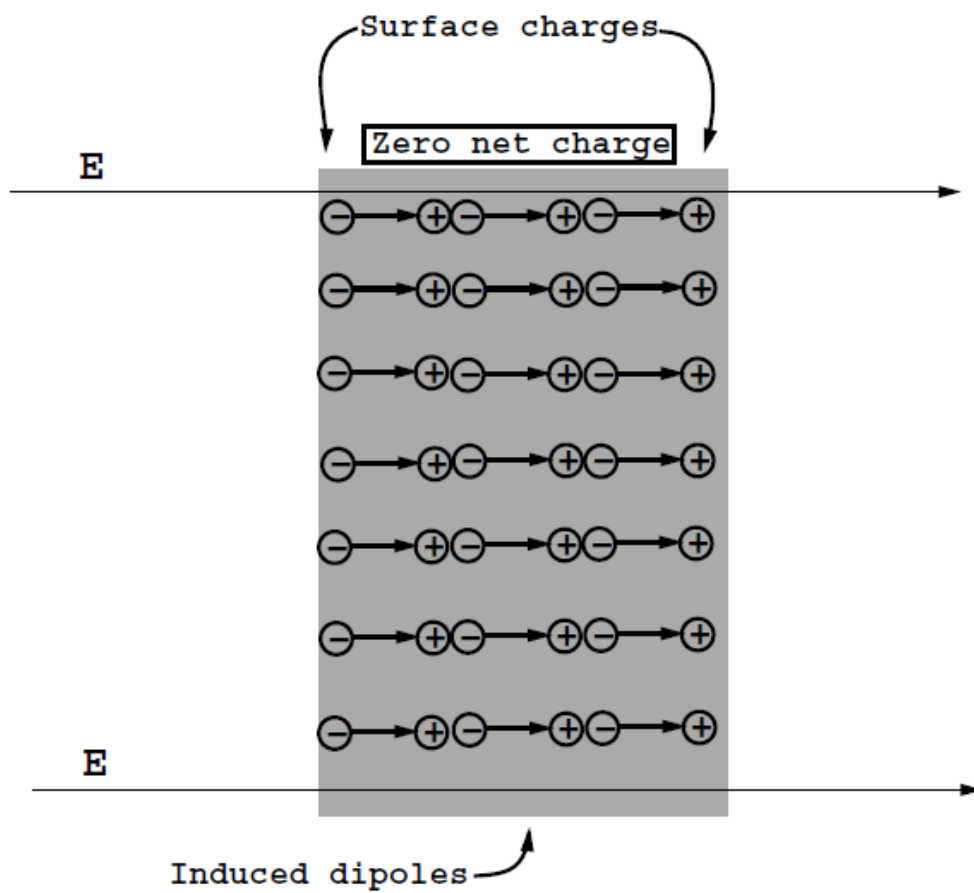


Figure 4-3. Formation of induced surface charges at the edge of a protein in an electric field (E). The electric field magnifies the intrinsic dipole of the backbone amides which cancel out except at the surface.

an effect (Figure 4-3). An electric field across a dielectric boundary will induce a surface charge which itself acts as a new field source. Therefore, when a charge is located within a low dielectric medium, it will create an electric field at the dielectric boundary, which will then induce a surface charge with an opposite sign. The influence of the induced surface charge will

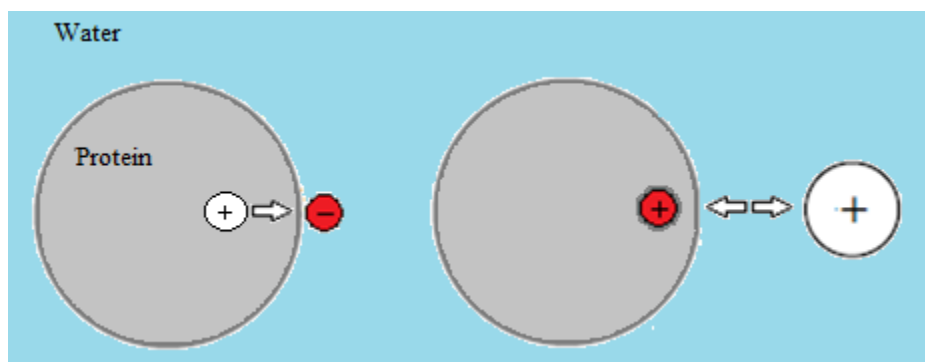


Figure 4-4. Left) A charge located in a low dielectric medium is attracted to the induced surface charge, which can be represented by placing an opposite charge directly across the dielectric boundary in the high dielectric medium (red circle). Right) Because of solvation effects, a charge located in a high dielectric medium will be repelled by a low dielectric medium. The effect of the charge can be represented by placing a mirror-image charge in the low dielectric medium (red circle).

be equivalent to placing a point charge of opposite sign in the high dielectric medium directly across from the original charge. In other words, the intrinsic charge is attracted towards the surface of the protein (Figure 4-4). To consider the effect that a point charge located in a high dielectric medium will have on the low dielectric medium, the concept of solvation must be revisited. The solvation of an atom or a molecule will be determined by several factors, including the hydrophobic effect and van der Waals interactions, and electrostatic energy. When a charge is placed in a solvent, it will polarize the solvent, which in turn produces a reaction potential (i.e. a surface charge). Subsequently, the original charge will interact with the induced surface charge, thereby stabilizing itself (Figure 4-4). Now when a solvated charge approaches a dielectric boundary, it will repel the low dielectric medium to remain optimally solvated. Conversely, a

charge located within a high dielectric medium placed next to a low dielectric medium will wish to maximize its solvation energy by immersing itself in the high dielectric medium. Therefore the influence of the point charge in the high dielectric medium can be represented by placing a charge of the same sign in the low dielectric medium, which in the case of this work is a protein (Figure 4-4). This repulsion of the point charge (i.e. salt) and the low dielectric medium (i.e. protein) is an unfavorable interaction, leading to the destabilization of the protein. At high salt concentrations, the entropy of the system will force the salt species to be in the near vicinity of the protein. As the concentration of the salt increases, so will the number of induced point mirror-image charges, and at a certain point the number of unfavorable interactions between the salt and the induced mirror-image charges within the protein will lead to protein aggregation and precipitation.

Leading up to that point however, the induced point charges will actually stabilize the folded state of the protein. Since proteins can exist in the folded state or unfolded state, the total surface area of the protein can vary (Figure 4-5). While both forms of the protein will have destabilizing induced point mirror-image charges, the folded form of the protein will have less since it has a smaller surface area than the unfolded state. In other words, the larger surface area of the unfolded state will have more room to interact with the ionic species present in solution,

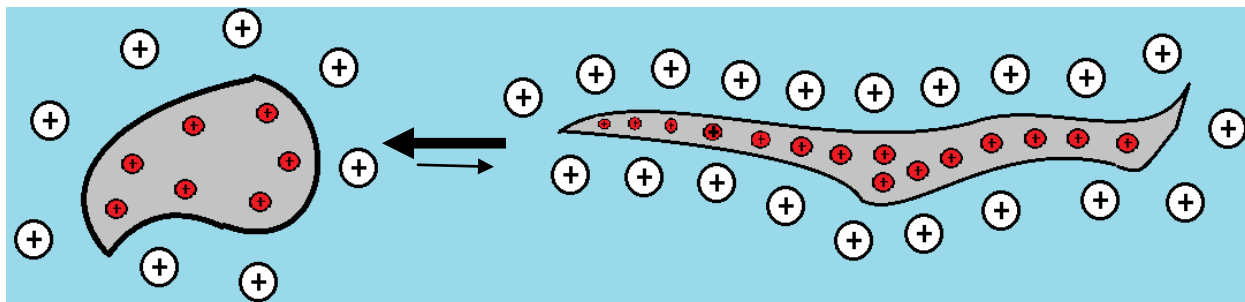


Figure 4-5. Illustration representing the relative effect of induced point image charges on the folded and unfolded states of a protein. The folded state (left) of a protein will be stabilized relative to the unfolded state (right) since it has a smaller surface area and therefore fewer destabilizing interactions between the cations in solution and their induced point mirror-image charge.

leading to a greater number of induced point mirror-image charges and a greater number of unfavorable interactions. Therefore, since it will have less induced point mirror-image charges, the folded state will be stabilized relative to the unfolded state of the protein.

In 2005, the model of Kirkwood and Tanford was expanded by Zhou (1). This model characterizes the reasons for the increase in protein solubility at low salt concentrations ($< 0.2\text{M}$) and the decrease in solubility observed at high salt concentrations ($> 0.3\text{M}$) (1) and offers a quantitative method to determine the amount of work necessary to salt-out a protein (1). Zhou concluded that the work necessary to salt-out a protein has a quadratic dependence on the square root of the ionic strength of the solvent (1). Afterwards, they demonstrate the validity of their model by characterizing the relationship between the salt concentration and the conformational stability of FK506-binding protein (12) and cold shock proteins (13). They clearly demonstrate that, under high salt concentrations, the induced point image charges will contribute significantly to the stability of the protein. The work presented here will use this theoretical analysis to study the impact of the aforementioned interactions by characterizing their effect on the model protein RNase t1.

4.2 Characterizing the thermodynamics of RNase t1 unfolding

The fluorescence spectrum of RNase t1 is sensitive to its environment. In the folded state (solid line Figure 4-6a), the maximal emission wavelength is $\sim 320\text{nm}$, while in the unfolded state (dashed line Figure 4-6a) the maximal emission red shifts to $\sim 355\text{nm}$ (14). However, the peak at 320nm has a strong contribution from the water Raman band, which is evident in the unfolded state spectrum (dashed line Figure 4-6a), and so the unfolding of the protein will be monitored by following the ratio of the emission at 330nm (F_{330}) and 350nm (F_{350}). This technique has been used repeatedly by different research groups to characterize the unfolding of RNase t1

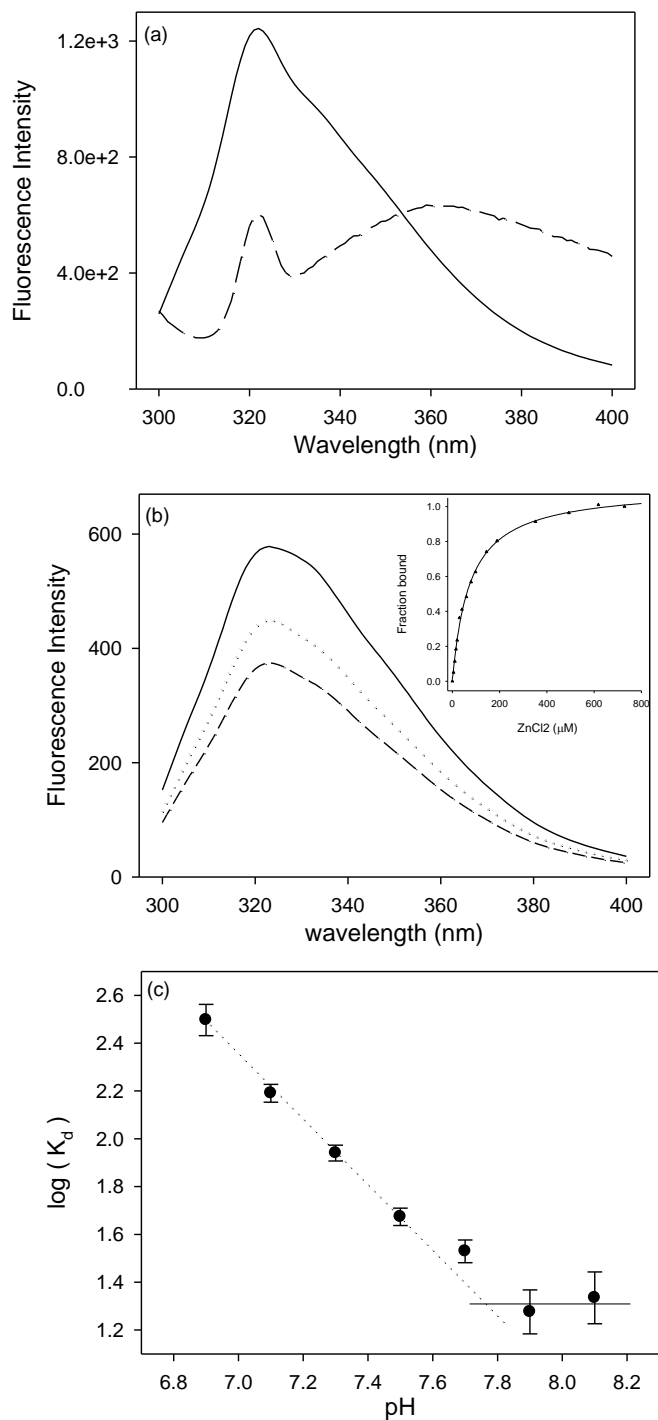


Figure 4-6 a) The fluorescence spectrum of RNase t1 in the folded (solid line) and unfolded (dashed line) forms, showing the Raman peak at 320 nm. b) The fluorescence spectrum of the folded state of RNase t1 in the presence of 0 μM ZnCl₂ (solid line), 50 μM ZnCl₂ (dashed line) and 50 μM ZnCl₂ and 100 mM MgCl₂ (dotted line). The inset fits the data to a hyperbolic binding curve. c) The pH dependence of the dissociation constant, K_d , of the Zn²⁺ ligand concentration in μM units.

(15, 16-19). As a control, I measured the fluorescence spectrum of RNase t1 in high salt concentration and I found no significant change in fluorescence intensities, with the exception of $ZnCl_2$, which quenches the fluorescence of RNase t1 upon binding (dashed line Figure 4-6b). The quenching of RNase t1 fluorescence by zinc can be fit to a hyperbolic binding profile (inset Figure 4-6b). To characterize the effects of chloride salts on the conformational stability of RNase t1, I first measured the unfolding of RNase t1 at low ionic strength by monitoring the ratio F_{330}/F_{350} . Figure 4-7 plots the changes in F_{330}/F_{350} versus the denaturant concentration. As discussed in the first chapter of this work, the thermodynamic unfolding pathway of RNase t1 is a two-state mechanism, and so the unfolding free energy ($\Delta G_{unfolding}^o$) can be easily obtained using the following equation (20):

$$\frac{F_{330}}{F_{350}} = y = \frac{y_f + m_f[\text{urea}] + (y_u + m_u[\text{urea}]) \exp\left(-\frac{\Delta G_{unfolding}^o - m[\text{urea}]}{RT}\right)}{1 + \exp\left(-\frac{\Delta G_{unfolding}^o - m[\text{urea}]}{RT}\right)} \quad (4-1)$$

where y_f and m_f , y_u , and m_u are the slope and intercept of the pre and post-transition baselines, $[\text{urea}]$ is the concentration of urea, $\Delta G_{unfolding}^o$, is the standard free energy for protein unfolding and m is a measure of the cooperativity of $\Delta G_{unfolding}^o$ on the urea concentration. The specific fit in Figure 4-7 yields the following parameters: $\frac{\Delta G_{unfolding}^o}{RT} = 10.01 \pm 0.01$, $\frac{m}{RT} = 2.012 \pm 0.001$ and $[\text{urea}]_{1/2} = 5.10 \pm 0.05M$, where $[\text{urea}]_{1/2}$ is the midpoint concentration of the unfolding curve. It is important to note that since these unfolding experiments are done on samples that are each individually prepared and left to stand overnight, issues of sample variations and reproducibility become important. In order to have reliable data, about 20 measurements of the

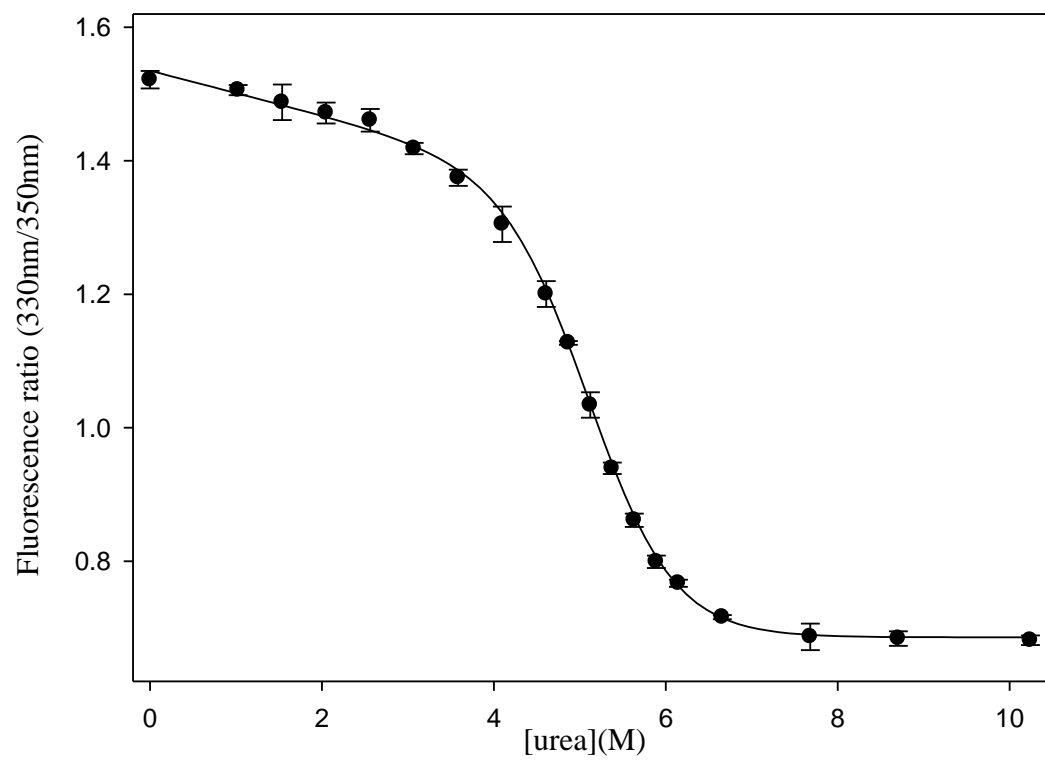


Figure 4-7. The unfolding of RNase t1 dissolved in pH 7 buffer at low ionic strength. The solid line is the best fit to equation 4-1.

unfolding of RNase t1 in pH 7 buffer at low ionic strength (50mM NaCl) have been performed. All these fits are well correlated with equation 4-1 and the following mean values of the parameters from fitting the 20 repetitions are obtained: $\frac{\Delta G_{unfolding}^0}{RT} = 9.6 \pm 0.5$, $\frac{m}{RT} = 2.9 \pm 0.1$ and $[urea]_{1/2} = 5.2 \pm 0.3M$. These values are consistent with literature values (21, 22).

4.3 Effect of alkali chlorides on the unfolding of RNase t1

Now that I have a reliable method to determine the free energy of unfolding of RNase t1, I can determine the relative impact of monoprotic chlorides on the unfolding of RNase t1. Figure 4-8a, 4-9a and 4-10a show the effects of the alkali chloride salts NaCl, KCl and LiCl respectively on the unfolding profile of RNase t1 as defined by the F_{330}/F_{350} ratio. As can be seen in Figure 4-8, 4-9 and 4-10, the addition of salt dramatically increases the stability of the enzyme. All of the data has been fitted to equation 4-1 and the fitting parameters $\frac{\Delta G_{unfolding}^0}{RT}$, $\frac{m}{RT}$ and the R^2 values are listed in Table 4-1 for the alkali chlorides. In addition, the contribution of the salt to the standard unfolding energy of RNase t1, $\frac{\Delta\Delta G_{unfolding}^0}{RT}$, have been listed in Table 4-1. This value at any given salt concentration is defined as $\frac{\Delta\Delta G_{unfolding}^0[S]}{RT} = \frac{\Delta G_{unfolding}^0[S]}{RT} - \frac{\Delta G_{unfolding}^0[NaCl_{0.05M}]}{RT}$.

The free energy of unfolding of a protein is often correlated with the ionic strength of the solvent (23, 24). I have plotted the $\frac{\Delta\Delta G_{unfolding}^0[S]}{RT}$ against the ionic strength of the solvent in Figures 4-8b, 4-9b, and 4-10b and fit the data to equation 4-2:

$$\frac{\Delta\Delta G_{unfolding}^0[S]}{RT} = a * I \quad (4-2)$$

The results of fitting the data from Figure 4-8b, 4-9b and 4-10b to equation 4-3 are listed in Table 4-4. The data is indeed well correlated with equation 4-3, but as will be discussed the next

section, interpreting our results on the basis of equation 4-3 is problematic.

$$\frac{\Delta\Delta G_{unfolding}^{\circ}[S]}{RT} = \Delta n \ln(1 + K * [ligand]) \quad (4-3)$$

4.4 The effect of zinc on the unfolding of RNase t1

In addition to alkali chloride salts, I have investigated the effect of zinc on the unfolding of RNase t1. As was mentioned above, Zn^{2+} binds specifically to RNase t1 and inhibits catalysis through a pH dependent mixed mechanism at micromolar concentrations (26). Additionally, the binding of Zn^{2+} ions quenches RNase t1 fluorescence through an electron transfer mechanism since there is no spectral overlap between the absorbance of $ZnCl_2$ and RNase t1 fluorescence, thereby ruling out FRET. Also zinc has an ionization potential of $\sim -9.39eV$ (27) and can therefore accept an electron from an excited tryptophan that has an ionization potential of $\sim 7.8eV$ (28).

I have also studied the temperature dependence of $ZnCl_2$ on binding to RNase t1. The results show that between 5 and 40°C, the binding constant K_b , defined as $\log(K_d) = 6 - \log(K_b)$ follows a linear Van't Hoff behavior that is expressed by the linear equation $\ln K_b = -(13,000 \pm 2,000) * \frac{1}{T} + (35 \pm 4)$. I observed this strong temperature dependence solely in the case of zinc binding, indicating a strong enthalpic contribution. I have also noted a strong pH dependence to zinc binding, shown in Figure 4-6c. The data from Figure 4-6c demonstrates that the binding of zinc involves a moiety with a pK_a close to 7.7, a value far removed from the pK_a values ~ 4 of surface carboxylates (29, 30). Since RNase t1 lacks free cysteines, who have can have pK_a values from 7.4-9.1 in polypeptides (31), I suggest that it is likely that histidine residue(s) are involved in the zinc binding process. The effect of $ZnCl_2$ on the RNase t1 folding

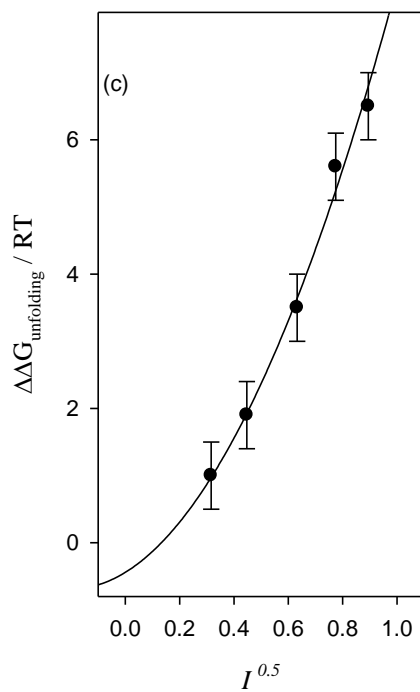
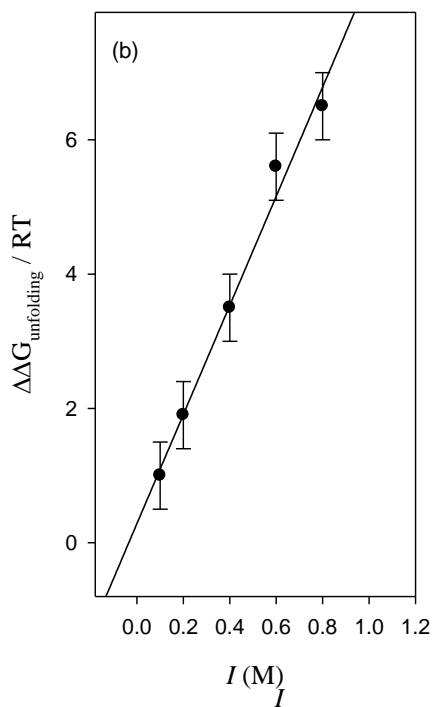
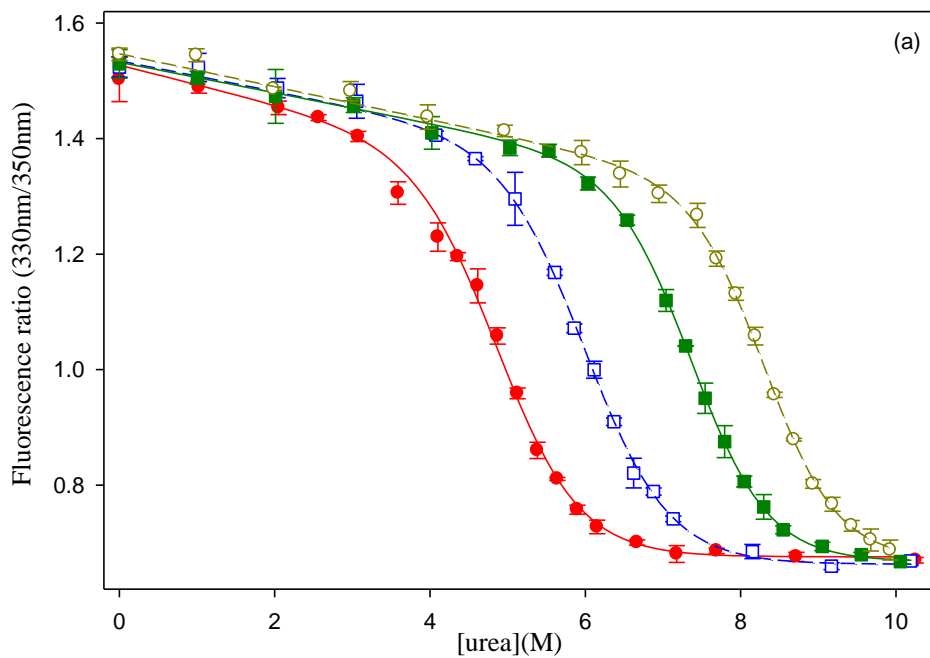


Figure 4-8 a) The unfolding profile of RNase t1 at increasing NaCl concentrations (0.05-1M). b) The dependence of $\frac{\Delta\Delta G_{\text{unfolding}}^0}{RT}$ on the ionic strength of the solvent. The solid line is the best fit to equation 4-2. c) The dependence of $\frac{\Delta\Delta G_{\text{unfolding}}^0}{RT}$ on the square root of the ionic strength of the solvent. The solid line is the best fit to equation 4-11.

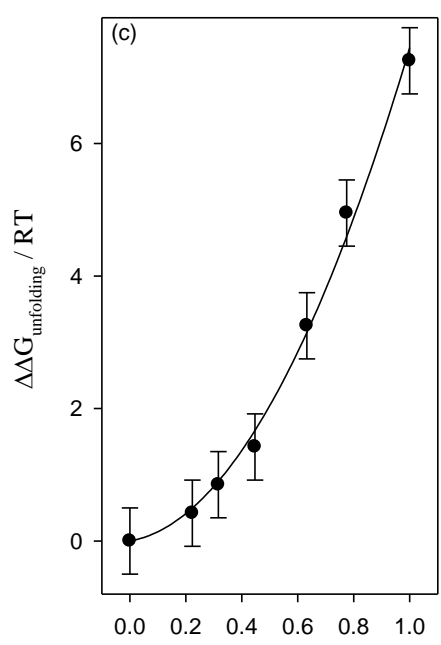
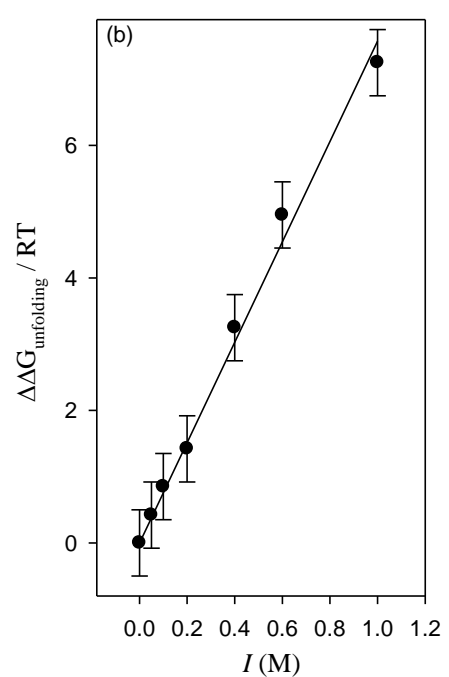
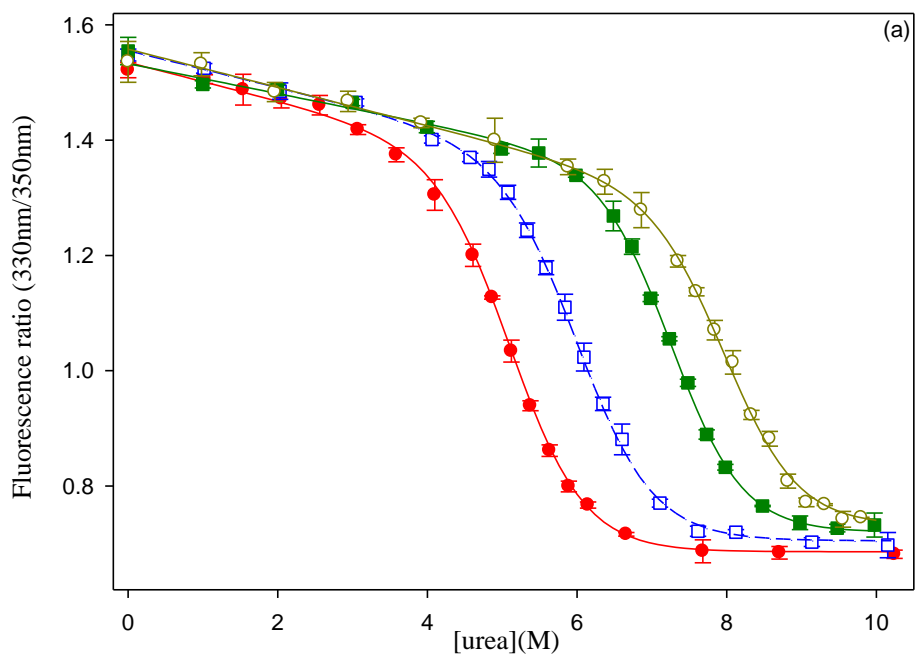


Figure 4-9 a) The unfolding profile of RNase t1 at increasing KCl concentrations (0.1-1M). b) The dependence of $\frac{\Delta\Delta G_{unfolding}^0}{RT}$ on the ionic strength of the solvent. The solid line is the best fit to equation 4-2. c) The dependence of $\frac{\Delta\Delta G_{unfolding}^0}{RT}$ on the square root of the ionic strength of the solvent. The solid line is the best fit to equation 4-11.

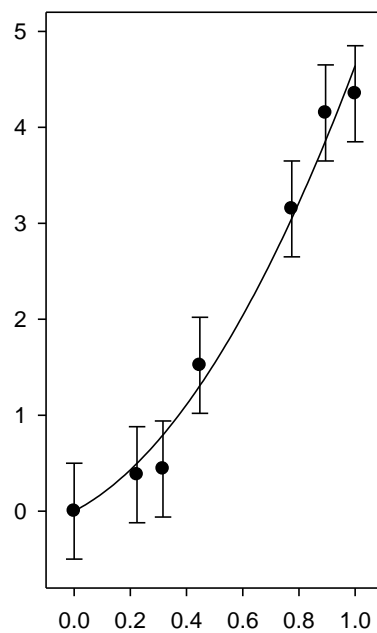
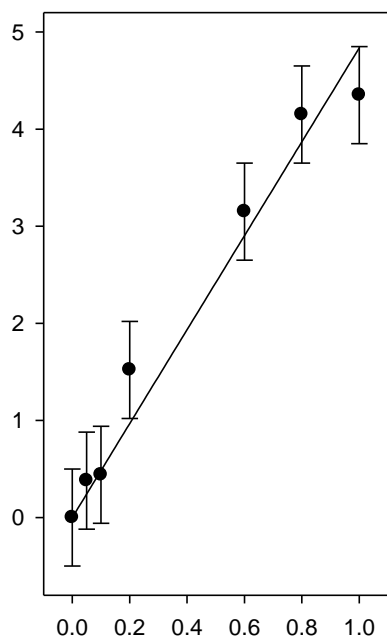
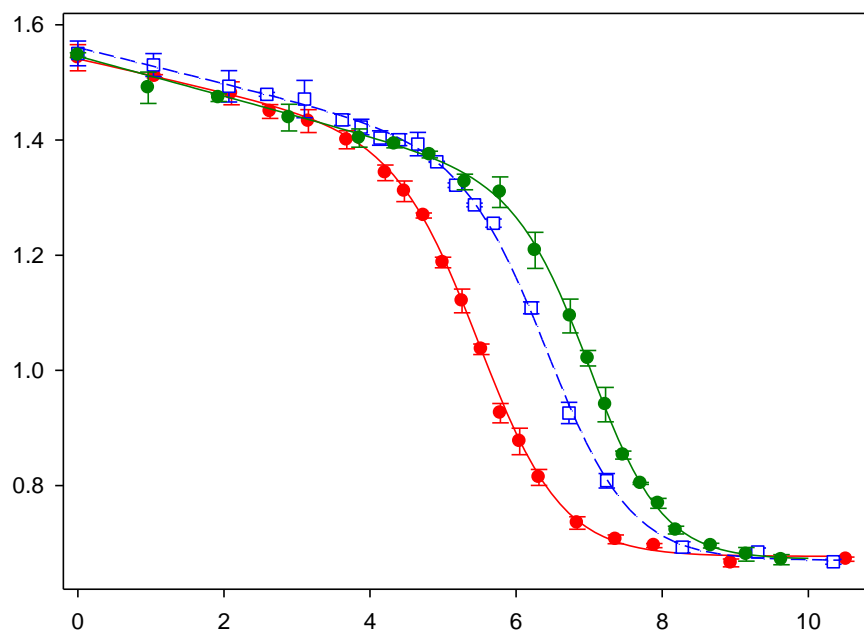


Figure 4-10 a) The unfolding profile of RNase t1 at increasing LiCl concentrations (0.1-1M). b) The dependence of $\frac{\Delta\Delta G_{unfolding}^0}{RT}$ on the ionic strength of the solvent. The solid line is the best fit to equation 4-2. c) The dependence of $\frac{\Delta\Delta G_{unfolding}^0}{RT}$ on the square root of the ionic strength of the solvent. The solid line is the best fit to equation 4-11.

Table 4-1. The effect of alkali chloride salts on the unfolding profile of RNase t1.

(M)	$\frac{\Delta G_{unfolding}^o}{RT}$	$\frac{m}{RT}$	R^2	$\frac{\Delta\Delta G_{unfolding}^o}{RT}$
[NaCl]				
0.1	10.64 ± 0.01	1.882 ± 0.002	0.999	1.0 ± 0.5
0.2	11.51 ± 0.02	1.851 ± 0.003	0.998	1.9 ± 0.5
0.4	13.07 ± 0.01	1.862 ± 0.001	0.999	3.5 ± 0.5
0.6	15.24 ± 0.03	2.014 ± 0.004	0.998	5.6 ± 0.5
0.8	16.14 ± 0.02	1.991 ± 0.002	0.997	6.5 ± 0.5
1.0	18.04 ± 0.01	2.121 ± 0.001	0.999	8.4 ± 0.5
[KCl]				
0.05	10.02 ± 0.01	2.010 ± 0.001	0.999	0.4 ± 0.5
0.1	10.45 ± 0.02	2.012 ± 0.003	0.999	0.9 ± 0.5
0.2	11.02 ± 0.01	1.946 ± 0.001	0.999	1.4 ± 0.5
0.4	12.85 ± 0.03	1.861 ± 0.004	0.999	3.3 ± 0.5
0.6	14.55 ± 0.02	2.102 ± 0.001	0.999	5.0 ± 0.5
1.0	16.85 ± 0.02	2.031 ± 0.002	0.999	7.3 ± 0.5
[LiCl]				
0.05	9.98 ± 0.01	1.734 ± 0.002	0.999	0.4 ± 0.5
0.1	10.04 ± 0.01	1.701 ± 0.003	0.998	0.5 ± 0.5
0.2	11.12 ± 0.04	1.737 ± 0.001	0.996	1.5 ± 0.5
0.6	12.75 ± 0.01	1.830 ± 0.004	0.995	3.2 ± 0.5
0.8	13.75 ± 0.03	1.962 ± 0.002	0.997	4.2 ± 0.5
1.0	13.95 ± 0.02	1.993 ± 0.005	0.996	4.9 ± 0.5

Table 4-2. The effect of divalent salts on the unfolding profile of RNase t1.

(M)	$\frac{\Delta G_{unfolding}^o}{RT}$	$\frac{m}{RT}$	R^2	$\frac{\Delta\Delta G_{unfolding}^o}{RT}$
[MgCl ₂]				
0.05	11.90 ± 0.01	2.071 ± 0.002	0.996	2.3 ± 0.5
0.2	14.02 ± 0.03	1.923 ± 0.003	0.998	4.4 ± 0.5
0.4	16.04 ± 0.01	2.042 ± 0.001	0.999	6.4 ± 0.5
0.8	18.60 ± 0.03	1.926 ± 0.004	0.999	9.0 ± 0.5
1.0	19.92 ± 0.01	2.023 ± 0.001	0.997	10.3 ± 0.5
[ZnCl ₂]				
0.0001	10.02 ± 0.01	2.010 ± 0.001	0.999	0.4 ± 0.5
0.0002	10.45 ± 0.02	2.012 ± 0.003	0.999	0.9 ± 0.5
0.0004	11.02 ± 0.01	1.946 ± 0.001	0.999	1.4 ± 0.5
0.0006	12.85 ± 0.03	1.861 ± 0.004	0.999	3.3 ± 0.5

Table 4-3. Parameters obtained from fitting data listed in Table 4-1, 4-2 to equation 4-2.

Salt	a	R^2
NaCl	8.5 ± 0.1	0.992
KCl	7.5 ± 0.1	0.992
LiCl	4.8 ± 0.2	0.966
MgCl ₂	3.8 ± 0.4	0.844

Table 4-4. Parameters obtained from fitting data in Table 4-1, 4-2 to equation 4-3.

Salt	Δn	$K (M^{-1})$	R^2
NaCl	12 ± 3	0.2 ± 0.1	0.995
KCl	9 ± 3	0.4 ± 0.1	0.997
LiCl	1.8 ± 0.3	1.9 ± 0.4	0.990
MgCl ₂	1.9 ± 0.2	10 ± 2	0.992
ZnCl ₂	Set to 1	6000 ± 200	0.980

Table 4-5. Parameters obtained from the data in Table 4-1 using equation 4-11.

Salt	b'	c'	R^2
NaCl	1.0 ± 0.3	7.3 ± 0.4	0.995
KCl	0.7 ± 0.3	6.7 ± 0.3	0.994
LiCl	1.5 ± 0.4	3.1 ± 0.4	0.982

profile has been investigated and is shown in Figure 4-11a. The concentration of ZnCl_2 is less than 1 mM and therefore cannot affect the protein through electrostatic interactions. And so I can conclude that the observed increase in protein stability is due to ligand binding, rather than electrostatic or salting-in effects. The data in Figure 4-11a has been fit to equation 4-2 and the fitting parameters are listed in Table 4-2. The obtained values of $\frac{\Delta\Delta G_{unfolding}^0}{RT}$ are plotted against ZnCl_2 and the data is fit to equation 4-3 with only 1 binding site yielding a binding constant $K = 6,000 \pm 200\text{M}^{-1}$, which is similar to the result obtained from Figure 4-6c. The fitting parameters of equation 4-3 have been listed in Table 4-4. It is important to note that all ZnCl_2 concentrations have been kept below the solubility limit of zinc hydroxide.

4.5 The effect of magnesium on the unfolding of RNase t1

Finally, the effect of MgCl_2 on the unfolding of RNase t1 has been investigated. As can be seen in Figure 4-12, magnesium significantly increases the unfolding energy of the enzyme. The data has been fit to equation 4-1, and the values of $\frac{\Delta G_{unfolding}^0}{RT}$, $\frac{\Delta\Delta G_{unfolding}^0}{RT}$, $\frac{m}{RT}$ and the R^2 have been listed in Table 4-2. I have also examined the effect of MgCl_2 on the fluorescence spectrum of RNase t1. As was discussed earlier, the addition of ZnCl_2 quenches the fluorescence of RNase t1, however when I add 100mM MgCl_2 to a solution of RNase t1 containing 50 μM ZnCl_2 , I see a 30% recovery of fluorescence (Figure 4-6b). None of the alkali salts caused a similar recovery of fluorescence. Because the Mg^{2+} ion cannot receive an electron from an excited tryptophan residue, it is likely that this fluorescence recovery is due to the magnesium ion binding to the enzyme and replacing some of the zinc ligands. This demonstrates that the Mg^{2+} ion behaves similarly to the Zn^{2+} ion and binds to RNase t1. I can confirm this by plotting the data in Figure 4-12 to the classical binding model (equation 4-3), the result of which is shown in Figure 4-13.

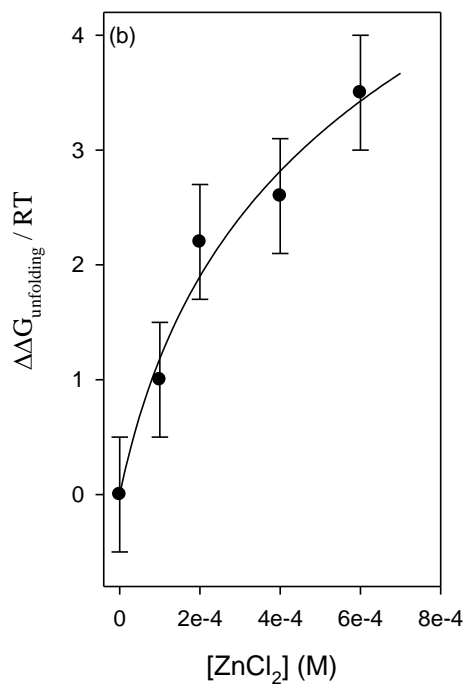
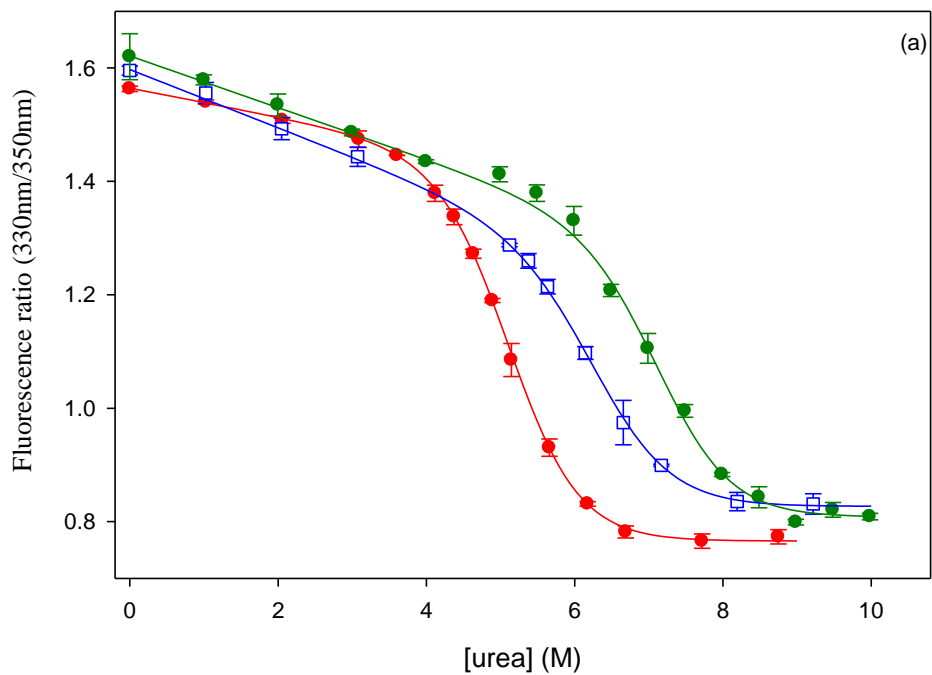


Figure 4-11. a) The unfolding profile of RNase t1 at increasing ZnCl₂ concentrations (100-600 μM) b) The dependence of $\frac{\Delta\Delta G_{\text{unfolding}}^0}{RT}$ on the ZnCl₂ concentration. The solid line is the best fit to equation 4-3.

The parameters obtained from this fit are shown in Table 4-4 with a very reasonable fit ($R^2 = 0.992$). A binding constant of $\sim 10M^{-1}$ for magnesium is obtained.

4.6 Applicability of the binding model

My study of salt effects on the unfolding free energy of RNase t1 has shown that the presence of NaCl, KCl and LiCl in solution stabilizes the folded form of RNase t1 relative to the unfolded form. It has been suggested that the observed increase in protein stability is due to cation binding to surface carboxylates of the protein (21, 32). However the results of my work again argue against this explanation. First of all, there is an apparent contradiction that exists between the extremely small binding constants of sodium and potassium coupled with their high number of binding sites. Conversely, the smaller, more penetrable ion lithium has only two binding sites coupled with a much larger binding constant than either sodium or potassium (see data in Table 4-3). Therefore, a paradox seems to exist, namely that the weaker interacting ions (sodium and potassium) interact with a larger number of sites on the enzyme surface.

The pH-dependent studies of Zn^{2+} binding also disagree with previous finding. The data in Figure 4-6c suggests there is a low probability that carboxylate residues are involved in cation binding for zinc and magnesium ions, and perhaps other cations as well. The reason for this discrepancy is that Saenger (32) obtained his crystals at pH 5.2, in which according to Figure 4-6c and enzyme inhibition studies, zinc binding is at a minimum. The crystals cannot be collected at neutral pH because zinc ion precipitates out as zinc hydroxide at millimolar concentrations. However, if I simplify equation 4-3 by applying the linear approximation at small $K I$ I obtain:

$$\frac{\Delta\Delta G_{unfolding}^o[S]}{RT} = \Delta n \ln(1 + K * [ligand]) \approx \Delta n * K * [ligand] \quad (4-4)$$

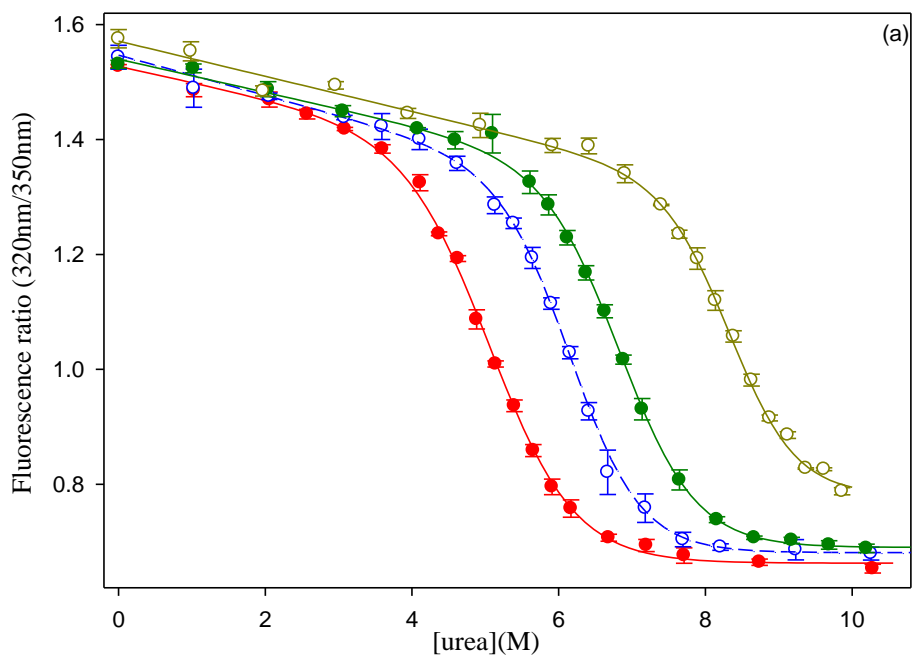


Figure 4-12. The unfolding profile of RNase t1 at increasing $MgCl_2$ concentrations (0.05-1M).

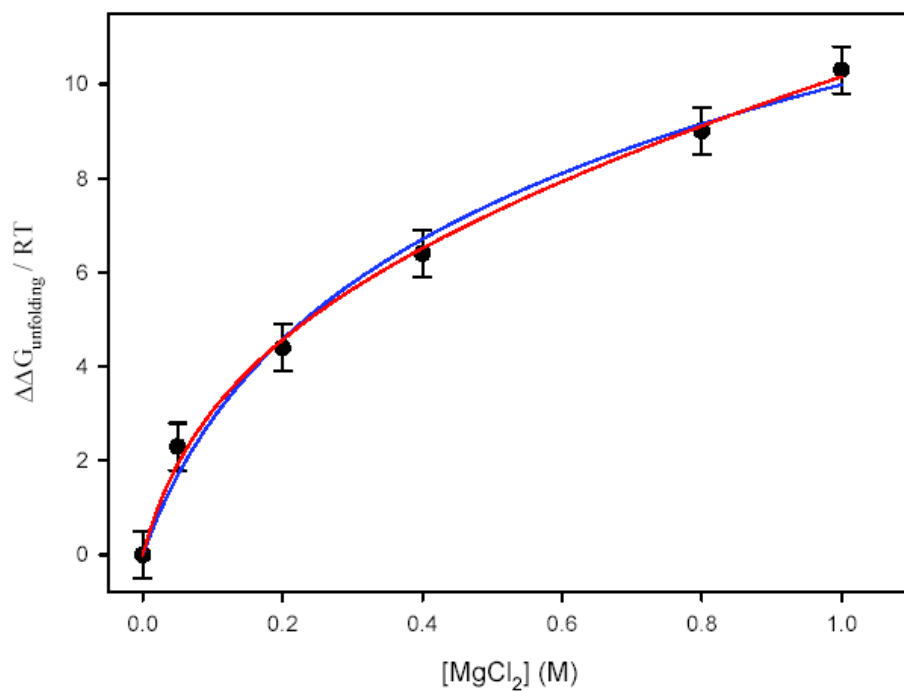


Figure 4-13. The dependence of $\frac{\Delta\Delta G_{unfolding}^0}{RT}$ on $MgCl_2$ concentration. The solid blue line is the best fit to equation 4-2 and the solid red line is the best fit to equation 4-18.

This type of a linear relationship is often seen in studies of the salt effect on protein; the linear relationship between unfolding free energy and ionic strength is usually attributed to chaotropic or kosmotropic salt effects (23, 33). This relationship is equivalent to the linear relationship of equation 4-2, and so $a = \Delta n * K$. The values of a (Table 4-3) follow the order $a_{\text{NaCl}} > a_{\text{KCl}} > a_{\text{LiCl}}$. If I consider the values of Δn to be identical for all monoprotic salts, the values of K will follow the same order: $K_{\text{NaCl}} > K_{\text{KCl}} > K_{\text{LiCl}}$. These obtained values seem more reasonable since it seems unlikely that the number of surface sites available for the small, very penetrable lithium ion will be significantly less than sodium. In fact, if the LiCl data is fitted to the classical binding equation (equation 4-2) and Δn is set as greater than 7, I obtain a reasonable fit ($R^2 > 0.97$). In addition, if Δn is set to 10 binding sites (the average of sodium and potassium), the values of K for all three monoprotic salts investigated would be smaller than 1 M^{-1} . The arbitrary manipulation of the number of binding sites has no effect on the quality of the fit; therefore the binding seems to be the result of a fitting artifact. Most importantly however, is the fact that when apparent binding constants (K) are so low, it is more appropriate to consider them as solvent exchange constants (34, 35), rather than binding constants. Applying classical binding models to these cases often lead to non-physical results, and the enhanced unfolding free energy observed is the results of salt exchanging with water molecules in the protein's hydration shell as opposed to any specific interaction between protein and salt (36).

4.7 Contributions of salting-in and salting-out effects to protein stability

I can now discuss the involvement of salting-in and salting-out effects in the stabilization of RNase t1. As was discussed earlier, the placing of a point charge (i.e. salt) in the near vicinity of a low-dielectric medium (i.e. proteins) will lead to increased salting-out effects via the induction

of a mirror-charge in the low-dielectric medium. However, the increased salt effect will also be accompanied by an increase in the ionic strength of the solvent, leading to an increase in the favorable salting-in effects. In the absence of any specific interaction, as is the case for some monoprotic salts studied here, the salt contribution to the standard unfolding energy $\left(\frac{\Delta\Delta G_{unfolding}^o}{RT}\right)$ of RNase t1 in the presence of salt can be defined as:

$$\begin{aligned} \left(\frac{\Delta\Delta G_{unfolding}^o}{RT}\right) &= \left(\frac{\Delta\Delta G_{unfolding}^o}{RT}\right)_{salting-out\ folded} + \left(\frac{\Delta\Delta G_{unfolding}^o}{RT}\right)_{salting-out\ unfolded} + \\ &\left(\frac{\Delta\Delta G_{unfolding}^o}{RT}\right)_{salting-in\ folded} + \left(\frac{\Delta\Delta G_{unfolding}^o}{RT}\right)_{salting-in\ unfolded} \end{aligned} \quad (4-5)$$

In the above equation, the salting-in contribution is due to Debye-Hückel interactions. This type of interaction has two aspects (charge screening and charge solvation) that will stabilize either the folded or unfolded form to a greater extent relative to the other.

4.7.1 Salting-in effects: charge solvation. As I saw in the first chapter, each charged residue on the protein will induce a counterion cloud in the solvent which will have a stabilizing effect when salt ions are present by affecting the solvation energy of the protein. The Poisson-Boltzman continuum model can be used to provide a description of solvation effects, but it is time consuming and computationally expensive. A relatively simple model, the generalized Born model, has been developed that gives a good account of the effects of Debye-Hückel interactions on protein stability. According to the generalized Born approximation method (37), the solvation energy of a charged group can be defined as:

$$\Delta G_{solvation} = \frac{Aq^2}{r} * \left(1 - \frac{e^{-\kappa r}}{\epsilon_s}\right) * f \quad (4-6)$$

where A is a unit dependent constant, q is the magnitude of the charge, ϵ_s is the dielectric constant of the solvent, r is the Born radius of the charge group, $\kappa = 0.3\sqrt{I}$ is the Debye-Hückel

screening parameter and f is the fraction of the area of the charged group that is solvent accessible. In the unfolded state, the fraction of the exposed charged residues on the surface of the protein would be greater than those same residues in the folded state ($f_{unfolded} \gg f_{folded}$). In addition, the increase in the local dielectric constant experienced by the charged residue would be greater in the unfolded state. This combination would cause the $\Delta G_{solvation-folded}$ to be smaller than the $\Delta G_{solvation-unfolded}$, which would cause a reduction of the magnitude of $\left(\frac{\Delta\Delta G_{unfolding}^0}{RT}\right)$ and effectively reduce the stability of the folded state relative to the unfolded state (12). That is to say the unfolded form of RNase t1 would be stabilized relative to the folded form by this first Debye- Hückel type interaction.

4.7.2 Salting-in effects: charge screening. The second Debye- Hückel type interaction will be manifest by the salts weakening interactions between charged residues located in close proximity in the protein (i.e. charge screening by salts). Interactions between two charged groups will have the form;

$$\Delta G_{screening} = B \frac{q_1 q_2}{\epsilon_s d} * \left(1 - \frac{e^{-\kappa d}}{\epsilon_s}\right) \quad (4-7)$$

where B is a unit dependent constant, q_1 , and q_2 are the magnitude of each charge, κ and ϵ_s have the same definition as in equation 4-6 and d is the distance between the two charges. Since the charged residues are much closer to each in the folded state than the unfolded state ($d_{folded} \ll d_{unfolded}$), the charge-charge interactions will be much stronger in the folded form of the protein and the charge screening will have a greater impact on the folded form of the protein (1). As I discussed earlier, the net effect of charge screening depends on the charge distribution of the protein in question. Charge screening will have a strong impact on RNase t1 specifically since it has a large number of charged residues (16) and 12 of those residues are negatively charged,

causing a strong overall negative charge. The repulsion of these negative residues is the dominant charge-charge interaction in the folded state of the protein and the introduction of salt will screen these repulsive interactions. This will cause an increase of the magnitude of $\left(\frac{\Delta\Delta G_{unfolding}^o}{RT}\right)$ and effectively stabilize the folded form of the enzyme. Therefore, the overall salting-in effect on highly charged proteins is a sum of Debye- Hückel interactions that stabilize both the unfolded (solvation energy) and folded form (charge screening) to almost the same extent. These contributions are clearly ionic strength dependent and are expressed as:

$$\left(\frac{\Delta\Delta G_{unfolding}^o}{RT}\right)_{salting-in\ folded} + \left(\frac{\Delta\Delta G_{unfolding}^o}{RT}\right)_{salting-in\ unfolded} = F(\sqrt{I}) \approx \alpha\sqrt{I} + \beta I + \dots \quad (4-8)$$

The function $F(\sqrt{I})$ depends entirely on ionic strength. Given that the $\left(\frac{\Delta\Delta G_{unfolding}^o}{RT}\right)$ terms are nearly equivalent, $F(\sqrt{I})$ is significantly smaller than either of the $\left(\frac{\Delta\Delta G_{unfolding}^o}{RT}\right)$ terms and can therefore be expanded as a polynomial around I , shown above in equation 4-8. It must be emphasized that none of the terms in equation 4-8 depend on the nature of the salt; salting-in interactions depend solely on the ionic strength of the solvent.

4.7.3 Salting-out effects. In the case of salting-out interactions, it can be assumed that the

magnitude of $\left(\frac{\Delta\Delta G_{unfolding}^o}{RT}\right)_{salting-out\ folded}$ will be much smaller than $\left(\frac{\Delta\Delta G_{unfolding}^o}{RT}\right)_{salting-out\ unfolded}$. This is because the surface area of the folded state is

much smaller than the surface area of the unfolded state. Theoretical work done by Zhou et al.

has shown that $\left(\frac{\Delta\Delta G_{unfolding}^o}{RT}\right)_{salting-out\ unfolded}$ follows the form:

$$\left(\frac{\Delta\Delta G_{unfolding}^o}{RT}\right) = b * \sqrt{I} + c * I \quad (4-9)$$

The parameter b is dependent on the “exclusion diameter” of the salts and is inversely proportional to the exclusion diameter of the salt, while the parameter c is not size-dependent (1). Therefore if I combine equation 4-8 and equation 4-9, the total salt contribution to the standard free energy of unfolding of RNase t1 can be expressed as:

$$\left(\frac{\Delta\Delta G_{unfolding}^o}{RT}\right) = b * \sqrt{I} + c * I + (\alpha\sqrt{I} + \beta I + \dots) = (\alpha + b) * \sqrt{I} + (\beta + c) * I \quad (4-10)$$

In Figure 4-8c, 4-9c and 4-10c, the dependence of $\left(\frac{\Delta\Delta G_{unfolding}^o}{RT}\right)$ on the square root of the ionic strength is shown. The data are fitted to a quadratic of the form:

$$\left(\frac{\Delta\Delta G_{unfolding}^o}{RT}\right) = b' * \sqrt{I} + c' * I \quad (4-11)$$

Where I is once again the ionic strength and b' and c' are constants. The lines in Figure 4-8c, 4-9c and 4-10c are obtained by fitting the data to equation 4-11 and the parameters obtained are listed in Table 4-5. All of $\left(\frac{\Delta\Delta G_{unfolding}^o}{RT}\right)$ values are well correlated with the quadratic equation 4-11 indicating that the contribution of higher terms from equation 4-8 do not contribute significantly. As can be seen in equation 4-10, the experimentally obtained parameter b' is a sum of b (contribution from salting out) and from α (contribution from salting-in). According to the simple continuum model (1), the parameter b decreases as the salt exclusion diameter increases (1) while α is solely dependent on the ionic strength of the solvent. As can be seen below, this trend is indeed observed in the monoprotic data:

$$b'_{KCl}(0.7) < b'_{NaCl}(1.0) < b'_{LiCl}(1.5) \quad (4-12a)$$

and b' follows the opposite trend of d_{ex} :

$$d_{ex-KCl}(3.98\text{\AA}) > d_{ex-NaCl}(3.52\text{\AA}) > d_{ex-LiCl}(3.18\text{\AA}) \quad (4-12b)$$

This observed trend confirms the prediction made by Zhou (1) and indicates that the interaction between the ions in close proximity to the protein and their induced mirror-image charges in the protein play a significant role to the observed salt-induced stability of the protein.

As can be seen from equations 4-10 and 4-11, c' is the sum of contributions of β (from salting-in) and of c (from salting-out). The model also predicts that the parameter c should not significantly change with different monoprotic salts. Additionally, similar to the parameter α , the parameter β should not change as well. Therefore unlike b' , the parameter c' should remain constant for any monoprotic salt. However, the experimentally obtained parameter c' follows the trend:

$$c'_{NaCl}(7.3) \approx c'_{KCl}(6.7) > c'_{LiCl}(3.1) \quad (4-13)$$

As can be seen, the lithium parameter c' differs significantly and does not follow the trend predicted by theory. These values demonstrate that sodium and potassium stabilize the protein to a similar extent but more so than lithium. This trend does not conform to the theoretical prediction (1) but does follow the trend of the Hofmeister series. The parameter c' is modeled simply as an embedded point charge (1), and so any deviation observed experimentally must be due to a salt specific effect. Because chloride is the common counterion in all three monoprotic salts studied, the deviation seen in the trend shown in equation 4-13 must be due to the nature of the cation.

4.8 Return of the lithium anomaly

What distinguishes lithium from potassium and sodium is the aforementioned “lithium anomaly”. As was discussed earlier, lithium has been shown to interact weakly with the amide

bond of peptides (38) and with certain hydrophobic moieties (39). These weak interactions help solubilize the molecules via direct interaction and can counteract the unfavourable salting-out effect. The weak interactions are not localized to specific locations on the protein, and have comparable strength to water molecules interacting with the amide bond of the polypeptide backbone (36). The weak interaction of lithium is analogous to the mode of action of urea which has also been shown to weakly interact with amide bonds through hydrogen bonds (40). However, it must be emphasized that these interactions are not site specific; they are considered to be the sum of a large number of weak interactions that encompass the whole hydration surface of the protein. Thus, when lithium ions replace water molecules in the protein hydration sphere, there are two competing interactions that are affecting the stability of the folded form of the protein. There is the stabilizing effect of salting-out interactions and the destabilizing effect of solubilizing amide bonds and hydrophobic moieties by specific interactions with lithium. This can be represented as:

$$\left(\frac{\Delta\Delta G_{unfolding}^o}{RT}\right)_{LiCl} = \left(\frac{\Delta\Delta G_{unfolding}^o}{RT}\right)_{electrostatic} + \left(\frac{\Delta\Delta G_{unfolding}^o}{RT}\right)_{solubiliziation} \quad (4-14a)$$

By combining with equation 4-11 can be rewritten as:

$$\left(\frac{\Delta\Delta G_{unfolding}^o}{RT}\right) = b' * \sqrt{I} + c' * I + \left(\frac{\Delta\Delta G_{unfolding}^o}{RT}\right)_{solubiliziation} \quad (4-14b)$$

The contribution of $\left(\frac{\Delta\Delta G_{unfolding}^o}{RT}\right)_{solubiliziation}$ is destabilizing and decreases the magnitude of

$\left(\frac{\Delta\Delta G_{unfolding}^o}{RT}\right)$ as the concentration of LiCl increases. At low salt concentrations, this parameter can be assumed to be linearly dependent on salt concentration

$$\left(\frac{\Delta\Delta G_{unfolding}^o}{RT}\right)_{solubiliziation} = -\sigma * I \quad (4-15a)$$

Which, when combined with equation 3-14b yields:

$$\left(\frac{\Delta\Delta G_{unfolding}^o}{RT}\right) = b' * \sqrt{I} + (c' - \sigma) * I \quad (4-15b)$$

The σ represents the destabilizing contribution of the weak lithium interactions, thereby providing an explanation for the inequality observed in equation 4-13.

4.9 Binding contribution of divalent cations to the conformational stability of RNase t1

Interpreting the data of the divalent salts, $MgCl_2$ and $ZnCl_2$, on RNase t1 stability is much simpler. As was expected, the $ZnCl_2$ data follows the classical binding model in a straightforward manner and provides a reasonable binding constant. The case of $MgCl_2$ is a little murkier; the binding model results in the following fit:

$$\frac{\Delta\Delta G_{unfolding}^o}{RT} = \Delta n \ln(1 + K * [ligand]) = 1.9 \ln(1 + 10 * [ligand]) \quad (4-16)$$

The value $n = 1.9$ implies the presence of two binding sites with an average binding constant of 10 M^{-1} . However, the classical binding model does not take into account the possible consequences of exchanging one unit of Mg^{2+} with one molecule of water at high $MgCl_2$ concentrations. This will have a definite impact on the thermodynamics of the folded form of the protein. The replacement of a water molecule by a magnesium ion in the hydration shell will stabilize the folded form of the protein via salting-out interactions, while simultaneously stabilizing the unfolded state via solubilizing interactions similar to those of lithium discussed in the previous section. The theoretical model described throughout this section has been derived using the Poisson-Boltzman distribution (41):

$$\nabla * \epsilon \nabla \Phi_{i0}(r|r_i) = -4\pi e_i \delta(r - r_i) \quad (4-17)$$

where e_i is a *single* point charge. This equation is applicable only when used with *monovalent*

ions. Since I am now discussing a *multivalent* ion (Mg^{2+}) it is not be appropriate to apply this model.

Nevertheless, the effects of point image charges and solubilizing interactions are still the result of a sum of large number of weak interactions. Therefore, in the case of low salt concentrations, I can modify equation 4-16 to obtain:

$$\frac{\Delta\Delta G_{unfolding}^o}{RT} = \Delta n \ln(1 + K * [ligand]) + \phi * c \quad (4-18)$$

The first term describes the contribution of binding and the second term is a linear term that approximates the effects of exchanging MgCl_2 with a water molecule in the protein hydration shell. If I set the number of binding sites to 1, I obtain values of $K = 24 \pm 1\text{M}^{-1}$, $\phi = 2.7 \pm 0.3$ with a very reasonable fit having an $R^2 = 0.997$ (Figure 4-13), without needing to postulate additional binding sites other than the zinc binding site. Therefore it seems reasonable to conclude that magnesium stabilizes the protein through both cation binding and through the salting-out effect.

4.10 Conclusions

This work has investigated the hypothesis that a major contributor to the salt-induced protein stability of the folded state of RNase t1 is the interaction between ions located in the immediate vicinity of the protein and their induced image charges in the low dielectric protein cavity. The data presented here is consistent with the predictions that relate salting-out effects with protein stability. First, the salt effects on RNase t1 manifest themselves via a quadratic dependence of the free energy of unfolding on the square root of the ionic strength of the solvent. Second, because RNase t1 is highly charged, this stabilization has manifested itself in only positive coefficients and third, the stabilization free energy does follow the dependence on salt exclusion

diameter as predicted by the theoretical model.

As a control, I have analyzed the data with the classical binding model. In the case of ZnCl_2 , a known ligand of RNase t1, the classical binding model effectively accounts for the increase in unfolding free energy. However, in the case of the monoprotic salts sodium, potassium and lithium, the classical binding model leads to physically unrealistic results and very small binding constants which would be better classified as solvent exchange constants. In the special case of the weakly interaction cation magnesium, contributions from binding and salting-out effects are necessary to account for the observed increase in protein stability. It must be noted that the “goodness of fit” was not the criterion used to reject the classical binding model. As a matter of fact, equation 4-3 gives a better fit to the data, yet the number of binding sites and strength of binding are contradictory and lead to physically unrealistic results.

Alternatively, the simple continuum model (1) provides a first principles description of the electrostatic interactions that occur when a formal unit of salt replaces one molecule of water that's located in its hydration shell. The fact that the salt-induced stabilization of RNase t1 follows the predictions of the simple continuum model supports its description of the salt-induced electrostatic interactions. The results support the notion that interactions between salt ions in the high dielectric solvent and their induced mirror-image charges in the low dielectric protein are significant contributors to the observed salt-induced increase in protein stability.

Understanding the effects of salts on electrostatic interactions and how they influence protein stability has important implications in the study of protein structure, function and dynamics. Electrostatic interactions play an important role in stabilizing protein structure and can be the origin of dynamic motions in proteins. The effect of salts on various dynamic motions in proteins

have been used to study the role of electrostatic interactions, however, until recently those studies have focused on the effect of salts on various charge-charge interactions and have neglected salting-out effects. The results demonstrate the significance of salting-out interactions on the stability of proteins. In fact, while studying charge-charge interactions, neglecting the contribution from salting-out interactions may lead to overestimating the importance of charge-charge interactions in the case of repulsive forces and underestimating those same interactions in the case of attractive forces.

A specific example of the potential importance of salt effects on protein stability is the study of the thermodynamics of proteins associated with halophilic organisms. Extensive work on halophilic enzymes has shown that the mechanisms by which halophilic and mesophilic variants of the same enzyme are very similar. However, these two types of enzymes are affected differently by high salt concentrations; high salt concentrations inactivate mesophilic enzymes while identical salt concentrations will activate halophilic enzymes. It is possible that this difference is caused by salting-out interactions affecting the mesophilic and halophilic enzymes differently, and so a thermodynamic analysis of the mesophilic and halophilic enzymes could be enlightening.

References

1. Huan-Xiang Zhou. Interactions of macromolecules with salt ions: An electrostatic theory for the hofmeister effect. *Proteins: Structure, Function, and Bioinformatics*. 2005;61:69-78.
2. Miriam Almagor, R. David Cole. In physiological salt conditions the core proteins of the nucleosomes in large chromatin fragments denature at 73°C and the DNA unstacks at 85°C. *The Jour.* 1988;264(11):6515-9.
3. Albrecht Wegner GI. 12-fold difference between the critical monomer concentrations of the two ends of actin filaments in physiological salt conditions. *Proceedings of the National Academy of Sciences*. 1983;80:4922-5.
4. Tamar Schlick, Bin Li, Wilma K. Olson. The influence of salt on the structure and energetics of supercoiled DNA. *Biophysical Journal*. 1994;67(6):2146-66.
5. Franz Hofmeister. Action of salts on proteins. *Arch. exper. Path. Pharma*. 1888;24:247-60.
6. Pierre Bauduin, Fawaz Nohmie, Didier Touraud, Roland Neueder, Werner Kunz, Barry W Ninham. Hofmeister specific-ion effects on enzyme activity and buffer pH: Horseradish peroxidase in citrate buffer. *Journal of Molecular Liquids*. 2005;123(1):14-9.
7. Raul Perez-Jimenez, Raquel Godoy-Ruiz, Beatriz Ibarra-Molero, Jose M Sanchez-Ruiz. The efficiency of different salts to screen charge interactions in proteins: A hofmeister effect? *Biophysical Journal*. 2004;86(4):2414-29.
8. Kim D. Collins. Ions from the hofmeister series and osmolytes: Effects on proteins in solution and in the crystallization process. *Methods*. 2004;34(3):300-11.
9. James M. Broering, Andreas S. Bommarius. Evaluation of hofmeister effects on the kinetic stability of proteins. *Journal of Physical Chemistry*. 2005;109(43):20612-9.
10. John G. Kirkwood. Acid-base equilibrium in solutions of ampholytes. *Annals of the New York Academy of Sciences*. 1941;41:321-8.
11. Charles Tanford, John G. Kirkwood. Theory of protein titration curves. I. general equations for impenetrable spheres. *Journal of the American Chemical Society*. 1957;79(20):5333-9.
12. Daniel S. Spencer, Ke Xu, Timothy M. Logan, Huan-Xing Zhou. Effects of pH, salt and macromolecular crowding on the stability of KF506-binding protein: An integrated experimental and theoretical study. *Journal of Molecular Biology*. 2005;351(1):219-32.
13. Xiaoqin Huang HZ. Similarity and difference in the unfolding of thermophilic and mesophilic cold shock proteins studied by molecular dynamics simulations. *Biophysical Journal*. 2006;91(7):2451-63.
14. Joseph R. Lakowicz. Principles of fluorescence spectroscopy, 3rd edition. *Analytical and Bioanalytical Chemistry*. 2008;390(5):1223-4.

15. Martin J. Scholtz, Gerald R. Grimsley, C. Nick Pace. Solvent denaturation of proteins and interpretations of the M value. *Methods in Enzymology*. 2009;466:549-65.
16. C. Nick Pace. Determination and analysis of urea and guanidine hydrochloride denaturation curves. *Methods in Enzymology*. 1986;131:266-80.
17. Samuel L.C. Moors, Abel Jonckheer, Marc De Maeyer, Yves Engelborghs, Arnout Ceulemans. Tryptophan conformations associated with partial unfolding in ribonuclease t1. *Biophysical Journal*. 2009;97(6):1778-86.
18. M.C. Shastry MRE. Reversible thermal unfolding of ribonuclease t1 in reverse micelles. *Biochemistry*. 1996;35(13):4094-101.
19. Margherita Ruoppolo, Robert B. Freedman. Refolding by disulfide isomerization: The mixed disulfide between ribonuclease t1 and glutathione as a model refolding substrate. *Biochemistry*. 1995;34(29):9380-8.
20. Marcelo M. Santoro, D.W. Bolen. Unfolding free energy changes determined by the linear extrapolation method. 1. unfolding of phenylmethanesulfonyl alpha- chymotrypsin using different denaturants. *Biochemistry*. 1988;27(21):8063-8.
21. Joeri Deswarte, Stefan De Vos, Ulrike Langhorst, Jan Steyaert, Remy Loris. The contribution of metal ions to the conformational stability of ribonuclease t1. crystal versus solution. *European Journal of Biochemistry*. 2001;268(14):3993-4000.
22. James A. Thomas, Bret A. Shirley, Gerald R. Grimsley, C. Nick Pace. Conformational stability and mechanism of folding of ribonucleae t1. *Journal of Biological Chemistry*. 1989;264(20):11614-20.
23. Miguel A. de los Rios, Kevin W. Plaxco. Apparent deby-huckel electrostatic effects in the folding of a simple, single domain protein. *Biochemistry*. 2005;44(4):1243-50.
24. Benben Song, Jae-Hyun Cho, Daniel P. Raleigh. Ionic-strength-dependent effects in protein folding: Analysis of rate equilibrium free-energy relationship and their interpretation. *Biochemistry*. 2007;46(49):14206-14.
25. C. Nick Pace, Gerald R. Grimsley. Ribonuclease t1 is stabilized by cation and anion binding. *Biochemistry*. 1988;27:3242-6.
26. Mitsuhiro Itaya YI. Steady-state kinetic studies of the inhibitory action of zinc on ribonuclease t1 catalysis. *Biochemical Journal*. 1982;297(2):357-62.
27. M. Vijayakumar MSG. Pair correlation energies and successive ionization potentials of atmos helium through zinc. *Journal of Chemical Physics*. 1992;97(9):6639-43.
28. Tiqing Liu, Patrik R. Callis, Ben H. Hesp, Mattijs de Groot, Wybren Jan Buma, Jaap Broos. Ionization potentials of fluoroindoles and the origin of nonexponential tryptophan fluorescence decay in proteins. *Journal of the American Chemical Society*. 2005;127(11):4104-13.

29. Normann Spitzner, Frank Lohr, Stefania Pfeiffer, Assen Koumanov, Andrey Karshikoff, Heinz Ruterjans. Ionization properties of titratable groups in ribonuclease t1 I. pKa values in the native state determined by two-dimensional NMR spectroscopy. *European Biophysics Journal*. 2001;30(3):186-97.
30. Fuyuhiko Inagaki, Yoshi Kawano, Ichio Shimada, Kenji Takahashi, Tatsuo Miyazawa. Nuclear magnetic resonance study of the microenvironments of histidine residues of ribonuclease t1 and carboxymethylated ribonuclease t1. *Journal of Biochemistry*. 1980;89:1185-95.
31. Grzegorz Bulaj, Tanja Kortemme, David P. Goldenberg. Ionization-reactivity relationships for cysteine thiols in polypeptides. *Biochemistry*. 1998;37(25):8965-72.
32. Jianping Ding, Hui Woog Choe, Joachim Granzin, Wolfram Saenger. Structure of ribonuclease t1 complexed with zinc(II) at 1.8Å resolution: A $Zn^{2+} \cdot 6H_2O \cdot \text{carboxylate clathrate}$. *Acta Crystallographica, Section B: Structural Science*. 1992;B48(2):185-91.
33. Lisa M. Gloss, Brandon J. Placek. The effect of salts on the stability of H2A-H2B histone dimer. *Biochemistry*. 2002;41(50):14951-9.
34. John A. Schellman. The relation between the free energy of interaction and binding. *Biophysical Chemistry*. 1993;45(3):273-9.
35. John A. Schellman. Protein stability in mixed solvents: A balance of contact interaction and excluded volume. *Biophysical Journal*. 2003;85(1):108-25.
36. Serge N. Timasheff. Thermodynamic binding and site occupancy in the light of the schellman exchange concept. *Biophysical Chemistry*. 2002;101-102:99-111.
37. Jayashree Srinivasan, Megan W. Trevathan, Paul Beroza, David A. Case. Application of a pairwise generalized born model to proteins and nucleic acids. inclusion of salt effects. *Theoretical Chemistry Accounts*. 1999;101(6):426-34.
38. Sanford Asher SB. Raman studies of solution polyglycine conformations. *The Journal of Physical Chemistry B*. 2010;114:6636-41.
39. Adrian H Elcock, Andrew S Thomas. Molecular dynamics simulations predict a favorable and unique mode of interaction between lithium (Li^+) ions and hydrophobic molecules in aqueous solutions. *Journal of Theory and Chemical Computation*. 2011;7(4):828-4.
40. Woon Ki Lim, Jorg Rosgen, S. Walter Englander. Urea, but not guanidinium, destabilizes proteins by forming hydrogen bonds to the peptide group. *Proceedings of the National Academy of Sciences of the United States of America*. 2009;106(8):2595-600.
41. Nikolai A. Simonov, Michael Mascagni, Marcia O. Fenley. Monte carlo-based linear poisson-boltzmann approach makes accurate salt-dependent solvation free energy predictions possible. *Journal of Chemical Physics*. 2007;127(18):185105/1,185105/6.

Chapter 5

Probing the effect of water-water interactions on enzyme activity with salt gradients: A case-study using ribonuclease t1

5.1 Overview

With a firm understanding of the effects of chloride salts on hydrophobicity and on the conformational stability of RNase t1, I will now be examining the effect of salts on the water hydrogen bond network in the hydration sphere of a protein and its subsequent effect on enzyme activity. Water interacts via hydrogen bonds, specifically through two types of hydrogen bonds: linear and bent hydrogen bonds. Vibrational spectroscopy has shown that salts will change the relative populations of bent and linear hydrogen bonds. In this chapter, I have studied the effect of these two types of hydrogen bonds by monitoring the enzymatic activity of RNase t1 in increasing concentrations of various chloride salts. The presence of salts inhibits the activity of RNase t1 and the results presented in this chapter demonstrate that the extent of the observed loss of enzyme activity correlates with the cationic species' ability to promote linear hydrogen bonds. I go on to show that the high population of linear hydrogen bonds stabilizes a more compact, a more rigid and less active conformation of RNase t1. This indicates that a protein's structure is sensitive to the nature of the hydrogen bond between the water molecules in its hydration shell.

5.2 Characterizing RNase t1 activity

The activity of RNase t1 was measured by monitoring the changes in absorbance at 280nm during the hydrolysis of the dinucleotide GpC. A typical kinetic trace is shown in Figure 5-1. The zero time is when RNase t1 was added to a solution containing 10 μ M GpC, and the subsequent data was fitted to equation 5-1:

$$A = A_0 + B(1 - e^{-kt}); \quad k = \frac{\{E\}k_{cat}}{K_M} \quad (5-1)$$

where A_0 and B are fitting parameters, k is the rate constant from which the specificity constant (k_{cat}/K_M) can be isolated. Since the concentration of GpC used is 1/20th that of its K_M value

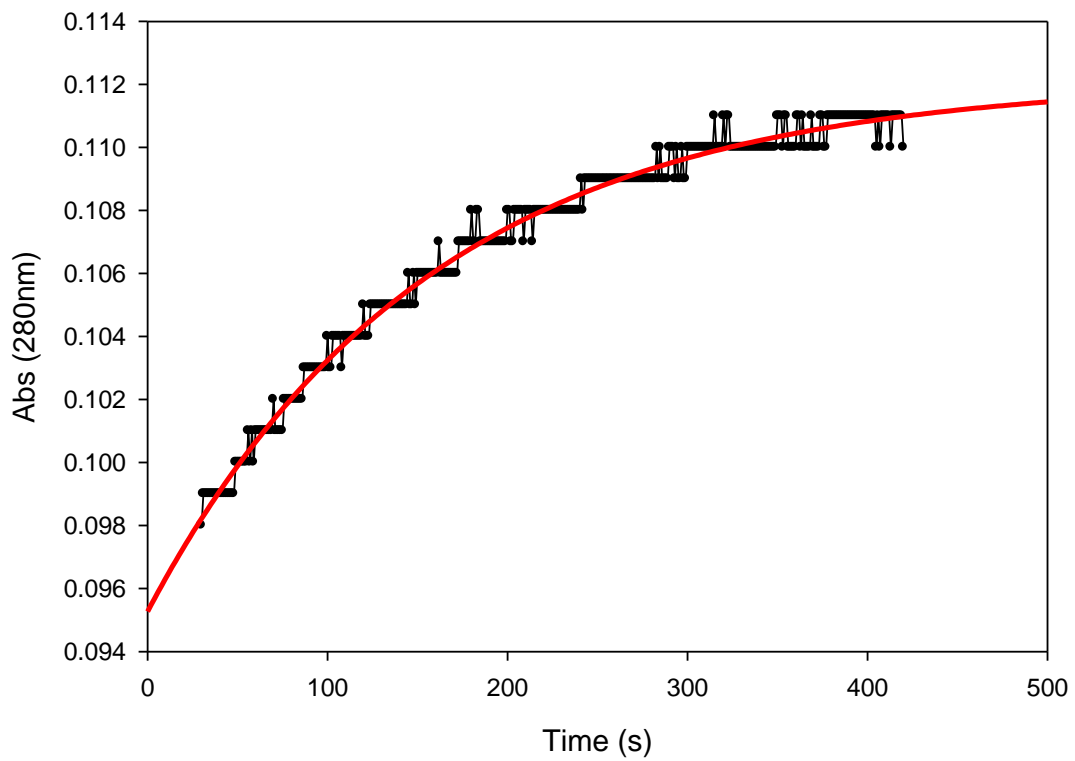


Figure 5-1. Typical kinetic trace obtained after adding RNase t1 (final concentration of 2.98nM) to a solution containing 10 μ M GpC at pH 5.5, 10mM bis-tris buffer.

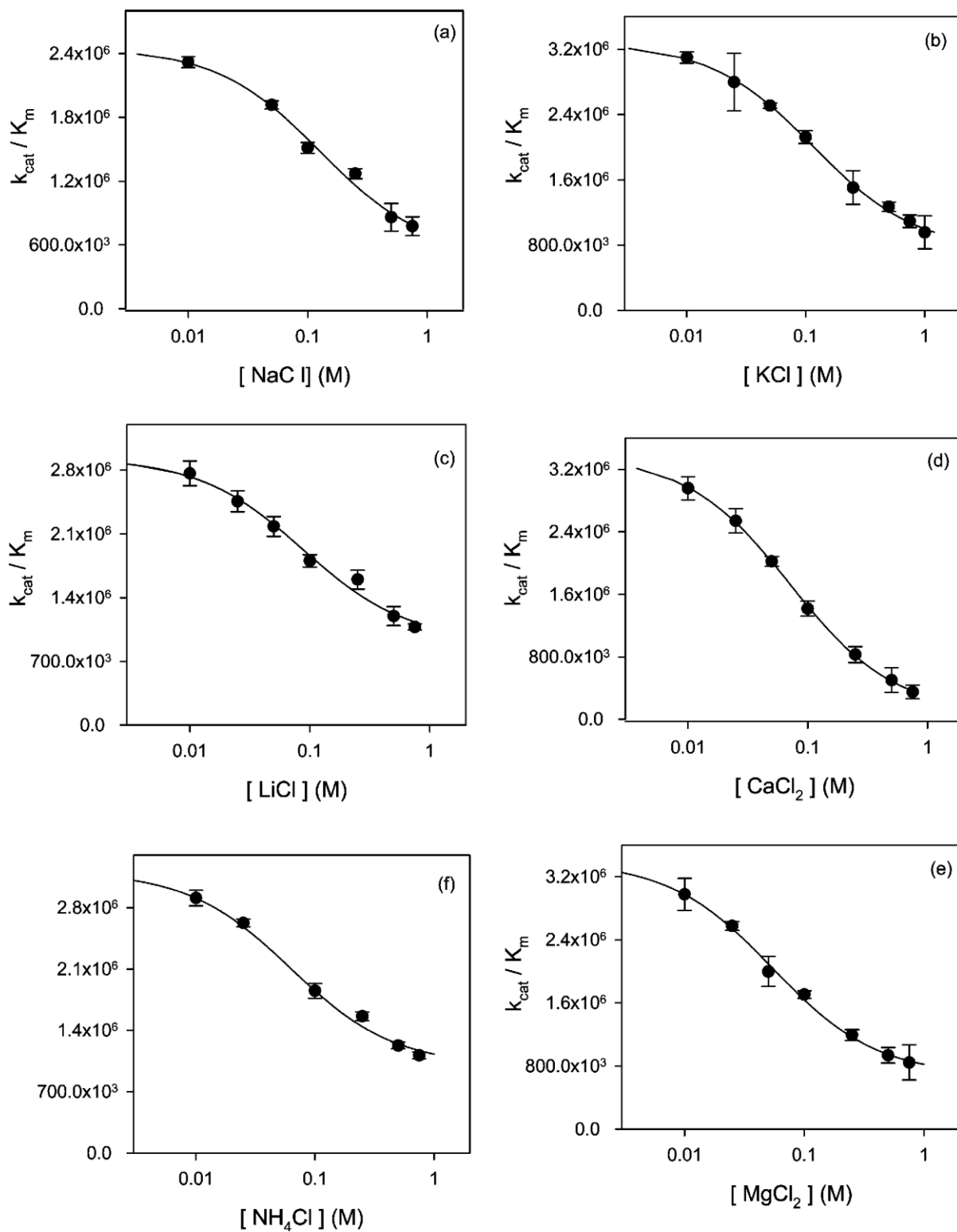


Figure 5-2. Effect of various chloride salts on the k_{cat}/K_m parameter of RNase t1 obtained from the enzyme-catalyzed hydrolysis of GpC. The catalytic efficiency is reduced universally upon addition of various salts.

(220 μ M) (1), the Michaelis-Menton equation can be reduced to the mono-exponential equation 5-1 (2), where k_{cat} and K_M are the Michaelis-Menton parameters. The salt effect on enzyme activity has been quantified by correlating the changes in activity, characterized by changes in k_{cat}/K_M , to increasing salt concentrations. The effect of various chloride salts on enzyme activity is shown in Figure 5-2. As can be seen, the salts cause a marked decrease in enzyme activity, the extent of which depends on the individual salt. It is important to note that the addition of salt at the indicated concentrations does not produce a decrease of fluorescence of a solution containing 0.5 μ M RNase. This precludes the possibility that the drop in enzyme activity is due to precipitation of the enzyme. Furthermore, diluting the high salt enzyme into a low salt solution restores the enzyme's catalytic properties, indicating the loss of activity is a reversible process. Furthermore, the obtained specificity constant values at low concentrations are similar to values found in the literature (2, 3).

5.3 Ligand binding and fluorescence

The binding of substrate-mimicking ligands has been investigated using steady-state fluorescence. Figure 5-3a and Figure 5-3c depict the effect of the ligand 5'-GMP on RNase t1 fluorescence upon excitation at 265 and 290nm respectively. The spectra shown in Figure 5-3a and 5-3c differ significantly from each other because different intrinsic fluorophores are being excited. In Figure 5-3c, the lone tryptophan (W59) is excited exclusively, whereas by exciting at 265nm (Figure 5-3a), the tyrosine residues are excited and obtain a different spectrum. The excited tyrosine residue and the tryptophan residue interact through frequency resonance energy transfer (FRET) between the excited tyrosine and the ground state tryptophan residue. In this spectrum contributions from both the tyrosine and the lone tryptophan residues are observed through FRET (4). The spectra in Figure 5-3 show how RNase t1 responds to the binding of a

ligand. As may be observed in Figure 5-3b, the fluorescence of RNase t1 is quenched by the inhibitor guanosine 5'-monophosphate (5'-GMP). When the enzyme is excited at 265nm, a hyperbolic dependence of fluorescence on 5'-GMP concentration is observed. As is seen in the inset of Figure 5-3b, the relationship follows a simple hyperbolic dependence. From this quenching profile, the fraction of bound ligand (f) is determined by using equations 5-2:

$$f = \frac{F - F_0}{F_{max} - F_0} \quad (5-2)$$

where F is the protein fluorescence at any given ligand concentration, F_0 is the protein fluorescence in the absence of ligand, and F_{max} is the protein fluorescence at the maximum ligand concentration. This dependence follows a simple hyperbolic dependence on ligand concentration depicted by equation 5-3 (5):

$$f = \frac{B[L]_{free}}{K_d + [L]_{free}} \quad (5-3)$$

where B is a fitting constant, K_d is the binding constant, and $[L]_{free}$ is the concentration of free 5'-GMP. A K_d of $50 \pm 7 \mu\text{M}$ and B_1 $1.14 \pm 0.03 \mu\text{M}$ are obtained by fitting the data to equation 5-3. These values are consistent with previous work found in the literature (6, 7).

When the enzyme is excited at 290nm, there is a drastic change in the fluorescence of RNase t1 after addition of 5'-GMP (Figure 5-3c). The binding of 5'-GMP causes an increase in RNase t1 fluorescence, and as can be observed in the inset of Figure 5-3d, the relationship does not follow a simple hyperbolic model but rather it follows a sigmoidal Hill equation (8):

$$f = y_0 + \frac{a([L]_{free})^b}{(K_d)^b + ([L]_{free})^b} \quad (5-4)$$

where K_d is the apparent binding constant, $[L]_{free}$ is the concentration of free ligand, a is a constant and b is the cooperativity constant, which reflects the extent of cooperativity amongst

multiple binding sites (8). Fitting the data in Figure 5-3d, a $K_d = 580 \pm 100\mu\text{M}$ and $b = 2.5 \pm 0.7\mu\text{M}$ is obtained, reaffirming that a secondary binding site exists for the guanylyl moiety and that this secondary binding site is cooperatively linked to binding to the first site (7). The above fluorescence results indicate that it is possible to probe the properties of the primary binding site of the guanylyl moiety without interference from the secondary site by selectively exciting the tyrosine residue at 265nm. The effect of salts on the binding of 5`-GMP to RNase t1 has been investigated using fluorescence spectroscopy with an excitation wavelength set to 265nm. The quenching profiles of RNase t1 upon addition of 5`-GMP were measured at increasing salt concentrations. The data in Figure 5-4 shows that increasing the salt concentration has a moderate effect on 5`-GMP binding, with MgCl_2 having the largest effect by increasing binding by 35%. The addition of salt had no appreciable effect on the secondary binding site of the guanylyl moiety.

5.4 The effect of salt on the structure of RNase t1

Finally, the effect of salt on the structure of RNase t1 was investigated using fluorescence quenching. The quencher used for this experiment is acrylamide because it has been shown to act as a probe to gauge the accessibility of an intrinsic fluorophore. The permeability of inert solutes, such as acrylamide, through proteins requires structural fluctuations of said protein (9), and one way to quantify these structural fluctuations is by using small molecules that are able to penetrate into a globular protein and quench its intrinsic fluorescence. The amount of quenching can be quantified by using the Stern-Volmer equation, which was previously discussed. The data in Figure 5-5 demonstrates that the addition of acrylamide quenches the fluorescence of RNase t1 and a Stern-Volmer constant of $2.02 \pm 0.04\text{M}^{-1}$ is obtained under low salt conditions and $1.53 \pm 0.04\text{M}^{-1}$ when 1M MgCl_2 is added. This significant decrease of the K_{SV} signifies that the high

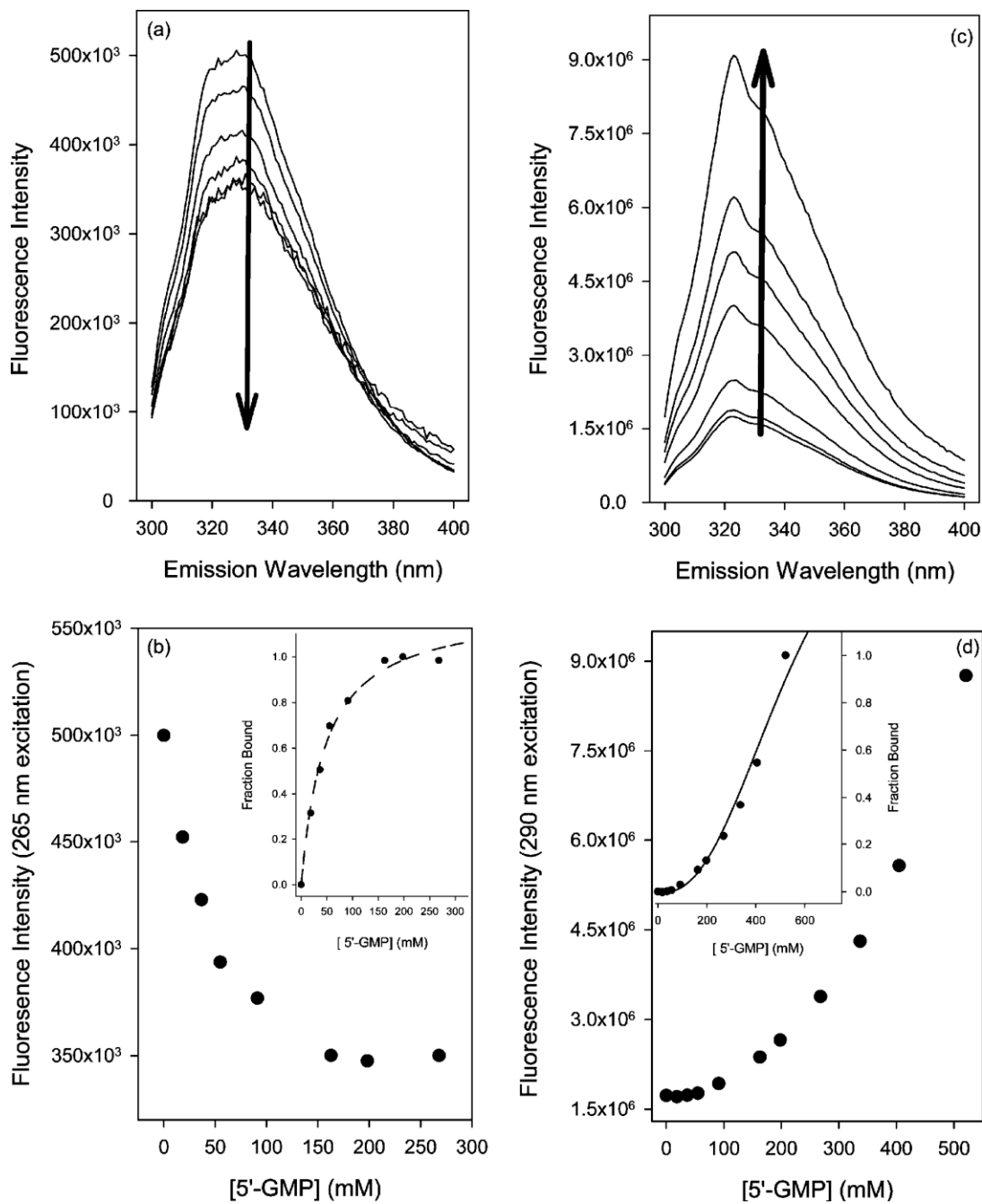


Figure 5-3. a) Steady-state fluorescence spectra of RNase t1 after addition of 0-200 μ M 5'-GMP, following the arrow, with excitation at 265nm. b) Fluorescence intensity maximum (330nm) of RNase t1 upon excitation at 265nm. c) Steady-state fluorescence spectra of RNase t1 after addition of 0-500 μ M 5'-GMP, following the arrow, with excitation at 290nm. d) Fluorescence intensity maximum (330nm) of RNase t1 upon excitation at 290nm.

salt concentration of the solvent has made the lone tryptophan of RNase t1 less accessible. This is most likely due to the salt stabilizing a more compact conformation of RNase t1 that has a more protected tryptophan residue (10). As a control, the experiment was repeated and the enzyme was replaced with N-acetyl tryptophanamide (NATA), a tryptophan residue analog. The data is once again fit to the Stern-Volmer equation and shown in Figure 5-5. The plots show the quenching of acrylamide is minimally affected by the addition of salt. The Stern-Volmer constant decreased from 22 ± 1 to $20 \pm 0.4\text{M}^{-1}$ after addition of 1M MgCl_2 . The slight decrease is expected because the viscosity of the solvent will increase at high salt concentration, causing a decrease in the Stern-Volmer constant. This observed insensitivity of NATA fluorescence after addition of MgCl_2 agrees with the assumption that the salt-dependent decrease of the Stern-Volmer constant is due to a change in the properties of the protein rather than a direct interaction between the salt ions and the tryptophan residue.

5.5 Potential explanations for the observed loss of enzyme activity

The data presented in Figure 5-2 demonstrates that each salt uniquely affects the catalytic efficiency of the model enzyme RNase t1. Traditionally, salt effects have been explained on the basis of the three following possibilities. First, the salt species affect the pK_a of key amino acid residues in the active site. Second, the salt species weaken Coulombic interactions between the substrate and the enzyme. Finally, the cations bind directly to the enzyme, thereby inhibiting catalysis. These three methods have been examined in detail and have been shown to be inadequate in explaining the observed decrease of enzyme catalysis upon addition of chloride salts. The data in this work offers a different explanation and suggests that the observed salt effect is due to the salt species changing the hydrogen bonding properties of the water molecules in the enzyme's hydration shell and in so doing indirectly stabilizing a more compact, less active

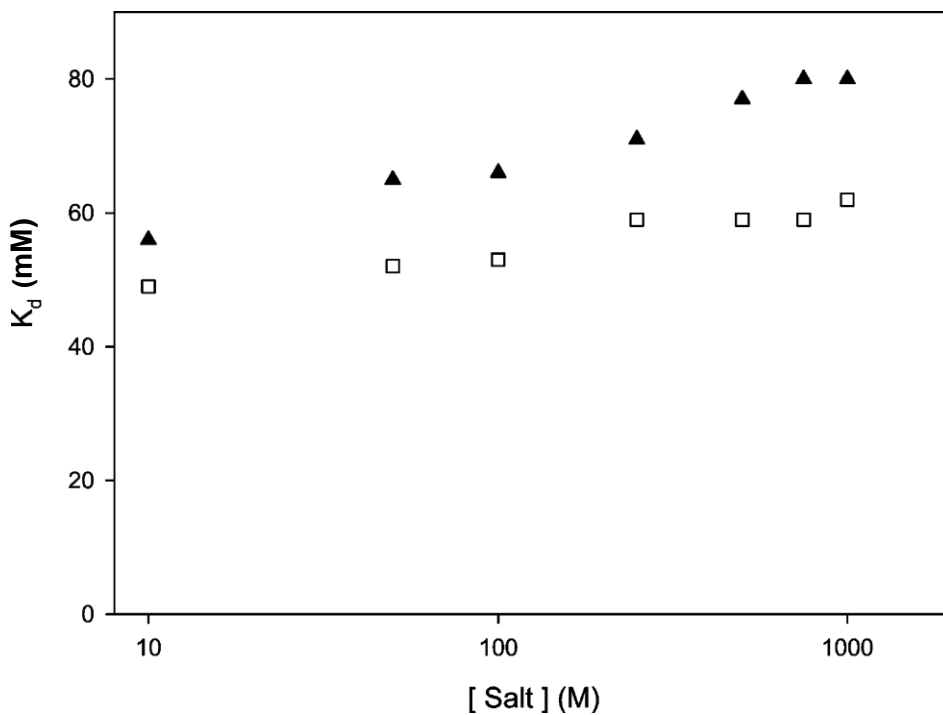


Figure 5-4. Effect of salt concentration on the binding of 5'-GMP to RNase t1. The K_d values measured upon addition of NaCl (\square) and $MgCl_2$ (Δ) at the indicated concentrations.

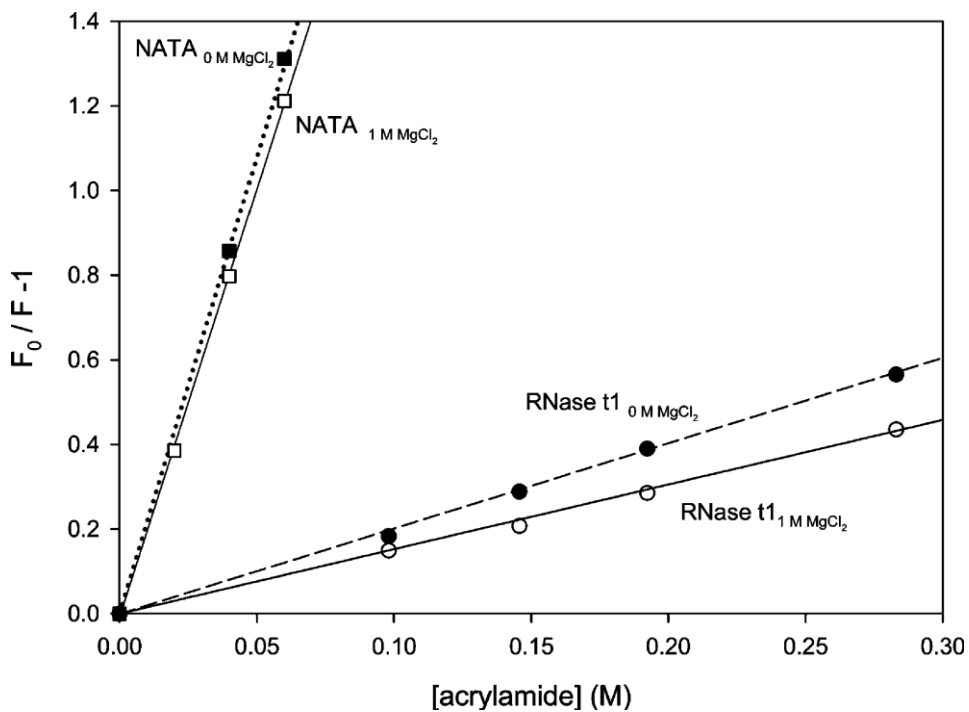


Figure 5-5. Stern-Volmer plots of the quenching of RNase (circles) and NATA (squares) in the absence (filled) and presence (open) of 1M $MgCl_2$.

form of RNase t1.

5.5.1 First possibility: Salt effect on pK_a values of key active site residues. The first traditional explanation is the possibility that the salt affect the pK_a values of key active-site residues. Those key active-site residues of RNase t1 have been identified as His40, His92, Glu58 and an unidentified carboxylate residue (11-13). Kinetic studies (12, 13) at varying pH values have shown that the protonation state of both histidine residues is crucial for proper catalysis. NMR studies have shown that the pK_a values of His40 and His92 are 7.7 and 7.4 respectively, and pK_a values of 3.9 and 3.2 have been assigned to Glu58 and the unidentified carboxylate (12, 13). NMR studies have also shown that salt concentrations indeed have a significant effect the pK_a values of histidine residues. Increasing the concentration of salt from a low (0.02M) to a high (1.5M) concentration can increase the pK_a value of histidine residues by a maximum of 0.3 units (14). This is most likely due primarily to the ionic strength dependence on the solvation energy of the residues (15). However, this increase in the pK_a value will not cause a change in the protonation state of His42 or His90 since the pH of the buffer used was 5.5 and will therefore have a negligible contribution to the observed decrease of the k_{cat}/K_m . The effect of salt concentration on glutamate and aspartate residues has also been extensively studied. As a general rule of thumb, a solution with a high salt concentration will increase the pK_a value of negatively charged residues by 0.3-0.7 pK_a units (16). Therefore even under high salt concentrations, the Glu58 and the unidentified carboxylate residue will not be protonated at pH 5.5, consistent with the assertion that it is unlikely that the increase of pK_a values of key active site residues will contribute significantly to the observed salt effect on k_{cat}/K_m .

5.5.2 Second possibility: The high salt concentration weakens the Coulombic interactions between the substrate and the enzyme. The second popular explanation for the observed salt

effect on enzyme catalysis has been that the salt species weaken Coulombic interactions between the substrate and the enzyme, a.k.a. the counterion effect. Salts can dramatically affect substrate binding if strong Coulombic interactions play a major role to the substrate-enzyme binding process (17, 18). Coulombic interactions contribute favourably to the substrate-enzyme binding process by increasing the overall entropy of the system through the formation of an ion pair that liberates water molecules and ions that were previously bound to the enzyme. As the substrate enters the enzyme's active site, strong electrostatic interactions exclude substrate counterions and/or enzyme counterions into the bulk solvent. This ion-pair formation is less favourable at high salt concentrations since the newly liberated ion needs to wrest a water molecule that is already bound to a solvent ion (19). Thermodynamically, substrate counterion release becomes less favourable as salt concentrations increase (19, 20), causing a decrease in substrate-enzyme binding affinity that will strongly affect the k_{cat}/K_m . A method has been developed by Raines et al. to quantify the counterion effect on enzyme catalysis, resulting in equation 5-5 (18, 19):

$$\frac{1}{k_{cat}/K_m} = \frac{1}{(k_{cat}/K_m)_{max}} + \frac{[salt]^n}{(k_{cat}/K_m)_{1M}} \quad (5-5)$$

where $(k_{cat}/K_m)_{max}$ is the k_{cat}/K_m limited only by the encounter of the substrate and the enzyme in solution, $(k_{cat}/K_m)_{1M}$ is the value of k_{cat}/K_m at 1 M salt concentration and n is a constant. In the case where the enzyme is "sluggish", that is to say the rate of substrate dissociation, k_{off} , from the encounter complex is significantly larger than the rate of catalysis, k_{cat} , the value of n is representative of the number of counterions released as the substrate binds the enzyme. Enzymes that interact with their substrate via strong Coulombic interactions will release a minimum of one counterion during substrate binding, leading to $n \geq 1$ (18-20). From temperature-jump kinetic experiments done on substrate-mimicking ligands (7), the value of k_{off} has been estimated to be larger than 2000 s^{-1} and the k_{cat} values for the enzyme using GpC are in the lower hundreds of

inverse seconds. Since the $k_{off} \gg k_{cat}$, RNase t1 can be classified as a sluggish enzyme and therefore the n value obtained from equation 5-5 will represent the number of counterions that will be released from the enzyme upon ligand binding. Figure 5-6a shows the data from Figure 5-2a replotted in order to fit equation 5-5. The parameter $n = 0.6 \pm 0.2$ is obtained, this value is significantly lower than 1, indicating that Coulombic interactions do not play an important role in GpC hydrolysis by RNase t1. This is consistent with previous work found in the literature (21).

Further evidence demonstrating the fact that Coulombic interactions do not play an important role is by examining the effect of salt on the binding of 5'-GMP. The GpC and 5'-GMP ligands have the same formal charge on their phosphate group at pH 5.5, therefore both ligands should have the same number of counterions if Coulombic interactions are important for this reaction. Once again using the work done by Raines et al. can be used to evaluate the salt effect on k_{cat}/K_m by using equation 5-6:

$$\frac{\delta(\log K_d)}{\delta(\log[\text{salt}])} = n' \quad (5-6)$$

In Figure 5-6b, the data from Figure 5-2 has been replotted to fit equation 5-6. If Coulombic interactions are present, the value n obtained from equation 5-5 should be close to the value n' obtained in equation 5-6. The best fit of equation 5-6 yielded $n' = 0.04 \pm 0.02$, which is significantly different from the value n obtained in equation 5-5. The small value of n' for 5'-GMP binding indicates that the binding of ligand-mimicking substrate is not accompanied by a significant counterion release. In addition, the large difference between the values of n and n' obtained from Figure 5-6 further demonstrates that the observed salt dependent decrease in k_{cat}/K_m is not caused by simple substrate-enzyme binding thermodynamics. And so I can conclude that Coulombic interactions are not responsible for the observed salt effect on enzyme

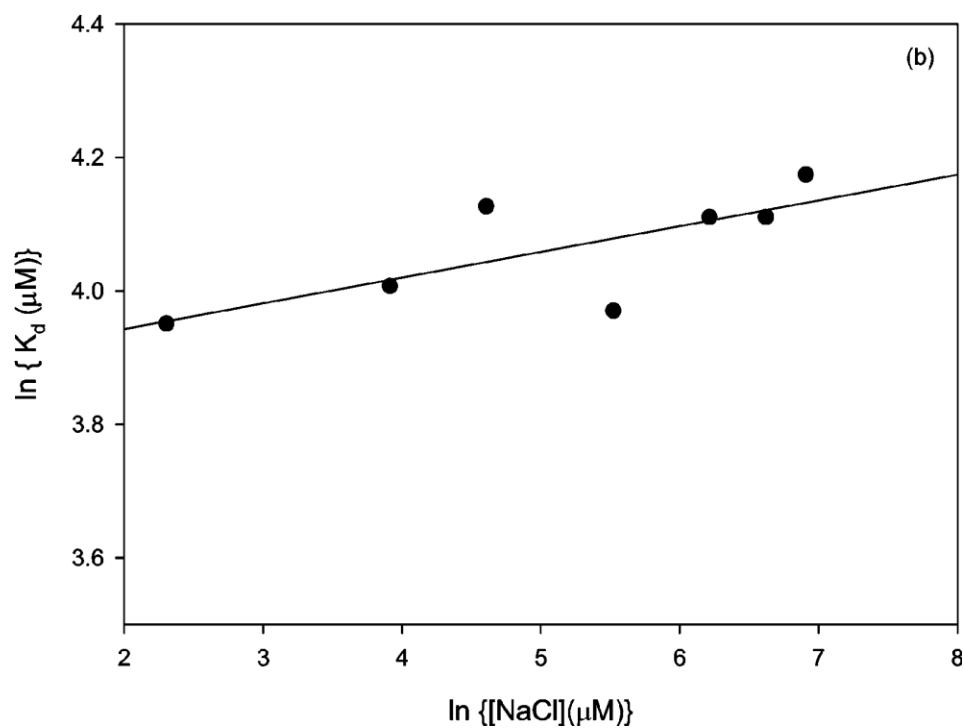
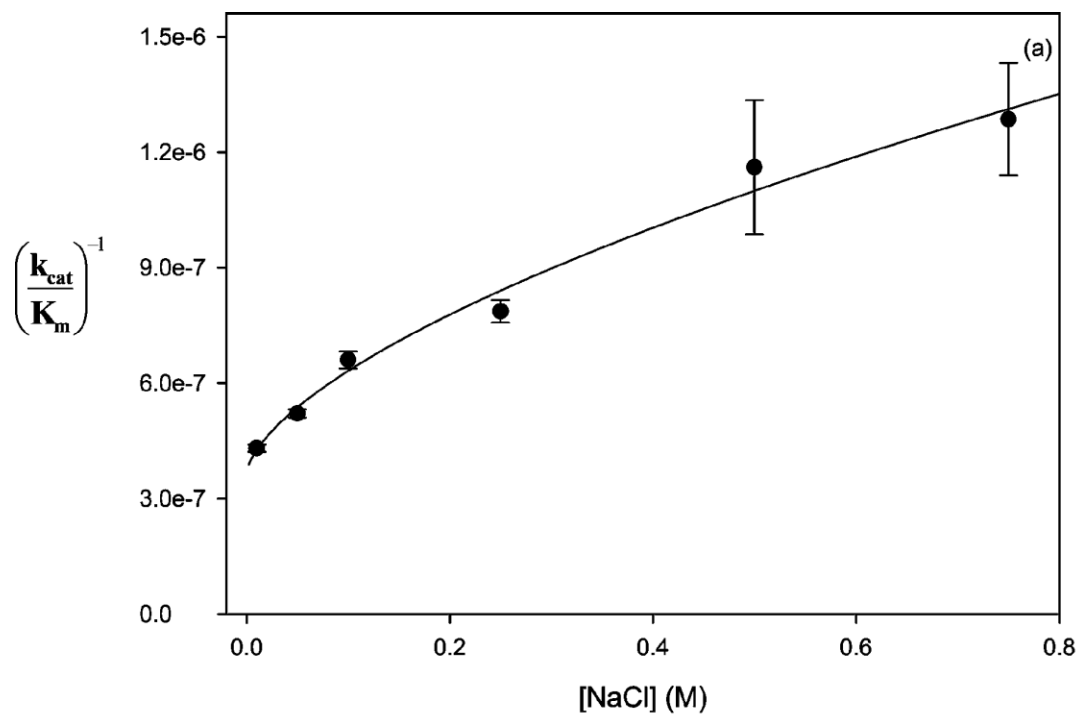


Figure 5-6 a) Effect of NaCl concentration on the parameter k_{cat}/K_m obtained from the enzyme catalyzed hydrolysis of GpC by RNase t1. The solid line represents the best fit to equation 5-6. b) Effect of NaCl concentration on the K_d values obtained from the binding of 5'-GMP to RNase t1.

catalysis.

5.5.3 Third possibility: Metal cations bind directly to the enzyme and inhibit catalysis. The final traditional explanation has been to treat the metal cation as a binding agent that directly inhibits the enzyme (22). This treatment implicitly assumes that the metal cation directly binds to a specific site on the enzyme and in so doing directly stabilizes a less active conformation (equation 5-7a), resulting in a decrease in enzyme activity. This loss of activity can be quantified using equation 5-7b:



$$\left(\frac{k_{\text{cat}}}{K_m}\right)_{\text{obs}} = \frac{\left(\frac{k_{\text{cat}}}{K_m}\right)_{\text{low salt}} + K_{\text{eq}}c\left(\frac{k_{\text{cat}}}{K_m}\right)_{\text{high salt}}}{1 + K_{\text{eq}}c} \quad (5-7b)$$

where $E_{\text{low salt}}$ is the enzyme in the active form in the low salt environment, E_{ion} is the enzyme bound to a metal cation and is the less active form, $\left(\frac{k_{\text{cat}}}{K_m}\right)_{\text{obs}}$ is the specificity constant at any given salt concentration, $\left(\frac{k_{\text{cat}}}{K_m}\right)_{\text{low salt}}$ is the active low-salt conformation, $\left(\frac{k_{\text{cat}}}{K_m}\right)_{\text{high salt}}$ is the specificity constant of the less active ion-bound form, K is the equilibrium constant of the ion to the enzyme and c is the concentration of salt. Upon the results of the fluorescence quenching data shown in Figure 5-5, it is reasonable to conclude that the high salt concentrations are forcing a conformational change the RNase t1 enzyme. This allows us to now analyze the data using equation 5-7b. The data in Figure 5-2 have been re-plotted using equation 5-7b to obtain equilibrium constants, K . The results of the best fit have been tabulated in Table 5-1 and since the K values of each salt are different, I can state that the cationic species are the inhibitors since all the anions are chloride.

Table 5-1. Values of the K parameter associated with RNase t1 for each data set by fitting the data depicted in Figure 5-2 to equation 5-7b.

Salt	K (M^{-1})
NaCl	8 ± 2
KCl	8.6 ± 0.8
LiCl	13 ± 1
CaCl ₂	14 ± 0.7
NH ₄ Cl	16 ± 3
MgCl ₂	21 ± 3

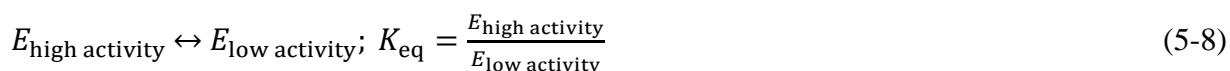
The values of K vary from 8 – 21 M^{-1} , which yields a free energy of interaction of 5 – 7.5 kJ/mol. These small K values present a dilemma in interpreting the binding data. While the model in equation 5-7b has been shown to be accurate for tightly binding metal cations (ligands that interact at submillimolar concentrations), it has been definitively shown that this model is inapplicable to weakly-binding ligands (23) and applying site-specific binding models to weak ligand-protein interactions leads to inaccurate and erroneous results (24) since this model doesn't take into account the binding competition between the ligand and solvent water molecules (23, 24). In this particular case, I am assuming that there is a specific metal-binding site on the surface of the enzyme.

It has been suggested that in a manner similar to the binding of Zinc and other heavy atoms (25), divalent cations bind to the surface carboxylate residue Asp49 (26). If the metal cations are in fact binding to RNase t1, then the binding of Mg^{2+} with a K of 21 M^{-1} should stabilize the protein by ~7.5 kJ/mol. Therefore, if Asp49 is mutated to Ala, the binding site is lost and the mutant protein should be destabilized by a minimum 7.5 kJ/mol relative to the wild type enzyme when dissolved in 1M $MgCl_2$. The unfolding free energy RNase t1 is 24.2 kJ/mol at low ionic strength, and in the presence of 1 M $MgCl_2$ is 43.7 kJ/mol, with the salt stabilizing the enzyme by ~ 20 kJ/mol. Mutating any of the surface carboxylate residues does not reduce the $\Delta G_{unfolding}^o$ by more than 2 kJ/mol (26). This result is inconsistent with a specific binding

model; if there was direct binding, I would expect a stabilization of the unfolding of RNase t1 to be 7.5 kJ/mol. Although it can still be concluded from the data in Figure 5-5 that the high salt concentration induces the adaptation of a more compact and rigid conformation, the data in Figure 5-6 suggests that it is very unlikely that this conformational change is mediated by cation binding to a specific site on the enzyme.

5.5.4 My proposed explanation: The observed salt effect is due to the salt interacting with the water molecules of the protein's hydration shell and modulating the hydrogen bonding, leading to the stabilization of a more rigid, more compact and less active conformation of RNase t1.

Now that the traditional explanations to explain the observed salt effect on enzyme catalysis have been discarded, I can offer an alternative explanation: the observed salt effect is due to the salts changing the hydrogen bonding properties of the water molecules in the protein's solvent shell. This indirectly stabilizes a less active conformation of the enzyme. As was seen, the salt species can alter the properties of the hydration layer of proteins. However, the effect to the thermodynamics of the system by a change in the hydration layer has not been discussed (27-29). If the premise that the salts are modifying the enzyme to give a high activity conformer ($E_{\text{high activity}}$) and a low activity conformer ($E_{\text{low activity}}$) is accepted, the following equilibrium can be written:



The addition of salt causes a shift in the above equilibrium and so K_{eq} can be represented by a polynomial function of salt concentration (equation 5-8a) where c is the concentration of any given salt and K_n is an equilibrium constant:

$$K_{\text{eq}} = \sum_0^n K_n c^n \quad (5-8a)$$

As a first linear approximation, let us assume that $K_{eq} \approx K_0 + Kc$, in which case the measured enzyme activity will then be:

$$\left(\frac{k_{cat}}{K_m}\right)_{obs} = \frac{\left(\frac{k_{cat}}{K_m}\right)_{low\ salt} + (K_0 + Kc)\left(\frac{k_{cat}}{K_m}\right)_{high\ salt}}{1 + (K_0 + Kc)} \quad (5-8b)$$

$$\left(\frac{k_{cat}}{K_m}\right)_{obs} = \frac{\left(\frac{k_{cat}}{K_m}\right)_{low\ salt} + K_0\left(\frac{k_{cat}}{K_m}\right)_{high\ salt} + Kc\left(\frac{k_{cat}}{K_m}\right)_{high\ salt}}{1 + (K_0 + Kc)} \quad (5-8c)$$

$$\left(\frac{k_{cat}}{K_m}\right)_{obs} = \frac{\left(\left(\frac{k_{cat}}{K_m}\right)_{low\ salt} + K_0\left(\frac{k_{cat}}{K_m}\right)_{high\ salt}\right)\frac{1}{1+K_0} + \frac{Kc\left(\frac{k_{cat}}{K_m}\right)_{high\ salt}}{1+K_0}}{1 + \left(\frac{K}{1+K_0}\right)c} \quad (5-8d)$$

Rearranging the above equation yields:

$$\left(\frac{k_{cat}}{K_m}\right)_{obs} = \frac{\left(\frac{k_{cat}}{K_m}\right)_{low\ salt} + c\left(\frac{K}{1+K_0}\right)\left(\frac{k_{cat}}{K_m}\right)_{high\ salt}}{1 + \left(\frac{K}{1+K_0}\right)c} \quad (5-9)$$

This equation has the same form as equation 5-7b, and because reasonable correlations are obtained from fitting the data to equation 5-9, the first linear approximation, that $K_{eq} \approx K_0 + Kc$, is validated. Therefore the values reported as K in Table 5-1 should be designated as $\frac{K}{1+K_0}$. This is an important distinction because variations between $\frac{K}{1+K_0}$ values associated with different cations indicate that K is not merely a function of ionic strength but is also salt specific. This distinction rules out simple polyelectrolyte repulsion screening (30) as the only contributor to the stabilization of the low-activity conformation in the high salt concentration. If the observed salt effect is indeed due to the changing of the hydrogen bonding network in the enzyme's hydration shell, then $\frac{K}{1+K_0}$ should depend on how each individual cation interacts with water.

The first method of characterizing salt-water interactions is by measuring the effect that dissolving salt has upon the viscosity of the solvent. It has long been known that salt influence

the viscosity of water, but it was Cox and Wolfenden who first connected viscosity with water structure (31). The viscosity of aqueous solutions containing salts has the following concentration dependence, depicted by the Jones-Dole equation (32):

$$\frac{\eta}{\eta_0} = 1 + A\sqrt{c} + Bc \quad (5-10)$$

where η is the viscosity of a salt solution and η_0 is the viscosity of pure water at the same temperature, c is the concentration of salt, A is an electrostatic term that is essentially 1 for moderate salt concentrations and B depends solely on the strength of the ion-water interactions versus the water-water interactions (32). The B coefficient is a measure of order or disorder of water molecules induced by a salt, with a negative B coefficient indicating a salt that lowers the viscosity, i.e. disrupts the order and a positive B coefficient indicates a salt that increases the viscosity, i.e. the structure of water (32, 33). The B coefficient can be expressed as $B = B_{(+)} + B_{(-)}$ in which $B_{(\pm)}$ is the contribution of the salt from each ion. Using the values of Marcus (34) for the $B_{(\pm)}$ coefficients, the $\frac{K}{1+K_0}$ values have been plotted as a function of the Jones-Dole B coefficient in Figure 5-7a. The data clearly demonstrates that with the exception of NH_4Cl , the $\frac{K}{1+K_0}$ parameter of all salts examined strongly correlates with the cation $B_{(+)}$ values.

Another method of measuring the strength of ion-water interactions is by using chromatographic and interfacial techniques (35, 36). These interactions have been characterized using Fourier transform infrared spectroscopy (FTIR) (35) and size exclusion columns (36) to determine the number of tightly bound water molecules that travel with an ion as it travels through the solvent, dubbed an ion's hydration number. The $\frac{K}{1+K_0}$ values have been plotted as a function of the hydration number of each cation in Figure 5-7b, and once again, with the exception of NH_4Cl , a strong correlation between the $\frac{K}{1+K_0}$ values and the cation hydration

numbers is observed.

Finally, if the results of the ammonium chloride salt are ignored, we observe that:

$$\left(\frac{K}{1+K_0}\right)_{\text{Mg}^{2+}} > \left(\frac{K}{1+K_0}\right)_{\text{Ca}^{2+}} > \left(\frac{K}{1+K_0}\right)_{\text{Li}^+} > \left(\frac{K}{1+K_0}\right)_{\text{Na}^+} \approx \left(\frac{K}{1+K_0}\right)_{\text{K}^+}$$

This ordering follows the kosmotrope ordering of cations in the Hofmeister series (33, 37). Hofmeister effects are defined as the effect of salts on hydrophobic interactions through the first and the second water shells around the ion. Kosmotropes of the Hofmeister series are defined as solutes that order water the Hofmeister series. The fact that my data follows the established Hofmeister series further supports the idea that salts affect the catalytic properties of RNase t1 by perturbing the properties of water molecules in its hydration shell.

While the above correlations support the hypothesis that salts affect enzyme catalysis indirectly by changing the structure of water in its hydration shell, they only correlate to hydration parameters that are determined from changes in the bulk solvent. A more meaningful correlation would be obtained if the $\frac{K}{1+K_0}$ parameter is correlated to parameters that measure water hydrogen bonding properties at a molecular level. Such a measure can be found in the work of Vanderkooi et al. According to the two-state model, liquid water can be considered to be a mixture of two conformations at equilibrium: a low-density, highly ordered form (icelike, water_{LD}) interacting via linear hydrogen bonds forming a tetrahedral network, and a high-density, less ordered form (water_{HD}) interacting via bent hydrogen bonds forming a non-regular bent tetrahedral network. The “linear” ($\theta_h \approx 12^\circ$) and “bent” ($\theta_h \approx 52^\circ$) angles are defined as the smallest O---O – H angle (θ_h) formed by two neighbouring water molecules (38). These two kinds of hydrogen bonds give rise to different signatures in the vibrational spectrum of water molecules in their hydration shell (33). The fact that the results mirror the ordering of cations in

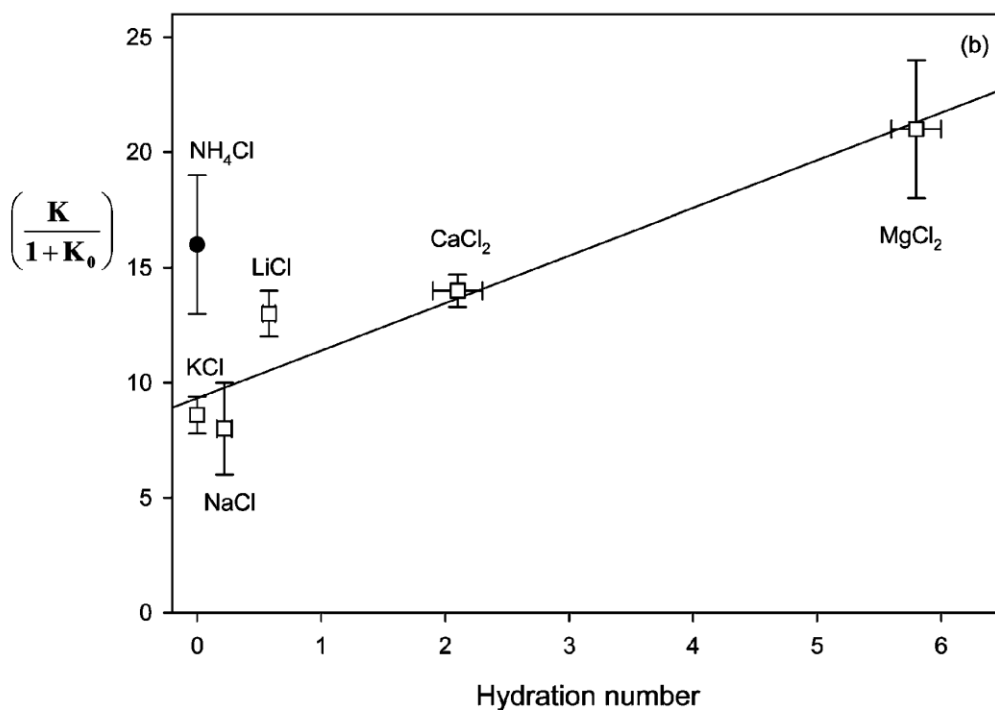
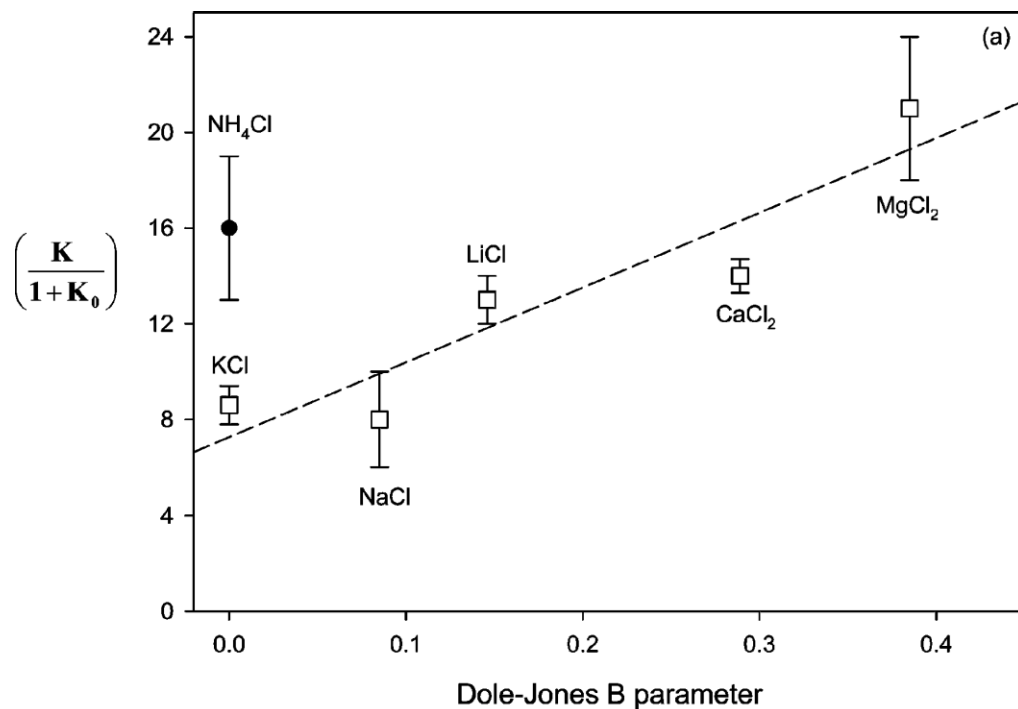


Figure 5-7. a) Dependence of the $\frac{K}{1+K_0}$ parameter, obtained by plotting the data from Figure 5-2 to equation 5-9, as a function of the Jones-Dole B coefficient of various chloride salts. b) Dependence of the $\frac{K}{1+K_0}$ parameter upon the cation hydration numbers of various salts.

when examined with FTIR spectroscopy which can then be deconvoluted to obtain the population distribution of equation 5-11.



Vanderkooi (39) went on to characterize the effects of adding various salts on the two types of hydrogen bonds of water using temperature excursion infrared spectroscopy (TEIR) in aqueous solutions having a salt concentration of 4.4 *m*, which corresponds to 12.5 water molecules per ion. This high concentration of salt allows only a few water molecules in the vicinity of each individual ion. Therefore I can consider the water molecules in the experiment to be in the immediate vicinity of ions in solution. By applying the two-state model (equation 5-11), Vanderkooi was able to quantify the perturbation of this equilibrium by characterizing the effective free-energy difference (ΔG°) between water_{HD} and water_{LD} . The ΔG° for transforming a water_{HD} to a water_{LD} in pure water is 250 cal/M, and the ΔG° values for different solutions of 4.4 *m* salt are (39) 55 (MgCl₂), 244 (NH₄Cl), 250 (CaCl₂), 278 (LiCl), 437 (KCl) and 448 cal/M (NaCl).

These values can be interpreted using the Mercedes-Benz (MB) model (33) developed by Dill et al. This model describes water molecules as two dimensional Lennard-Jones disks with three radial hydrogen bonding arms. These arms form hydrogen bonds when they are aligned and there is no distinction between hydrogen bond acceptors and donors (33, 37). One arm contains a positive charge about two-thirds of the way towards the periphery of the disk and a negative charge at the center of the disc. Dill has shown the ordering of the water molecules depends on either the strength of the electrostatic interactions between the ion and water molecule or the entropic contribution of the water molecules in the ions hydration shell. Dill has demonstrated that small ions order first-shell water molecules through electrostatic interactions. Ions with a

small radius will inherently have their charge closer to the outside edge and so be able to strongly interact with the dipole of the water. Therefore small ions will disrupt the hydrogen bonding network of the first-shell water molecules and orient them in the water_{HD} form. As the radius of the ion increases, the electrostatic interaction weakens and the entropic contribution of the surrounding water molecules becomes more important. Therefore as the sizes of the cations increase, the water molecules in the first solvation shell of the ion lose water_{HD} and approach the behavior of water molecules present near non-polar solutes (37). That is to say water molecules around large ions are organized to maximize hydrogen bonding.

These results suggest that since small ions order water molecules in their first hydration shell to the water_{HD} form, to satisfy the equilibrium in equation 5-11, water molecules in subsequent hydration shells will take the form of water_{LD}. Conversely, large ions will order water molecules in their first hydration shell to adopt the water_{LD} form, forcing subsequent shells to contain a high population of water_{HD}. Therefore the ΔG° values listed above are a measure of the salts ability to force water molecules to the water_{LD} conformation beyond their first hydration shell. For example, the ΔG° values for CaCl₂ and pure water are nearly identical; however, because the Ca²⁺ ion has a high charge density, it will orient the water molecules in its first hydration shell to the water_{HD} form, thereby forcing subsequent hydration shells to adopt the water_{LD} form. Therefore there will be a large concentrated population of water_{LD} in comparison to pure water. In fact, Bakker et al. have shown using dielectric relaxation spectroscopy and femtosecond time-resolved infrared vibrational spectroscopy that certain salts are able to order water molecules “far beyond their first solvation shell” (40), taking the theoretical work of Dill et al. one step further and confirming that salts stabilize the formation of water_{LD} in hydration shells beyond the first of the ion. This stabilization of water_{LD} prevents the solubilization of non-polar

groups in water because of the increase in the already large positive heat capacity of transfer (33) can't be lessened by an increase in the water_{HD} population. Having completed a rigorous thermodynamic analysis of protein unfolding, Cho et al. have shown that the solvation of hydrophobic moieties requires a population of water_{LD} that can be readily converted to water_{HD} (41). Therefore hydrophobic interactions will be enhanced by the fixed population of water_{LD} that cannot be converted to water_{HD} due to the presence of salts promoting water_{LD} .

As can be seen in Figure 5-8, the $\frac{K}{1+K_0}$ values correlate strongly with the ΔG^0 values of 4.4 *m* salt solutions, and contrary to the previous results in Figure 5-7, NH_4Cl also follows the correlation, suggesting that NH_4Cl can indeed order water molecules beyond its first solvation shell. The discrepancy of NH_4Cl in Figure 5-7 underlines the importance of the role that the counterion plays in ordering water molecules; the data in Figure 5-7 is correlated against parameters that measure the effects of the cation only and ignore the contribution from the anion. The effect of the counterion on the hydration structure of water molecules has been shown to be critically important (40) and the effect of ion and counterion to be interdependent (28, 40).

Based on the correlation seen in Figure 5-8, the following explanation is offered for the observed salt effect on the catalysis of RNase t1. Because the enzyme has an overall negative charge (six positively and nine negatively charged residues) at pH 5.5, cations will be attracted to the hydration shell of the enzyme and enrich the local concentration of cations. This increase in the concentration of salt in the enzyme's hydration layer will lead to a perturbation of the water_{HD} - water_{LD} equilibrium. Cations with a high charge density will promote the formation of water_{LD} in the protein's hydration shell which will enhance hydrophobic interactions. The enhanced hydrophobic interaction will inhibit the solvation of hydrophobic moieties and force a more compact, rigid and less active conformation of RNase t1 to be stabilized. This stabilization

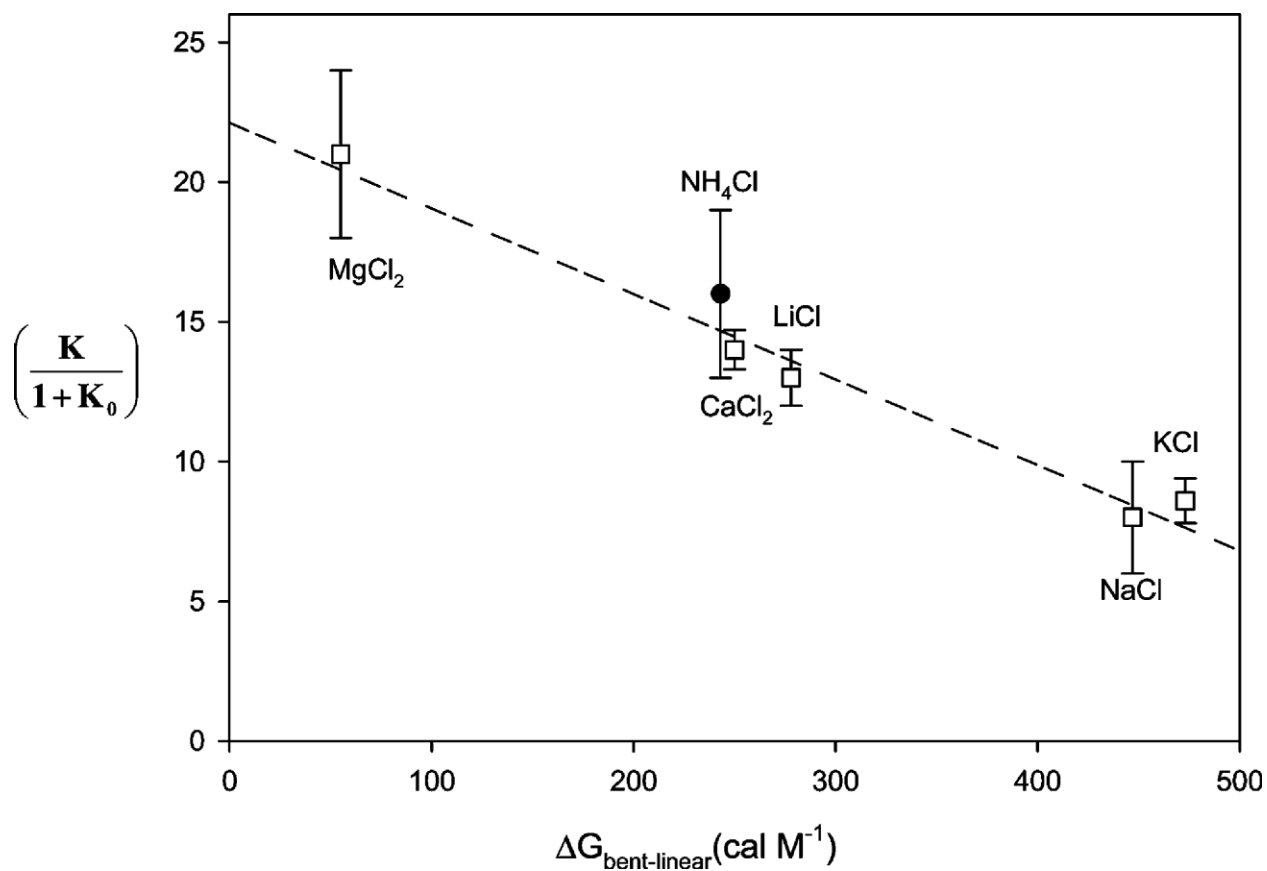


Figure 5-8. Dependence of the $\frac{K}{1+K_0}$ parameter of RNase t1 upon the amount of energy (ΔG^0) needed to convert water_{HD} to water_{LD} of various 4.4 m salt solutions.

leads to the observed decrease in enzyme activity.

It is of the utmost importance to note that these salt effects do not require the high, non-physiological concentrations of salt used in this study. The hydration layer of a protein such as RNase t1 contains approximately 250 – 275 water molecules (42). If only one of these water molecules is replaced by one formal unit of MgCl_2 , a concentration of 0.2 M is obtained in the immediate vicinity of the enzyme. However, the replacement of the on Mg^{2+} ion will affect 55 molecules of water, which encompasses the hydrogen bonding of approximately 20% of the water molecules of the protein hydration layer. Even a small amount of salt in the bulk solvent can potentially perturb the thermodynamic properties of the protein in a significant manner. In addition, these results pose a new challenge for theoreticians modeling protein structures in solution because they demonstrate that the hydration layer of proteins under physiological conditions may be very different than that of proteins in pure water.

5.6 Conclusions

In the final chapter of this work, I have studied the effect of various chloride salts on the enzymatic activity of RNase t1. I have revisited the fact that the addition of salts hinders the catalytic capabilities of the enzyme and observed that the degree of loss of enzyme activity is unique to each salt added in solution. I have demonstrated that the traditional explanations (change in pK_a of key active site residues, Coulombic interactions between enzyme and substrate, inhibition caused by direct metal binding) to the observed loss of enzyme activity in concentrated salt solutions are inadequate in explaining the observed loss of enzyme activity. I have also shown that the addition of salt promotes a more compact, more rigid and less form of the enzyme and that the salts ability to promote this less active conformation is directly

correlated to its ability to promote linear hydrogen bonds throughout the hydrogen bonding network of water. As was seen in the previous chapter, salts can affect proteins directly through electrostatic interactions and induced point charges, however I suggest here that salts can also indirectly influence protein stability by modulating the hydrogen bonding network of the water in the protein's hydration shell. My results are compatible with the hypothesis that linear water stabilizes a more compact form of RNase t1 and thereby inhibits its catalytic efficiency.

References

1. Jan Steyaert, Abdel Fattah Haikal, Lode Wyns, Patrick Stanssens. Subsite interactions of ribonuclease t1: Viscosity effects indicate that the rate-limiting step of GpN transesterification depends on the nature of N. *Biochemistry*. 1991;30(35):8661-5.
2. Jan Steyaert, Chris Opsomer, Lode Wyns, Patrick Stanssens. Quantitative analysis of the contribution of Glu46 and Asn98 to the guanosine specificity of ribonuclease t1. *Biochemistry*. 1991;30(2):494-9.
3. Kapil Kumar, Frederick G. Walz Jr. Probing functional perfection in substructure of ribonuclease t1: Double combinatorial random mutagenesis involving Asn43, Asn44, and Glu46 in the guanine binding loop. *Biochemistry*. 2001;40(12):3748-57.
4. Joseph R. Lakowicz. Principles of fluorescence spectroscopy, 3rd edition. *Analytical and Bioanalytical Chemistry*. 2008;390(5):1223-4.
5. C.R. Cantor PRS. The behavior of biological macromolecules; their biophysical chemistry, pt. 3. W.H. Freeman; 1980.
6. Cui Qing Hu, Julian M. Sturtevant. Thermodynamics of binding of mononucleotides to ribonuclease t1. *Journal of Physical Chemistry*. 1992;96(10):4052-6.
7. Y. Georgalis, A. Zouni, P. Zielenkiewicz, J.F. Holzwarth, R. Clarke, U. Hahn, W. Saenger. Modes of mononucleotide binding to ribonuclease t1. *Journal of Biological Chemistry*. 1992;267(15):10323-30.
8. James N. Weiss. The hill equation revisited: Uses and misuses. *Federation of American Societies for Experimental Biology*. 1997;11:835-41.
9. Giovanni B. Strambini, Margherita Gonnelli. Amplitude spectrum of structural fluctuations in proteins from the inner diffusion of solutes of increasing molecular size: A trp phosphorescence quenching study. *Biochemistry*. 2011;50(6):970-80.
10. Giovanni B. Strambini, Margherita Gonnelli. Acrylamide quenching of trp phosphorescence in liver alcohol dehydrogenase: Evidence of gated quencher penetrations. *Biochemical Journal*. 2009;48(31):7482-91.
11. Michael Zabinski, Frederick G. Walz Jr. Subsites and catalytic mechanism of ribonuclease t1: Kinetic studies using GpC and GpU as substrates. *Archives of Biochemistry and Biophysics*. 1976;175(2):558-64.
12. Harry L. Osterman, Frederick G. Walz Jr. Subsite interactions and ribonuclease t1 catalysis: Kinetic studies with ApGpC and ApGpu. *Biochemistry*. 1979;18(10):1984-8.
13. Jan Steyaert, Klaas Hallenga, Lode Wyns, Patrick Stanssens. Histidine-40 of ribonuclease t1 acts as base catalyst when the true catalyst base, glutamic acid-58, is replaced by alanine. *Biochemistry*. 1990;29(38):9064-72.
14. Yung0Hsiang Kao, Carolyn A. Fitch, Shibani Bhattacharya, Christopher J. Sarkisian, Juliette T.J. Lecomte, Bertrand Garcia-Moreno E. Salt effects on ionization equilibria of histidines in myoglobin. *Biophysical Journal*. 2000;79(3):1637-54.

15. Kelly K. Lee, Carolyn A. Fitch, Juliette T.J. Lecomte, Bertrand E. Garcia-Moreno. Electrostatic effects in highly charged proteins: Salt sensitivity of pK_a values of histidines in staphylococcal nuclease. *Biochemistry*. 2002;41(17):5656-67.
16. Yoshito Abe, Iwashita Tadashi, Hiroki Iwashita, Yoshio Hashimoto, Hiroyuki Motoshima, Yoshitugu Tanaka, Taiji Imoto. Effect of salt concentration on the pK_a of acidic residues in lysozyme. *Biochemistry*. 1995;118(5):946-52.
17. Barbara M. Fiser, Wayne L. Schultz, Ronald T. Raines. Coulombic effects of remote subsites on the active site of ribonuclease A. *Biochemistry*. 1998;37(50):17386-401.
18. Chiwook Park, Ronald T. Raines. Origin of the 'inactivation' of ribonuclease A at low salt concentrations. *Federation of European Biochemical Scientists Letters*. 2000;468(2,3):199-202.
19. Chiwook Park, Ronald T. Raines. Quantitative analysis of the effect of salt concentration on enzymatic catalysis. *Journal of the American Chemical Society*. 2001;123(46):11472-9.
20. Thomas M. Record, Timothy M. Lohman, Pieter De Haseth. Ion effects on ligand-nucleic acid interactions. *Journal of Molecular Biology*. 1976;107(2):145-58.
21. Frederick G. Walz Jr. Studies on the nature of guanine nucleotide binding with ribonuclease t1. *Biochemistry*. 1977;16(25):5509-15.
22. Erin M. Bowers, Lindsey O. Ragland, Larry D. Byers. Salt effects on β -glucosidase: PH-profile narrowing. *Biochimica et Biophysica Acta, Proteins and Proteomics*. 2007;1774(12):1500-7.
23. Serge N. Timasheff. Thermodynamic binding and site occupancy in the light of the schellman exchange concept. *Biophysical Chemistry*. 2002;101-102:99-111.
24. John A. Schellman. The relation between the free energy of interaction and binding. *Biophysical Chemistry*. 1993;45(3):273-9.
25. Mitsuhiro Itaya YI. Steady-state kinetic studies of the inhibitory action of zinc on ribonuclease t1 catalysis. *Biochemical Journal*. 1982;297(2):357-62.
26. Joeri Deswarte, Stefan De Vos, Ulrike Langhorst, Jan Steyaert, Remy Loris. The contribution of metal ions to the conformational stability of ribonuclease t1. crystal versus solution. *European Journal of Biochemistry*. 2001;268(14):3993-4000.
27. Andrew S. Thomas, Adrian H. Elcock. Molecular dynamics simulations of hydrophobic association in aqueous salt solutions indicate a connection between water hydrogen bonding and the hofmeister effect. *Journal of the American Chemical Society*. 2007;129:14887-98.
28. Feng Guo, Joel M. Friedman. Charge density-dependent modifications of hydration shell waters by hofmeister ions. *Journal of the American Chemical Society*. 2009;131(31):11010-8.
29. Christopher D. Cappa, Jared D. Smith, Kevin R. Wilson, Benjamin M. Messer, Mary K. Gilles, Ronald C. Cohen, Richard J. Saykally. Effects of alkali metal halide salts on the hydrogen bond network of liquid water. *Journal of Physical Chemistry*. 2005;109(15):7046-52.

30. Paul G. Higgs, Jean Francois Joanny. Theory of polyampholyte solutions. *Journal of Chemical Physics*. 1991;94(2):1543-54.
31. W.M. Cox JHW. Viscosity of strong electrolytes measured by a differential method. *Proceedings of the Royal Society of London*. 1934;145:475-88.
32. H. Donald B. Jenkins. Viscosity *B*-coefficients of ions in solution. *Chemical Reviews*. 1995;95(8):2695-724.
33. Ken A. Dill, Thomas M. Truskett, Vojko Valchy, Barbara Hribar-Lee. Modeling water, the hydrophobic effect, and ion solvation. *Annual Review of Biophysics and Biomolecular Structur*. 2005;34:173-99.
34. Yizhak Marcus. *Ion properties*. ; 1997.
35. Joseph B. Schlenoff, Amir H. Rmaile, Claudiu B. Bucur. Hydration contributions to association in polyelectrolyte multilayers and complexes: Visualizing hydrophobicity. *Journal of the American Chemical Society*. 2008;130(41):13589-97.
36. Michael Y. Kiriukhin, Kim D. Collins. Dynamic hydration numbers for biologically important ions. *Biophysical Chemistry*. 2002;99(2):155-68.
37. Barbara Hribar, Noel T. Southhall, Vojko Vlachy, Ken A. Dill. How ions affect the structure of water. *Journal of the American Chemical Society*. 2002;124(41):12302-11.
38. Kim A. Sharp, Bhupinder Madan, Eric Manas, Jane M. Vanderkooi. Water structure changes induced by hydrophobic and polar solutes revealed by simulations and infrared spectroscopy. *Journal of Phy*. 2001;114(4):1791-6.
39. Nathaniel V. Nucci, Jane M. Vanderkooi. Effects of salt on the hofmeister series on the hydrogen bond network of water. *Journal of Molecular Liquids*. 2008;143:160-70.
40. K.J. Tielrooij, N. Garcia-Araez, M. Bonn, H.J. Bakker. Cooperativity in ion hydration. *Science*. 2010;328(5981):1006-9.
41. G. Wilse Robinson, C.H. Cho. Role of hydration water in protein unfolding. *Biophysical Journal*. 1999;77:3311-8.
42. Serge N. Timasheff. Protein hydration, thermodynamic binding, and preferential hydration. *Biochemistry*. 2002;41(46):13473-82.

SUMMARY OF WORK

The work presented here examines the effect that salts in solution will have on i) the hydrophobic effect, ii) the conformational stability of a model enzyme and iii) the cumulative effect of i) and ii) on enzyme activity. In my examination of the effect of salts on the hydrophobic effect, I have taken a particular look at lithium, which does not conform to the theoretical predictions of many systems. With the simple model, I examined the effect of alkali chlorides on hydrophobicity and determine that lithium does indeed affect hydrophobicity as is predicted by theoretical work, as well as all other alkali metals examined. It was shown that the hydrophobic effect is modulated according to the charge density of the alkali salt present in solution.

I have also investigated the effect of point induced image charges on the conformational stability of RNase t1 using urea-induced unfolding. The work presented here seeks to determine the magnitude of the role that point induced image charges play in protein stability. The work presented here validates the theoretical model developed by Zhou et al. and goes on to show that induced image point charges contribute significantly to the stability of RNase t1 via salting-out interactions. I go on to demonstrate that the contribution depends on the nature of the salt and varies according to the nature of the interaction between the cation and the protein.

Finally, I have investigated the effect of salts on enzyme catalysis in terms of hydrophobicity and conformational stability. Through fluorescence spectroscopy and UV-Vis absorbance, I have determined that the addition of salts leads to the stabilization of a compact, rigid conformation of RNase t1 which inhibits the hydrolysis of the substrate GpC. The extent of the loss of enzyme activity once again depends on the nature of the salt and I have shown for the first time a strong correlation between enzyme activity and the type of hydrogen bonds in the

hydration shell of the enzyme. I have demonstrated that the magnitude of the loss of enzyme activity depends on the ability of the cation to induce linear hydrogen bonds in the protein hydration shell, thereby stabilizing a compact and rigid conformation of the enzyme.